MULTIFUNCTIONAL NANOCOMPOSITE REINFORCED BY GRAPHITE NANOPLATELETS

By

Huang Wu

A DISSERTATION

Submitted to
Michigan State University
in partial fulfillment of the requirements
for the degree of

DOCTOR OF PHILSOPHY

Chemical Engineering

2011

ABSTRACT

MULTIFUNCTIONAL NANOCOMPOSITE REINFORCED BY GRAPHITE NANOPLATELETS

By

Huang Wu

Nanoparticles have the potential to impart multiple desirable properties to polymers and composites due to their theoretical high properties and easier processing. Compared with other nanoparticles, graphite or graphene nanoplatelets are drawing more and more attention because of their combination of exceptional mechanical, electrical, thermal properties that are equal to carbon nanotubes but with the same two-dimensional platelet morphology as nanoclay, which also makes them capable of providing improved barrier properties in polymers. However, the 2D structure of graphite nanoplatelets also requires additional attention to be directed at the processing of these nanoparticles in polymers. Unlike symmetric nanofillers such as carbon black, the dispersion of 2D platelet fillers in a polymer matrix is more difficult due to the strong action between their surfaces. Besides getting good dispersion, the orientation of 2D particles also needs to be taken into account due to their anisotropic properties. However, if done properly, both dispersion and orientation can be controlled through nano-structuring to create novel materials with unique morphologies and properties.

In this research, graphite nanoplatelets were fabricated through exfoliation route to preserve the exceptional electrical and thermal properties. A novel polishing and

plasma etching process for scanning electron microscopic observation of these nanocomposite samples has been developed to study the relationships among processing, morphology and performance. As a result, the dispersion and orientation of GNP could be used to explain the mechanical and electrical properties of the composites. It was discovered that orientation of GNP particles is the main factor in achieving high mechanical properties. Orientation that causes high mechanical properties and low electrical conductivity can be controlled by annealing the composite under high temperature.

Based on these principles, methods for nanostructuring of the exfoliated graphite nanoplatelets were identified and investigated to optimize desired properties. First, composites with uniformly aligned filler particles can be produced by cast film extrusion. Improvement of both tensile modulus and strength along with barrier properties was observed compared with injection and compression molded samples. Second, pre-coating of polymer powder and solid state ball milling (SSBM) were used to create percolated networks at low GNP concentrations to enhance electrical conductivity. A combination of melt-extrusion and SSBM resulted in the composites with both high mechanical properties and high electrical conductivity. Third, GNP particles were assembled into a thin paper-like film to create a flexible, durable and light-weighted material with extremely high electrical conductivity (~2200 S/cm) and thermal conductivity (~313W/m/K), low permeability to small molecules and the engineering possibility to be incorporated into fiber reinforced composites.

To my wife and my parents

ACHNOWLEDGEMENTS

Firstly, I'd like to thank The Boeing Company for sponsoring this project. I'd also like to express my personal gratitude to Mr. Gregg Bogucki from Boeing for his help.

Then, I'd like to express my sincere appreciation to my advisor, Prof. Lawrence T. Drzal, for taking me as his student and helping me throughout my PhD research project. I am also thankful to my committee members, Prof. Greg Baker, Krishnamurthy Jayaraman, Ilsoon Lee and Ramani Narayan for their comments on my research. Furthermore, I'd like to thank department of Chemical Engineering and Material Science.

I am grateful to every CMSC staff, Per Askeland, Inhwan Do, Ed Drown, Hiroyuki Fukushima, Hazel-Ann Hosein, Karen Lillis, Wanjun Liu, Hwan-Man Park, Mike Rich, Brian Rook and Inger Weitlauf. Just like good neighbors, they are always there when I need help.

My awesome officemates, Pat, Xian, Anchita, Deb, Tao, Jinglei, Dee, Yan and Sanjib, inspired me a lot through our chatting in the office, lab and during coffee time. I enjoyed staying and working in EB1105 thanks to the friendly and joyful environment created by them.

Last but not least, I want to thank my wife and my parents for their unconditional love and infinite support in my life, especially their encouragement during my studies.

Table of Contents

List of Tables

List of Figures

Chapter 1 Introduction

Background and Literature Review

Multifunctional Polymer Composite

Polymer and polymer composites have been widely used to replace metal and metal alloys because of their light weight, good chemical resistance and lower manufacturing costs in automobile, aerospace, recreational goods, infrastructure, electronic devices, etc.. Although the modulus and strength may be the principal structural requirement for polymer composites, many applications would also benefit greatly if other properties could be added thereby increasing the functionality of the same material. For example, one inherent difference between polymer and metal is the electrical conductivity: most polymers are insulators while metals are conductors. Incorporating adequate electrical conductivity into polymers and polymer composites has been a major goal recently due to the increasing demand of lightning strike protection in polymer composites constructed aircraft. Similarly, any desirable property is thermal conductivity which is very low in polymer composites. Materials used in electronic packaging require high thermal conductivity to dissipate heat. Another example of the need for multifunctional composites is the material used in containers such as fuel tanks, which requires mechanical strength for structural purpose, electrical conductivity for static charge hazard prevention, and barrier properties to the fuel molecules.

Nanocomposite

One promising way to provide multifunctionality to a polymer composite is to add nanofillers. Polymer nanocomposites usually refer to a polymer matrix filled by high-surface-area reinforcing fillers [1] including carbon nanotubes (CNTs), carbon nanofibers, nanoclay, carbon black (CB), graphene platelets and so on. Since their discovery, nanoparticles were expected to function as substitute reinforcements for conventional reinforcement fibers because of the theoretically high particle properties and the significant improvement in nanocomposite properties attained at low loadings. Furthermore significant advantages were expected from gains in processing by eliminating the need for layer-by-layer assembly or autoclave processing. The functionality of the nanofillers is highly dependent on their morphology. For example, as conductive fillers, the zero-dimensional CB can improve composite electrical conductivity as a result of electrical percolation at low (~5%) loading for non-polar, low crystallinity thermoplastics [2], while high aspect ratio CNT filled composites with a similar matrix have a percolation threshold of 0.1vol% [3]. The high aspect ratio and linear shape of CNTs make it easier to form a percolated network with more contacts being formed between filler particles. Two-dimensional (nano-platelet) fillers such as alumino-silicate nanoclay can also produce composites with low gas permeability which cannot be achieved by CNTs or CB because of the highly tortuous path formed by their impenetrable nature. If properly aligned, the 2D particles will force the small molecules to travel through a tortuous zigzag path

instead of diffusing freely, resulting in much lower permeability [4-6] (Figure 1.1). Research also suggests that this kind of filler can also be used to improve the fire retardancy of its composite [7].

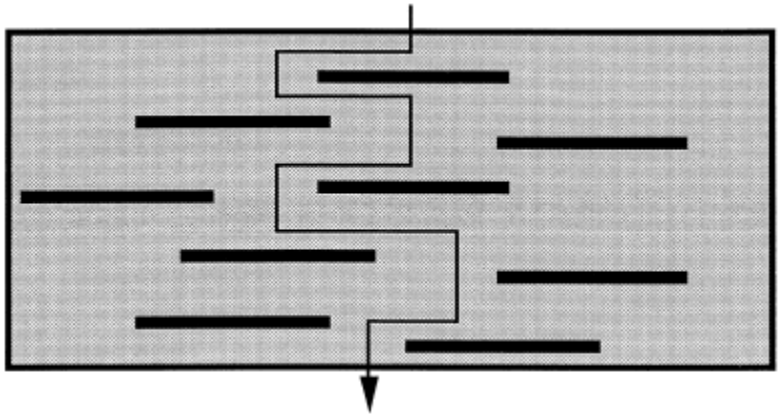

Figure 1.1, Proposed model for the tortuous zigzag diffusion path in a composite filled by aligned 2D particles (adapted from literature [4])

Despite the promising properties of CNTs, it is not advantageous to use them in commercial composites because of their expensive nature and limited availability. CB/rubber composites are the standard in the tire industry, and colloidal silica as a rubber additive is making inroads into the tire industry [8]. However, these two fillers do not possess the excellent electrical properties found in CNTs.

Exfoliated Graphite Nanoplatelet and its Composites

Graphene based nanoplatelet particles, which combine good electrical and thermal properties similar to CNTs and the two-dimensional morphology of alumino-silicate clays, are considered to be an excellent potential additive in terms of achieving multifunctionality for the composites. Graphite or graphene nanoplatelets have received growing interest because their high mechanical properties (~1TB for either

single layer or multi layer graphene theoretically [9, 10] and experimentally [11-13]), excellent electrical (~1.0×10^{-6} ohm/cm resistivity for pure graphene [14]), and thermal (~5000 W/m/K [15-18]) conductivity. The platelet shape of graphite also benefits the composites by enhancing barrier properties and coupled with the high thermal oxidative resistance of graphene, fire retardancy can be achieved as well as demonstrated in Figure 1.1. Such properties are considered to be essential for multifunctional composites.

The process of generating thin graphite platelets consisting of several layers of graphene sheets is relatively simple and cost-effective. Usually, three steps are involved in fabricating these nanofillers from natural graphite: (i) intercalation, where both proton-donor agents and electron acceptors can be intercalated in between graphene layers; (ii) exfoliation, where a large amount of heat is applied to expand the intercalated graphite through vaporization of the intercalant; (iii) pulverization, where the exfoliated graphite is reduced in size to smaller dimensions. As demonstrated in Drzal's group [19], exfoliated graphite nanoplatelets (GNP) consisting of small stacks of graphene can be fabricated by acid intercalation, microwave heating and ultrasonication pulverization and be scaled inexpensively into quantity production by this route. The size and thickness of GNP is controllable during fabrication. Typical sizes of the platelets range from submicron to 25 microns in diameter usually notated as GNP-1, GNP-5 and GNP-15 where the number refers to the average statistical diameter with thicknesses in the 5-10 nm range. Compared with the other popular fabrication route requiring formation of graphene oxide

followed by reduction of graphite oxide [20] back to graphene, the intercalation-expanding route avoids the disruption of sp^2 bonding of the graphite which is the key to its superior thermal and electrical properties as well as its economical price.

Processing of Nanocomposites

Because of the two dimensional nature of GNP and its high aspect ratio, final properties of GNP based nanocomposites can vary due to the processing methods selected. For example, the molding processes are important for their ability to make complex shaped integrated composites. Kim et al [21] have shown that differences in electrical conductivity of polycarbonate/graphene composites can be attained depending on whether they were made by injection molding or compression molding. Compression molded samples showed much better electrical conductivity than injection molded ones. Mohanty et al [22] found that post-molding treatment, such as annealing after injection molding can provide better flexural modulus and strength and alter the morphology of nanocomposites and thus their properties.

Typical compounding methods for thermoplastic matrix includes: (1) melt compounding, such as combining high density polyethylene (HDPE) and exfoliated graphite mixed in a Brabender mixer [23, 24] or twin-screw extruder [25]; (2) solution mixing, where a solvent is used to dissolve polymer and then disperse graphite [26, 27]; (3) in-situ polymerization, where the polymer is polymerized with presence of graphite [28, 29].

While being the most widely used method in industrial applications, melt-extrusion falls short in the electrical conductivity and percolation threshold achieved in the resulting composite [30, 31]. Solution mixing is capable of separating and dispersing nano particles which results in lower percolation threshold [32], but the presence of solvent may cause problems while processing the composite and increase the cost of manufacture. In-situ polymerization only applies to limited category of polymers, and the energy cost for exfoliating graphite during the process is a large concern. Efforts have been made to find a practical and efficient way to disperse the nano graphite particles in order to achieve lower percolation. Some researchers used melt-extrusion of unsaturated polyester resin (UPR) to modify expanded graphite [33] which resulted in a percolation threshold at 5.7wt%, instead of 22.2wt% for composites with conventional graphite. Recently, Drzal's group [30] developed a GNP pre-coating method to achieve low percolation threshold where a non-solvent of the polymer is used to disperse GNP particles. While adding polymer powder into the suspension, the GNP particles are coated onto the polymer surface. The GNP forms a complete continuous coating on the surface of the polymer powder. Subsequent compression molding results in nanocomposites with the continuous GNP phase intact after the molding process.

Dynamic percolation behavior of CB composites has been studied by Wu et al [34] who found that due to Brownian motion, CB particles are able to reposition themselves locally under high temperature during which the viscosity of the polymer matrix is low. Particles of platelet shape such as alumino-silicates and graphene

might not be affected to the same extent by Brownian motion because of their larger dimensions. Researchers have shown faster particle re-organization in layered alumino-silicate/polymer composites than expected compared to Brownian motion theory [35-37]. The real driving force might be the elastic restoring force of the polymeric matrix to its stress free state generated during processing though no widely-accepted conclusion has been drawn yet. Kim [21] proposed a disorientation mechanism for graphene composites based on X-ray scattering and rheology data, pointing out that at low loadings (<3wt%) of graphite filler, the rotation experienced by the particles caused by annealing still cannot increase particle contact with each other, while at high loadings (>12wt%), the movement of filler particles is restricted due to excluded volume interactions between particles.

Paper Form Nanocomposite

Reassembly of nano material into macro-scale structures has become one interesting approach to utilize the nanofillers. The reassembled structure can also be incorporated into a composite. Carbon nanotubes (CNT) Bucky paper [38-48] and graphite oxide (GO) paper [20, 49, 50] have been widely studied. The paper form of these materials can be self-standing and show good flexibility [20, 46]. Electrical conductivity is reported to be 200 S/cm for Bucky paper with aligned CNT [46] and 350 S/cm for reduced GO paper [49]. The paper fabricated from ref. [46] and [49] are claimed to be binder-free but other types of paper made with a polymeric binder would have lower values. Compared with natural graphite which has a conductivity

of ~2000 S/cm, these values are still one order of magnitude lower. The reason is, for CNT, the contact resistance between each tube is high due to the curvature of the contacting surfaces resulting in point-to-point contacts; for GO paper, the chemically reduced graphite oxide is not as conductive as pristine graphite. Li et al [51] and Biswas et al [52] both fabricated Langmuir-Blodgett thin films from exfoliated graphite nanoplatelets. The electrical and thermal conductivity were reported to be over 1000 S/cm [52] and 380 W/m/K [53], respectively.

Dissertation Objective

The major objective of this research is to investigate the feasibility of using GNP particles to impart the polymer composite with multifunctionality, and find the optimum way to achieve these desired multifunctional properties. The major polymer matrix used during this research is the polyetherimide (PEId, Ultem®) (Figure 1.2). PEId is a high temperature amorphous engineering thermalplastic. The glass transition temperature for PEId is 216℃. PEId has excellent chemical resistance and thermal stability. Moreover, it is inherently flame resistant and only generates a very small amount of low-density gas when burned, making it an ideal material for applications in advanced structures such as submarine, airplane and high-floor offices [54].

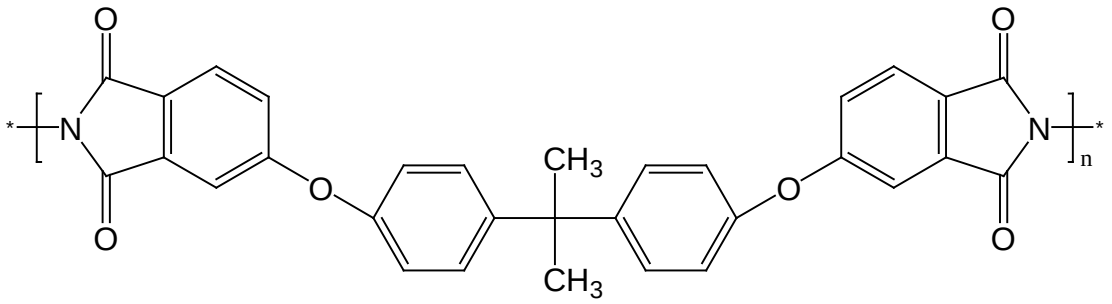

Figure 1.2, Molecular structure of PEId

In order to establish a viable method for producing multifunctional GNP composites for different applications, the relationships among common processing methods, the morphology and the performance of the GNP composite are first studied. A novel approach of SEM sample preparation has been developed for revealing the internal polymer nanocomposite morphology. The effect of injection and compression molding on the mechanical properties, electrical conductivity and coefficient of thermal expansion is investigated and explained based on the morphology. The remaining part of this dissertation is directed at how to design and nanostructure the GNP in the composites for desired properties based on what has been learned. Eventually, a nanostructured film or paper form of GNP composite is shown to the best way to achieve the full potential of the GNP nanoparticle.

REFERENCES

REFERENCES

1. Vaia, R.A. and E.P. Giannelis, *Polymer nanocomposites: Status and opportunities.* Mrs Bulletin, 2001. **26**(5): p. 394-401.

2. Huang, J.C., *Carbon black filled conducting polymers and polymer blends.* Advances in Polymer Technology, 2002. **21**(4): p. 299-313.

3. Bauhofer, W. and J.Z. Kovacs, *A review and analysis of electrical percolation in carbon nanotube polymer composites.* Composites Science and Technology, 2009. **69**(10): p. 1486-1498.

4. LeBaron, P.C., Z. Wang, and T.J. Pinnavaia, *Polymer-layered silicate nanocomposites: an overview.* Applied Clay Science, 1999. **15**(1-2): p. 11-29.

5. Kim, J.K., et al., *Moisture barrier characteristics of organoclay-epoxy nanocomposites.* Composites Science and Technology, 2005. **65**(5): p. 805-813.

6. Yano, K., et al., *SYNTHESIS AND PROPERTIES OF POLYIMIDE CLAY HYBRID.* Journal of Polymer Science Part a-Polymer Chemistry, 1993. **31**(10): p. 2493-2498.

7. Porter, D., E. Metcalfe, and M.J.K. Thomas, *Nanocomposite fire retardants - A review.* Fire and Materials, 2000. **24**(1): p. 45-52.

8. Schaefer, D.W. and R.S. Justice, *How nano are nanocomposites?* Macromolecules, 2007. **40**(24): p. 8501-8517.

9. Chang, T.C. and H.J. Gao, *Size-dependent elastic properties of a single-walled carbon nanotube via a molecular mechanics model.* Journal of the Mechanics and Physics of Solids, 2003. **51**(6): p. 1059-1074.

10. Meo, M. and M. Rossi, *Prediction of Young's modulus of single wall carbon nanotubes by molecular-mechanics based finite element modelling.* Composites Science and Technology, 2006. **66**(11-12): p. 1597-1605.

11. Lee, C., et al., *Measurement of the elastic properties and intrinsic strength of monolayer graphene.* Science, 2008. **321**(5887): p. 385-388.

12. Zhao, H., K. Min, and N.R. Aluru, *Size and Chirality Dependent Elastic Properties of Graphene Nanoribbons under Uniaxial Tension.* Nano Letters, 2009. **9**(8): p. 3012-3015.

13. Wong, C.L., et al., *Characterization of nanomechanical graphene drum structures.* Journal of Micromechanics and Microengineering, 2010. **20**(11).

14. Tune, L., *Physicists Show Electrons Can Travel More Than 100 Times Faster in Graphene (https://newsdesk.umd.edu/scitech/release.cfm?ArticleID=1621)*. 2008.

15. Watanabe, E., et al., *Ballistic thermal conductance of electrons in graphene ribbons.* Physical Review B, 2009. **80**(8).

16. Jiang, J.W., J.S. Wang, and B.W. Li, *Thermal conductance of graphene and dimerite.* Physical Review B, 2009. **79**(20).

17. Saito, K., J. Nakamura, and A. Natori, *Ballistic thermal conductance of a graphene sheet.* Physical Review B, 2007. **76**(11).

18. Balandin, A.A., et al., *Superior thermal conductivity of single-layer graphene.* Nano Letters, 2008. **8**(3): p. 902-907.

19. Fukushima, H., *Graphite Nanoreinforcements in Polymer Nanocomposites*, in *Department of Chemical Engineering and Materials Science*. 2003, Michigan State University: East Lansing.

20. Stankovich, S., et al., *Synthesis of graphene-based nanosheets via chemical reduction of exfoliated graphite oxide.* Carbon, 2007. **45**(7): p. 1558-1565.

21. Kim, H. and C.W. Macosko, *Processing-property relationships of polycarbonate/graphene composites.* Polymer, 2009. **50**(15): p. 3797-3809.

22. Mohanty, A.K., et al., *Effect of process engineering on the performance of natural fiber reinforced cellulose acetate biocomposites.* Composites Part a-Applied Science and Manufacturing, 2004. **35**(3): p. 363-370.

23. Wang, Y.S., M.A. Ogurkis, and J.T. Lindt, *ELECTRICAL-PROPERTIES OF EXFOLIATED-GRAPHITE FILLED POLYETHYLENE COMPOSITES.* Polymer Composites, 1986. **7**(5): p. 349-354.

24. Krupa, I. and I. Chodak, *Physical properties of thermoplastic/graphite composites.* European Polymer Journal, 2001. **37**(11): p. 2159-2168.

25. Zheng, W., X.H. Lu, and S.C. Wong, *Electrical and mechanical properties of expanded graphite-reinforced high-density polyethylene.* Journal of Applied Polymer Science, 2004. **91**(5): p. 2781-2788.

26. Zheng, W.G., S.C. Wong, and H.J. Sue, *Transport behavior of PMMA/expanded graphite nanocomposites.* Polymer, 2002. **43**(25): p. 6767-6773.

27. Zheng, W. and S.C. Wong, *Electrical conductivity and dielectric properties of PMMA/expanded graphite composites.* Composites Science and Technology, 2003. **63**(2): p. 225-235.

28. Pan, Y.X., et al., *A new process of fabricating electrically conducting nylon 6/graphite nanocomposites via intercalation polymerization.* Journal of Polymer Science Part B-Polymer Physics, 2000. **38**(12): p. 1626-1633.

29. Zou, J.F., et al., *Conductive mechanism of polymer/graphite conducting composites with low percolation threshold.* Journal of Polymer Science Part B-Polymer Physics, 2002. **40**(10): p. 954-963.

30. Kalaitzidou, K., H. Fukushima, and L.T. Drzal, *A new compounding method for exfoliated graphite-polypropylene nanocomposites with enhanced flexural properties and lower percolation threshold.* Composites Science and Technology, 2007. **67**(10): p. 2045-2051.

31. Kim, S., I. Do, and L.T. Drzal, *Multifunctional xGnP/LLDPE Nanocomposites Prepared by Solution Compounding Using Various Screw Rotating Systems.* Macromolecular Materials and Engineering, 2009. **294**(3): p. 196-205.

32. Ansari, S. and E.P. Giannelis, *Functionalized Graphene Sheet-Poly(vinylidene fluoride) Conductive Nanocomposites.* Journal of Polymer Science Part B-Polymer Physics, 2009. **47**(9): p. 888-897.

33. She, Y.H., G.H. Chen, and D.J. Wu, *Fabrication of polyethylene/graphite nanocomposite from modified expanded graphite.* Polymer International, 2007. **56**(5): p. 679-685.

34. Wu, G.Z., et al., *A delay of percolation time in carbon-black-filled conductive polymer composites.* Journal of Applied Physics, 2000. **88**(3): p. 1480-1487.

35. Schmidt, G., et al., *Shear orientation of viscoelastic polymer-clay solutions probed by flow birefringence and SANS.* Macromolecules, 2000. **33**(20): p. 7219-7222.

36. Solomon, M.J., et al., *Rheology of polypropylene/clay hybrid materials.* Macromolecules, 2001. **34**(6): p. 1864-1872.

37. Ren, J.X., et al., *Disorientation kinetics of aligned polymer layered silicate*

nanocomposites. Macromolecules, 2003. **36**(11): p. 4188-4194.

38. Liu, J., et al., *Fullerene pipes.* Science, 1998. **280**(5367): p. 1253-1256.

39. Cooper, S.M., et al., *Gas permeability of a buckypaper membrane.* Nano Letters, 2003. **3**(2): p. 189-192.

40. Wang, Z., et al., *Processing and property investigation of single-walled carbon nanotube (SWNT) buckypaper/epoxy resin matrix nanocomposites.* Composites Part a-Applied Science and Manufacturing, 2004. **35**(10): p. 1225-1232.

41. Endo, M., et al., *'Buckypaper' from coaxial nanotubes.* Nature, 2005. **433**(7025): p. 476-476.

42. Gonnet, P., et al., *Thermal conductivity of magnetically aligned carbon nanotube buckypapers and nanocomposites.* Current Applied Physics, 2006. **6**(1): p. 119-122.

43. Gou, J.H., *Single-walled nanotube bucky paper and nanocomposite.* Polymer International, 2006. **55**(11): p. 1283-1288.

44. Kim, Y.A., et al., *Fabrication of high-purity, double-walled carbon nanotube buckypaper.* Chemical Vapor Deposition, 2006. **12**(6): p. 327-+.

45. Zheng, F., et al., *Single-walled carbon nanotube paper as a sorbent for organic vapor preconcentration.* Analytical Chemistry, 2006. **78**(7): p. 2442-2446.

46. Wang, D., et al., *Highly oriented carbon nanotube papers made of aligned carbon nanotubes.* Nanotechnology, 2008. **19**(7).

47. Xu, G.H., et al., *The feasibility of producing MWCNT paper and strong MWCNT film from VACNT array.* Applied Physics a-Materials Science & Processing, 2008. **92**(3): p. 531-539.

48. Dumee, L.F., et al., *Characterization and evaluation of carbon nanotube Bucky-Paper membranes for direct contact membrane distillation.* Journal of Membrane Science, 2010. **351**(1-2): p. 36-43.

49. Chen, H., et al., *Mechanically strong, electrically conductive, and biocompatible graphene paper.* Advanced Materials, 2008. **20**(18): p. 3557-+.

50. Park, S., et al., *Graphene oxide papers modified by divalent ions - Enhancing*

mechanical properties via chemical cross-linking. Acs Nano, 2008. **2**(3): p. 572-578.

51. Li, X.L., et al., *Highly conducting graphene sheets and Langmuir-Blodgett films.* Nature Nanotechnology, 2008. **3**(9): p. 538-542.

52. Biswas, S. and L.T. Drzal, *A Novel Approach to Create a Highly Ordered Monolayer Film of Graphene Nanosheets at the Liquid-Liquid Interface.* Nano Letters, 2009. **9**(1): p. 167-172.

53. Xiang, J.L. and L.T. Drzal, *Thermal Conductivity of a Monolayer of Exfoliated Graphite Nanoplatelets Prepared by Liquid-Liquid Interfacial Self-Assembly.* Journal of Nanomaterials, 2010.

54. http://www.sabic-ip.com. Last visited: March 2011

Chapter 2 A novel method of revealing the morphology of nanocomposites by Scanning Electron Microscope

Abstract

Revealing the morphology of the nanocomposites explicitly helps to understand the relationship between particle structure, method of processing and performance. A novel SEM sample preparation process involving epoxy fixation of the sample, mechanical polishing and O2 plasma etching is developed, leading to images with excellent morphological information as a result of good contrast between GNP particles and the matrix. Such good contrast enables important information to be collected for further analysis such as particle size and orientation by the image-processing software. For samples with a porous structure or cracks, fluorescent images can be used to locate the epoxy fixation material and reveal the real structure of the material without the complicating effects of the fixation agent..

Introduction

“Seeing Is Believing.” Since the natural state of the fillers such as their distribution, dispersion and orientation is the bridge between the processing route and the

performance of the polymer nanocomposites, it is critical to be able to actually see the internal morphology, at a micro scale. Modern microscopic techniques have given researchers various ways to observe the morphology for micro-scale devices and materials. Scanning electron microscope (SEM) and transmission electron microscope (TEM) are the most widely used techniques. SEM is useful for checking the fracture surface of a composite. However, when the size of the filler particle is in hundreds of nanometers to a few microns range, it is hard to distinguish the filler morphology from the features generated by the polymer matrix [1, 2]. TEM is extremely useful to investigate the dispersion state of nanofillers such as nano-silicate [3, 4], carbon nanotubes (CNT) [2, 5]. However, only a small portion of the sample can be observed at one time, making it difficult to understand the overall condition of the fillers throughout the entire sample.

Recently, graphite nanoplatelet (GNP)/polymer composites have drawn a lot of attention. To get a clear picture of the dispersion, distribution and orientation of the GNP particles in GNP/polymer composite, a new time-efficient approach for making SEM samples has been developed. After adequate polishing and oxygen plasma etching, the prepared cross-section of the composite sample shows excellent contrast between the nanofillers and the matrix. The images can be processed in software to gather information such as particle size, number density and degree of alignment, which is crucial to understanding the performance of the composite and guiding the nanostructuring for desired properties.

Experimental Details and Discussion

SEM Sample Preparation

For a composite that is reinforced by anisotropic fillers, 2D images of merely cross-section of the sample cannot tell everything. Especially in injection molded coupons, particles are forced to align in the flow direction while still confined by the sample geometry. In this research, an injection molded sample was prepared by sectioning in three directions: along the flow (0 degree), width (90 degree) and thickness (z) directions (Figure 2.1).

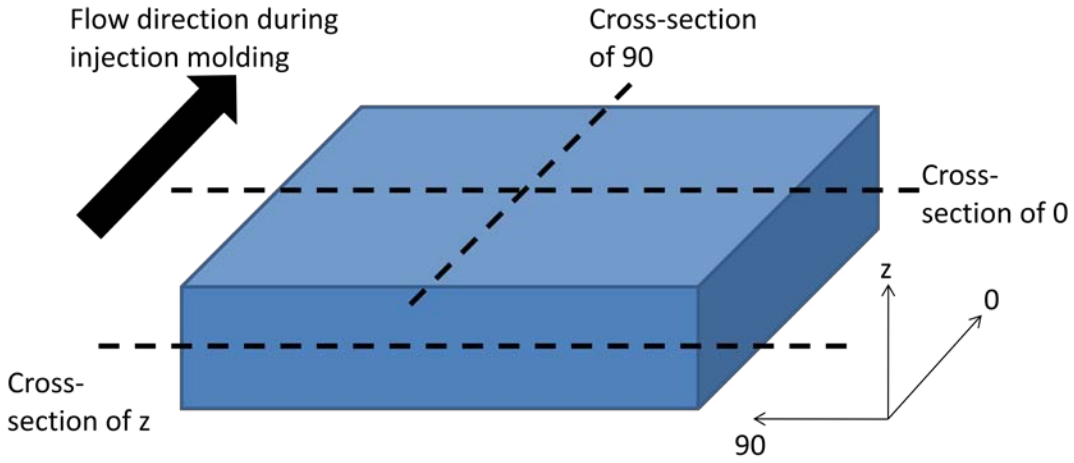

Figure 2.1, Sectioning injection molded coupon. Dash lines indicate the directions of sectioning (For interpretation of the references to color in this and all other figures, the reader is referred to the electronic version of this dissertation).

After sectioning, the to-be-observed surface was attached to an aluminum substrate by double-sided tape. A plastic ring holder was placed around the sample. An epoxy fixative agent was added into the holder and cured under room temperature. The sample-embedded epoxy puck was then polished by SiC polishing paper with finish

up to #4000 grit. This was followed by polishing with 1 micron and 0.05 micron alumina powder/water slurry.

The alumina powder/water polished sample has a very smooth surface with few polishing artifacts. However, it is not suitable for SEM observation since the contrast under SEM relies most on topographical differences i.e. height difference. In order to create height difference between the GNP particles and polymer matrix, O_2 plasma was applied to the polished surface. The sample was placed in a chamber with the polished surface facing up. The chamber was evacuated and then purged by O_2, which was ionized under a power source of 400 watts. The total time used for GNP/polymer composite was 1 hour. The polymer materials on the polished sample including the polymer matrix and the epoxy fixative are slowly removed as a result of the plasma etching while the GNP particles are mostly unaffected by the plasma due to its stable sp^2 structure. The effect of plasma etching on polished polyetherimide (PEId) surface is shown in Figure 2.2.

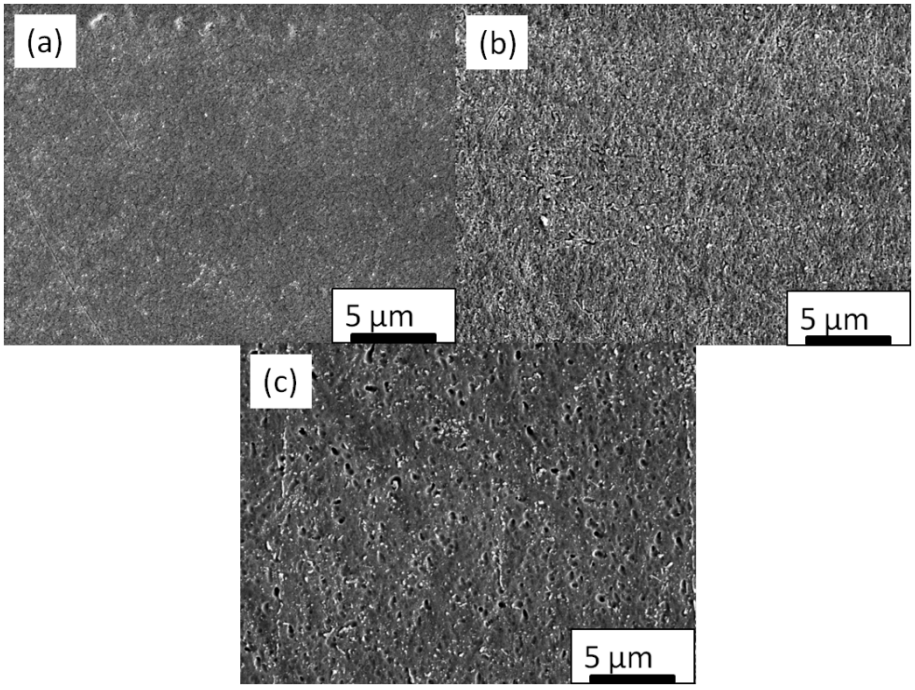

Figure 2.2, Neat polyetherimide surface under plasma etching: (a) no plasma, (b) 30 min plasma, (c) 90 min plasma.

If no plasma is applied, the polished surface shows a smooth morphology. After 30 min plasma treatment, the surface becomes rougher. After 90 min, many pores with features of a few hundred of nanometers appear on the surface. This indicates that the O_2 plasma is very effective at etching away polymer.

The comparison between SEM images taken from a fractured surface, a polished surface and a plasma etched surface is shown in Figure 2.3. Compared with un-etched surfaces, the plasma treated one shows the best contrast between GNP particles and the matrix. In Figure 2.3(c), the white lines stand for the cross-section of the GNP particles. The dark part is occupied by the matrix. On the fractured surface (Figure 2.3(a)), it is hard to distinguish GNP particles from the matrix due to the roughness of sample. Although polished surface can show some contrast, it is not as clear as the etched one, and a lot of smaller particles are invisible due to the

entrapment of polymer matrix (Figure 2.3(b)).

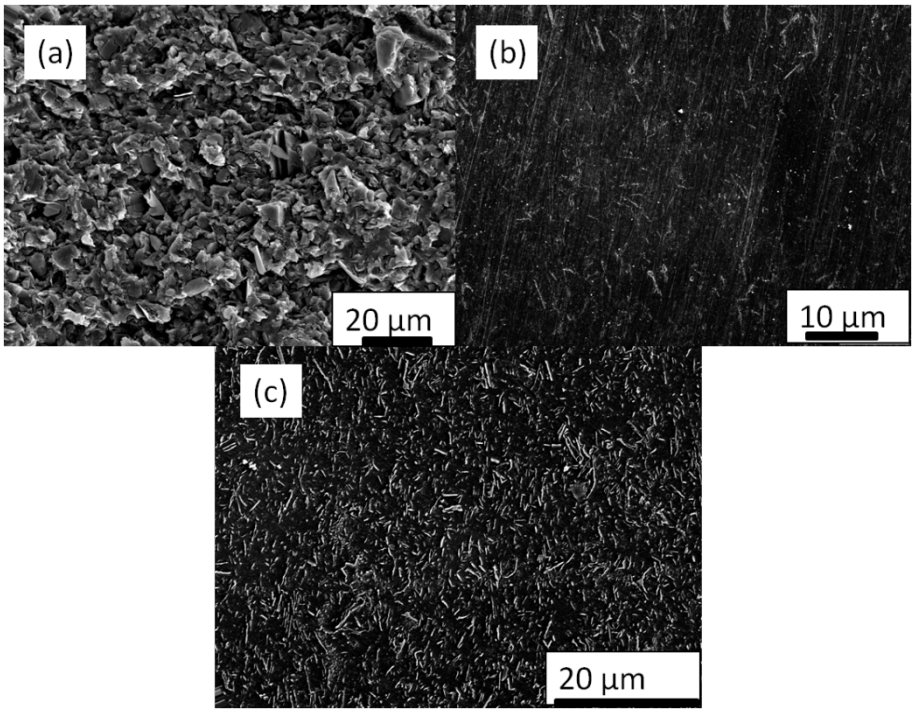

Figure 2.3, Comparison between fractured, polished, and plasma etched surfaces. Images were taken from 5wt% GNP/PEId composites: (a) fractured surface, (b) polished surface, (c) plasma etched surface

Kalaitzidou et al [6] developed a novel approach to fabricate GNP nanocomposites by coating the GNP particles onto a polymer powder surface (pre-coating process). After compression molding, the coated structure forms a continuous GNP phase and helps the electrical percolation. In their work a fractured surface was used to demonstrate the percolated structure. However, it is hard to interpret due to surface roughness. Figure 2.4 shows the comparison between the fractured surface adapted from literature [6] and the plasma etched surface for the sample made from the same process. While Figure 2.4(a) suffers from a mixed morphology of GNP particles and the roughness of the matrix, Figure 2.4(b) explicitly shows the continuous phase of the GNP (white lines).

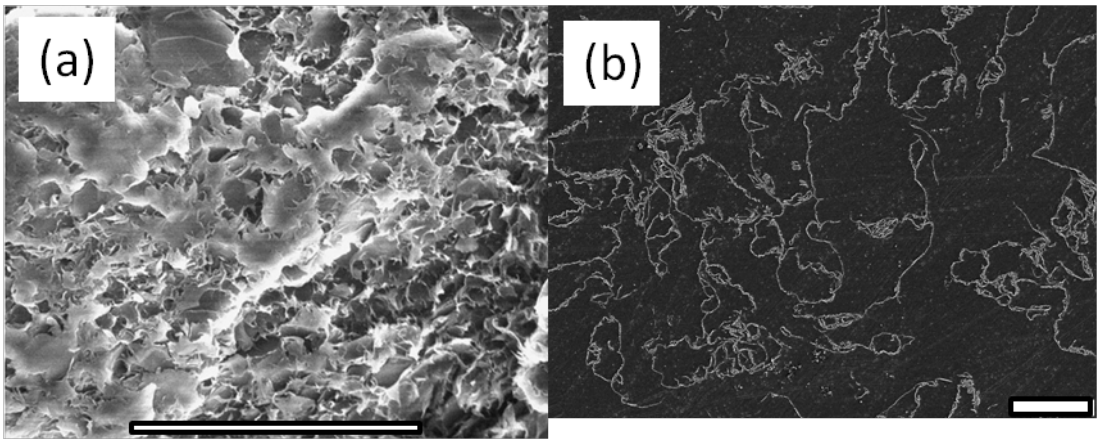

Figure 2.4, Comparison between fractured surface and plasma etched surface for pre-coated composite (a) fractured surface of GNP/PP, adapted from literature [6] and (b) plasma etched surface of GNP/PEId (scale bars: (a)150 micron, (b)20 micron)

Image Processing

Image-Pro Plus software (Media Cybernetics, Inc.) was used to gather information from the SEM images. This software is capable of distinguishing one phase from another based on the contrast of the image. In our image, the GNP phase always stands out from the matrix, resulting in bright (high intensity) spots surrounded by dark phase. Two properties of the particles are of extreme interest: the degree of alignment and the size. Figure 2.5 summarizes the type of information about the GNP particles obtained by the Image-Pro software.

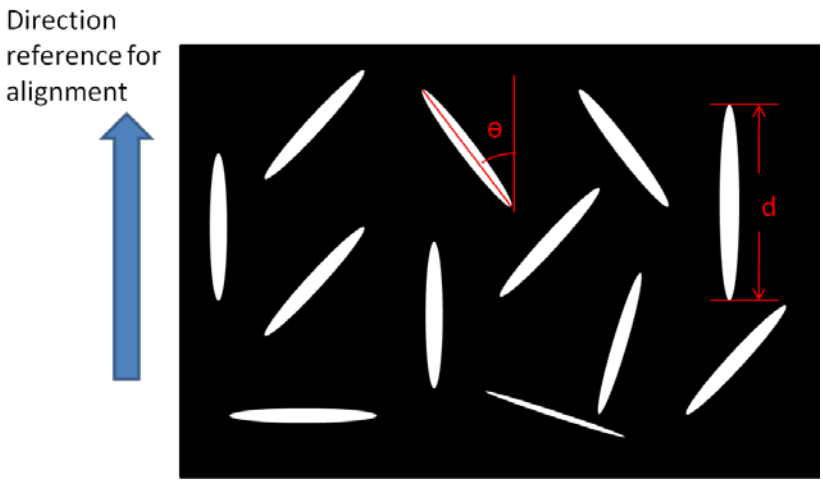

Figure 2.5, Schematics of image processing, white objects stand for the projection of GNP particles on the observed plane, θ is the angle between the length direction of the projection and the reference direction, d is the larger dimension of the projection. (For interpretation of the references to color in this and all other figures, the reader is referred to the electronic version of this dissertation)

Note that the thickness of GNP particles cannot be obtained from this kind of SEM images, because the projected thickness of the white object is actually the projection of part of the GNP basal plane, which is much larger than the real thickness of the platelet.

Getting good contrast makes it possible to process the images in the software. Figure 2.5 shows the schematics of gathering information from the SEM image. In this thesis, two properties are majorly of interest: the average size of the particle in the composite, and the degree of alignment. The size of an individual particle, d, can be calculated by the Image-Pro software by counting the pixels between the two ends of the largest dimension of the particle. The length that a pixel represents can be obtained by comparing it with the scale bar. Assuming every particle has the same thickness, the volume-weighted average size of the particles can be expressed as:

$$< d >= {\sum d_i^3}/{\sum d_i^2} \quad (1)$$

The direction of the projection of GNP particle on the observed plane can be represented by the angle (θ) between the projected radius and the reference direction. The degree of alignment is defined as:

$$a =< cos^2\theta > \quad (2)$$

Since the sample size for SEM can be relatively large, it is possible to survey the whole cross-section of a composite sample. An automated navigation stage can be used to move the SEM sample a few microns in a step and SEM images can be taken at each location. The information of interest, such as degree of orientation, can be plotted as a function of position for the entire sample (Figure 2.6).

Figure 2.6 shows the alignment situation ($a =< cos^2\theta >$) on the entire cross-section of an injection molded coupon. In practice, over 900 images were taken from one sample but not all the images were processed to get the a value. Due to its symmetric nature, only one quarter of the surface needs to be surveyed, e.g. from (0, 0) to (1500, 6300) in Figure 2.6, while the other portion can be mirrored.

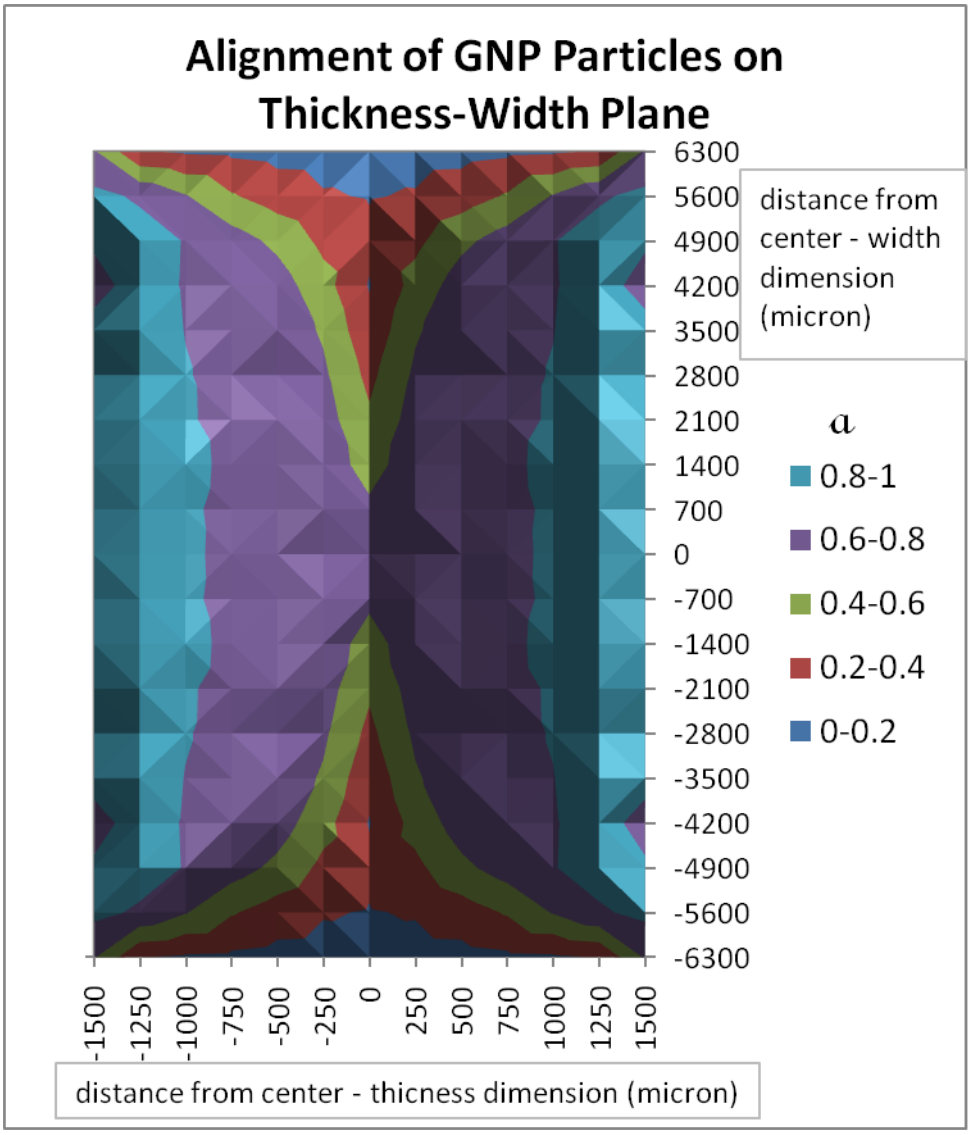

Figure 2.6, Degree of Alignment on the entire thickness-with plane (cross-section of 10wt% GNP-5/PEId injection molded coupon)

Fluorescent Imaging

Epoxy fixative is useful as a support during polishing. However, when a porous or crack-containing sample is to be observed, the epoxy can fill into the pores and compromise the results such as porosity one can get from image analysis. To solve this problem, a complementary fluorescent imaging approach is developed. During SEM sample preparation, the epoxy fixative was mixed with a fluorescent dye. After

polishing and plasma etching, the sample was first observed with a confocal microscope with a laser source. The well dispersed fluorescent dye molecules are excited by the laser beam and emit a fluorescence signal, which can be detected by the confocal microscope. By comparing with the SEM images, one can tell the original polymer matrix phase from the epoxy fixative phase.

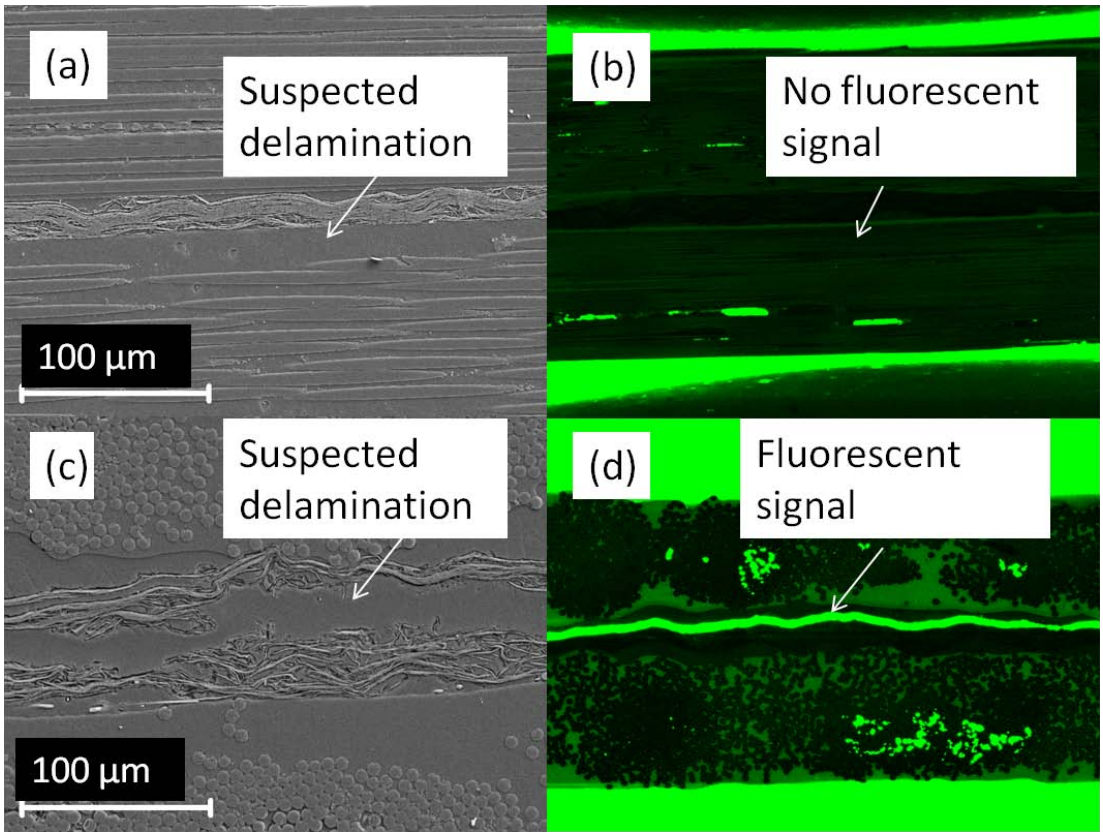

Figure 2.7, Comparison between SEM and fluorescent images. Images were taken from carbon fiber (CF)/GNP/epoxy composite with one layer of GNP in between of two layers of carbon fiber stacks (details available in Chapter 8)

In Figure 2.7(a), a polymer-rich region presents between the GNP layer and CF layer. However, in the corresponding fluorescent image (Figure 2.7(b)), no fluorescence signal is present at the same position. This indicates that the polymer is the matrix of the composite, not the epoxy fixative, so the sample is fully consolidated with no delamination. Meanwhile, Figure 2.7(c) shows a polymer-rich region inside the GNP

layer. The corresponding fluorescent image (Figure 2.7(d)) confirms that the material there is from the epoxy fixative because of the strong fluorescent signal.

Conclusions

The sectioning-polishing-O_2 plasma etching process is found to be very effective in revealing the morphology of the GNP/polymer nanocomposites. Artifact free images can be obtained by SEM imaging of the sample prepared in this way. As a result of the good contrast between nanofillers and the matrix, the image can be processed by Image-Pro software and information such as particle size and orientation can be gathered for further analysis. The complementary fluorescent image can identify the epoxy fixative material used in the sample preparation process and helps interpret the morphology of samples with internal porosity.

REFERENCES

REFERENCES

1. Kalaitzidou, K., H. Fukushima, and L.T. Drzal, *Mechanical properties and morphological characterization of exfoliated graphite-polypropylene nanocomposites.* Composites Part a-Applied Science and Manufacturing, 2007. **38**(7): p. 1675-1682.

2. Tang, W.Z., M.H. Santare, and S.G. Advani, *Melt processing and mechanical property characterization of multi-walled carbon nanotube/high density polyethylene (MWNT/HDPE) composite films.* Carbon, 2003. **41**(14): p. 2779-2785.

3. Giannelis, E.P., *Polymer-layered silicate nanocomposites: Synthesis, properties and applications.* Applied Organometallic Chemistry, 1998. **12**(10-11): p. 675-680.

4. Lan, T. and T.J. Pinnavaia, *CLAY-REINFORCED EPOXY NANOCOMPOSITES.* Chemistry of Materials, 1994. **6**(12): p. 2216-2219.

5. Ginic-Markovic, M., et al., *Synthesis of new polyaniline/nanotube composites using ultrasonically initiated emulsion polymerization.* Chemistry of Materials, 2006. **18**(26): p. 6258-6265.

6. Kalaitzidou, K., H. Fukushima, and L.T. Drzal, *A new compounding method for exfoliated graphite-polypropylene nanocomposites with enhanced flexural properties and lower percolation threshold.* Composites Science and Technology, 2007. **67**(10): p. 2045-2051.

Chapter 3 Effect of Molding and Annealing on Dispersion and Orientation on the Mechanical Properties and Electrical Conductivity of Graphene Nanoplatelet -Polyetherimide Composites

Abstract

In this research, exfoliated graphene nanoplatelets (GNP, ~10 nm thick and ~5 microns in diameter)) and Polyetherimide (PEId) were compounded via melt-extrusion in a Leistritz twin-screw extruder. Both injection molding and compression molding were used to fabricate GNP-PEId nanocomposites at various concentrations for measurement of their mechanical properties and electrical conductivity. It was found that the electrical percolation threshold of the composites processed by compression molding (<3wt%) was much lower than those made by injection molding (>10wt%). However, the composites that were made by injection molding showed higher modulus and strength. Scanning electron microscopy (SEM) investigation of the morphology found that injection molding led to higher GNP orientation, although the degree of orientation varied from the surface to the center

of the sample. Modification of the Annealing of the samples made by injection molding under the same temperature as during compression molding was found to increase the electrical conductivity with the annealing time. The largest improvement in electrical conductivity with annealing was in the through-plane direction (perpendicular to flow direction in injection molding). SEM images confirmed an increase in the random orientation of the GNP after annealing. Tandon-Wang equation with respect to the nanoparticle orientation resulted in good agreement with the experimental results.

Introduction

Polymer nanocomposites usually refer to a polymer matrix filled by high-surface-area reinforcing fillers [1] including carbon nanotubes (CNTs), carbon nanofibers, nanoclay, carbon black (CB), graphene platelets and so on. Since their discovery, nanoparticles were expected to function as substitute reinforcements for conventional reinforcement fibers because of the theoretically high particle properties and the significant improvement in nanocomposite properties attained at low loadings. Furthermore significant advantages were expected from gains in processing by eliminating the need for layer-by-layer assembly or autoclave processing. The functionality of the nanofillers is highly dependent on their morphology. For example, as conductive fillers, the zero-dimensional CB can improve composite electrical conductivity as a result of electrical percolation at low (~5%) loading for non-polar, low crystallinity thermoplastics [2], while high aspect ratio CNT filled composites with

a similar matrix have a percolation threshold of 0.1vol% [3]. The high aspect ratio and linear shape of CNTs make it easier to form a percolated network with more contacts being formed between filler particles. Two-dimensional (nano-platelet) fillers such as alumino-silicate nanoclay can also produce composites with low gas permeability which cannot be achieved by CNTs or CB because of the highly tortuous path formed by their two-dimensional nature [4, 5]. Research also suggests that this kind of filler can also be used to improve the fire retardancy of its composite [6].

Despite of the promising properties of CNTs, it is not advantageous to use them in commercial composites because of their expensive nature and limited availability. CB/rubber composites reached the expectation of the tire industry, and colloidal silica is showing a promising future in the same area [7]. However, these two fillers do not possess the excellent electrical properties as found in CNTs.

Graphene based nanoplatelet particles, which combine good electrical and thermal properties similar to CNTs and the two-dimensional morphology as alumino-silicate clays, are considered to be the excellent filler in terms of multifunctionality. The process of generating thin graphite platelets consisting of several layers of graphene sheets is relatively simple and cost-effective. Usually, three steps are involved in fabricating these nanofillers from natural graphite: (i) intercalation, where both electron-donor agents and electron acceptors can be intercalated in between graphene layers; (ii) exfoliation, where a large amount of heat is applied to expand the intercalated graphite through vaporization of the intercalant; (iii) pulverization, where the exfoliated graphite is reduced in size to smaller dimensions. As

demonstrated in Drzal's group [8], exfoliated graphite nanoplatelets (GNP) consisting of small stacks of graphene can be fabricated by acid intercalation, microwave heating and ultrasonication pulverization and be scaled inexpensively into quantity production by this route. The size and thickness of GNP is controllable during fabrication. Typical sizes of the platelets range from submicron to 25 microns in diameter usually notated as GNP-1, GNP-5 and GNP-15 where the number refers to the average statistical diameter with thicknesses in the 5-10 nm range.

Because of the two dimensional nature of GNP and its high aspect ratio, final properties of GNP based nanocomposites can vary due to the processing methods selected. For example, the molding processes are important for their ability to make complex shaped integrated composites. Kim et al [9] have shown that differences in electrical conductivity of polycarbonate/graphene composites can be attained depending on whether they were made by injection molding or compression molding. Compression molded samples showed much better electrical conductivity than injection molded ones. Mohanty et al [10] found that post-molding treatment, such as annealing after injection molding can provide better flexural modulus and strength and alter the morphology of nanocomposites and thus their properties. Dynamic percolation behavior of CB composites has been studied by Wu et al [11] who found that due to Brownian motion, CB particles are able to reposition themselves locally under high temperature during which the viscosity of the polymer matrix is low. Particles of platelet shape such as alumino-silicates and graphene, might not be subject to Brownian motion because of their larger dimensions. Researchers have

shown faster particle re-organization in layered alumino-silicate/polymer composites than expected compared to Brownian motion theory [12-14]. The real driving force might be the elastic restoring force of the polymeric matrix generated during processing though no widely-accepted conclusion has been drawn yet. Kim proposed a disorientation mechanism for graphene composites based on X-ray scattering and rheology data, pointing out that at low loadings (<3wt%) of graphite filler, the rotation experienced by the particles caused by annealing still cannot increase particle contact with each other, while at high loadings (>12wt%), the movement of filler particles is restricted due to excluded volume interactions between particles.

The purpose of this research is to understand the relationship between processing, morphology and properties of the GNP/polyetherimide (PEId) nanocomposites. PEId has a high glass transition temperature, extremely good chemical resistance and excellent thermal stability and is an amorphous thermoplastic material. Melt-extrusion in a twin-screw extruder was used to compound GNP and PEId pellets which were either injection molded or compression molded. Annealing under confinement at the molding temperature (340℃) was investigated for its effect on mechanical and electrical properties.

Experimentation

Materials

Polyetherimide (PEId, Ultem 1010) was provided by Sabic Americas, Inc. (Houston,

TX). GNP-5 was provided by XG Sciences, Inc. (East Lansing, MI) with an average diameter of 3.9 micron and a specific surface area of 40m^2/g.

Melt-extrusion

Melt-extrusion was carried on a Leistritz co-rotating twin-screw extruder (MIC27/6L-48D). Barrel temperatures were set to 310C with a melt temperature at 340C. The die pressure was ~5.5MPa. Screw speed was set at 150 rpm.

Molding

After extrusion compounding, part of the composite material was compression molded in a CARVER Laboratory Press (Model 2731, Fred S. Carver Inc.). A picture-frame mold was used with a dimension of 76mm × 76mm × 3.3mm. The material was heated up to 340C and held for 15 min. A compression pressure of 20MPa was applied to the material and was held for 15 min. After that, the press was cooled with water. The other part of the composite material was injection molded with a Milacron VSX 85-4.44 (Cincinnati, OH) injection molder with a Master Precision tensile coupon die (Series No. 24157, Greenville, MI). The melt pressure during injection molding was 90MPa. The central part of the injection molded tensile bars were cut into a 12.7mm by 12.7mm square and annealed in a mold of the same size under a pressure of 23MPa at 340C for 1 hour.

Characterization

The resistance of GNP/PEId composites was measured in two directions: the 'through-plane direction' which through the coupon thickness and was the same direction as the applied pressure in compression molding while the 'in-plane direction' which in the direction of flow in the injection molded coupon and was perpendicular to the pressure in the compression molded coupon. The resistance value was then converted into resistivity by taking into account the sample dimensions. Flexural strength and modulus were tested under ASTM 790 standard on a UTS SFM-20 machine (United Calibration Corp.) at room temperature. The test was performed at a flexural rate of 0.03 in/min. according to ASTM 790 standard, the sample strain should not exceed 5% during flexural test, so the strength value was calculated from the force at 5% strain if the sample hadn't failed before that. Tensile strength and modulus were tested under ASTM D638 with a straining rate of 0.02 in/min.

The morphology of the nanocomposites was observed by Scanning Electron Microscope (JSM-6400, Jeol, Tokyo, Japan). In order to investigate the distribution and orientation of the fillers, the tensile bar coupons were cut along as well as perpendicular to the material flow direction as in injection molding and put into an epoxy holder to undergo a series of polishing steps. Oxygen plasma was used after the final polishing to etch away a layer of polymer in order to expose the GNP particle. The polished surface was then sputter coated with gold.

Results and Discussions

Compression molding

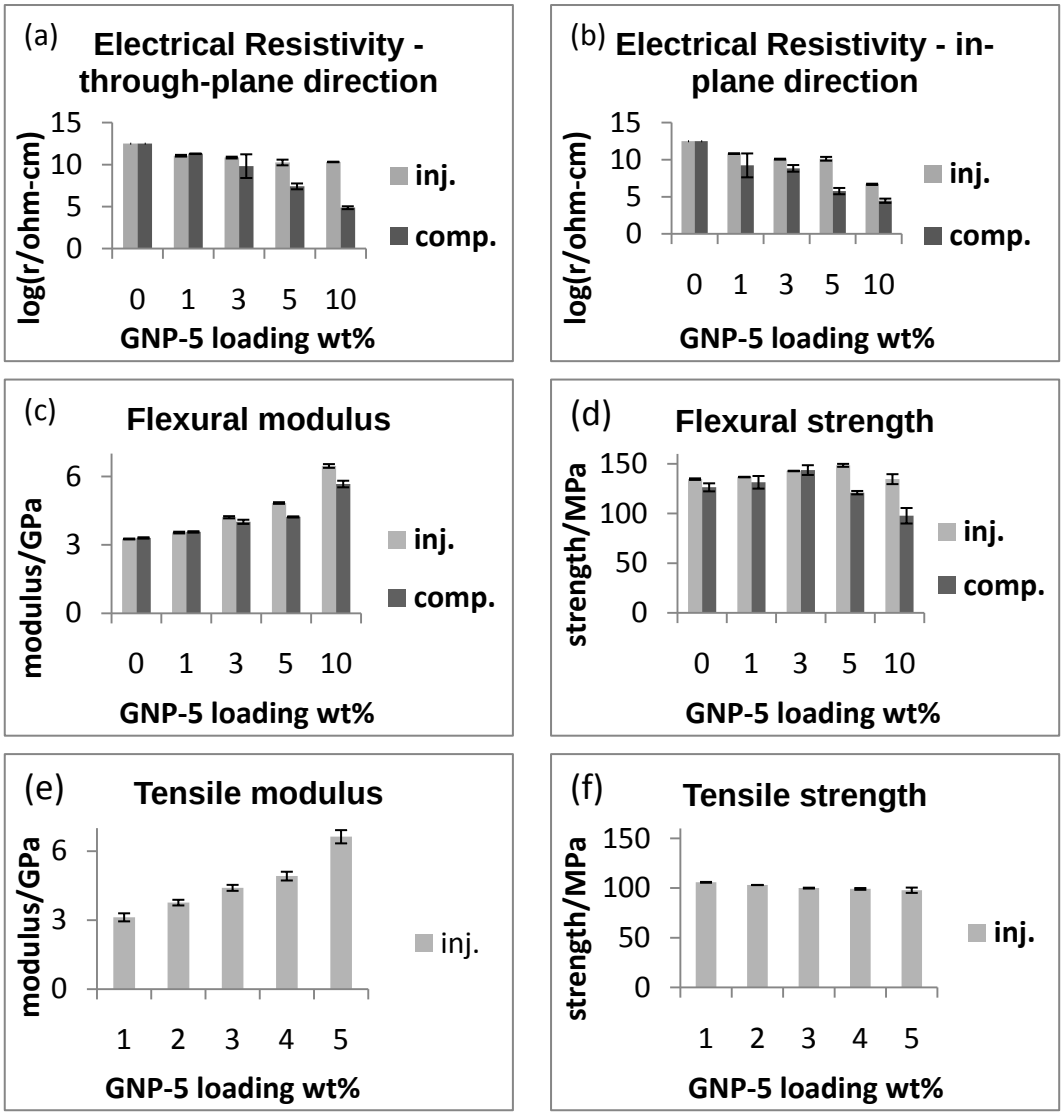

Figure 3.1, Comparison between GNP-5/PEId composites made from injection molding and compression molding

The flexural modulus and strength and electrical resistivity of the GNP-5/PEId composites made from compression molding are shown in Figure 3.1. It is found that

the electrical percolation threshold is around 3wt% for the through-plane direction and 1 wt% for the in-plane direction. This is the results of the GNP particles having a slightly preferential alignment direction because of the compressive force during molding as shown in Figure 3.2(a). The flexural modulus of the composites is increased with an increase of GNP content. At 10wt% loading, a 70% improvement of modulus is observed. For flexural strength, an increase is seen with the GNP content up to 3wt%, while a decrease is recorded afterwards. Interestingly, 3wt% loading is around the electrical percolation threshold of the composites, suggesting the forming of a continuous filler phase is producing strength reducing defects in the composite.

Injection molding

The orientation of the GNP particles in the injection molded coupons is much more complicated because of the material flow and the walls of the mold. The injection molded coupons show anisotropic behavior due to material flow. GNP orientation should be present at in two cross-sections: one surface perpendicular to the flow direction and the other one along the flow direction (Figures 3.2 (b) and (c)). In Figure 3.2(b), different orientations of the GNP particles can be seen at different position of the cross-section. The portion of the samplethat is close to the wall has almost perfect orientation parallel to it, while a change of orientation can be observed at the corner. As the distance between the particle and the wall increase, the GNP particle undergoes less orientation. This is because viscous melt of the

composite has the highest shear rate at the wall and the lowest at the center of the coupon.

The orientation of the filler particles leads to differences in the mechanical behavior between the compression and injection molded samples. In Figure 3.1 (c), the modulus of the GNP-5/PEId composites made from injection molding is higher than the ones made from compression molding. At 10wt%, the modulus is improved by 100% as compared to the neat polymer. The strength of the injection molded coupons increases steadily with the increase of GNP loading up to 5wt% while at 10wt% it remains constant at the same level as the neat polymer. For tensile modulus, the same trend is observed as flexural modulus, while tensile strength drops steadily with the increase of the filler loading.

The electrical resistivity of the injection molded samples is much higher than the compression molded ones. It is found that in the through-plane direction, the GNP particles do not percolate even at 10wt% loading. For the in-plane direction, the 10wt% sample shows percolated behavior, but the resistivity is two orders of magnitude higher than its compression molded counterpart.

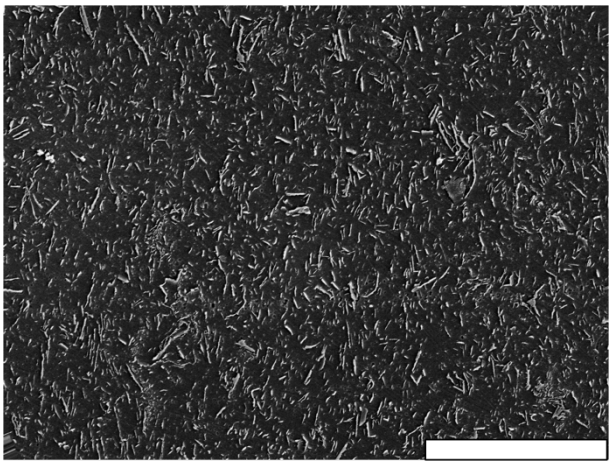

(a)

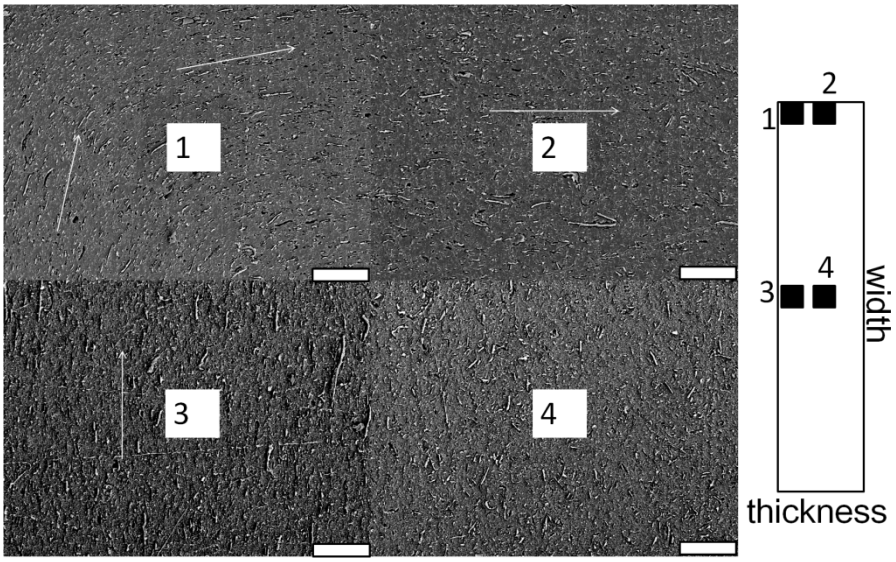

(b)

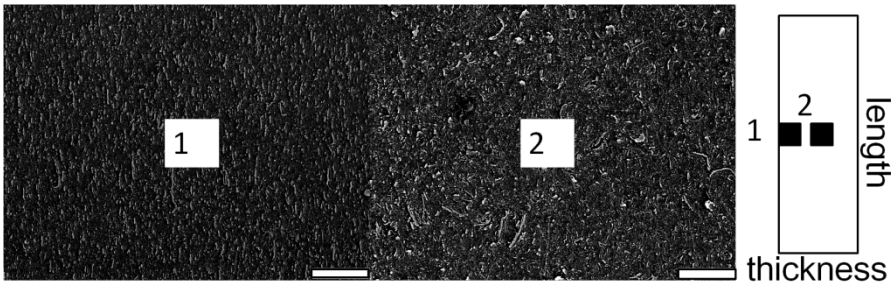

(c)

Figure 3.2, Orientation of GNPGNP particles observed on: (a) cross-section of a compression molded coupon; (b) the cross-section of an injection molded coupon perpendicular to the flow direction & (c) along the flow direction (the scale bars represent 20 micron)

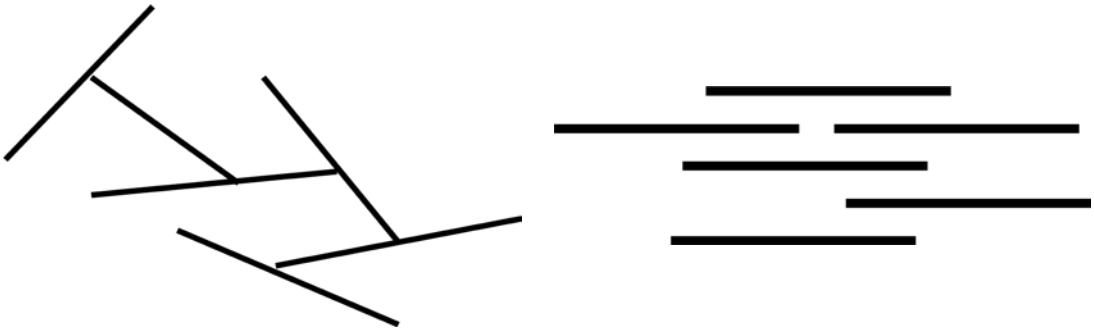

(a) (b)

Figure 3.3, Schematics of alignment situation of GNP particles in PEId matrix: (a) random orientation after compression molding, (b) aligned orientation after injection molding

As shown in Figure 3.3(a), the particles are randomly oriented. The connection between particles is good. However, in Figure 3.3(b), most of the particles are aligned. The alignment not only prevents the particles from connecting with each other in the through-plane direction, but also places the particles apart in the in-plane direction.

Model prediction of modulus

Because of the complicated orientation situation of GNP/PEId composites, it's not easy to predict their mechanical behavior. Figure 3.4 shows the calculated modulus value of the composites using the Tandon-Weng equation [15].

$$\frac{E_{11}}{E_m} = \frac{1}{1+\phi(-2\upsilon_m A_3+(1-\upsilon_m)A_4+(1+\upsilon_m)A_5 A)/2A} \quad (1)$$

In equation (1), E_{11}, E_m are the Young's modulus of the composite and neat matrix polymer, respectively. ϕ is the volume fraction of the filler. υ_m is the Poisson's ratio of the matrix. A and A_i are functions of ϕ, U_m and Eshelby's tensor. Tandon and Weng gave formulas for both uni-directional and randomly oriented [16]

situations. The values of the parameters used in the equation are listed in Table 3.1.

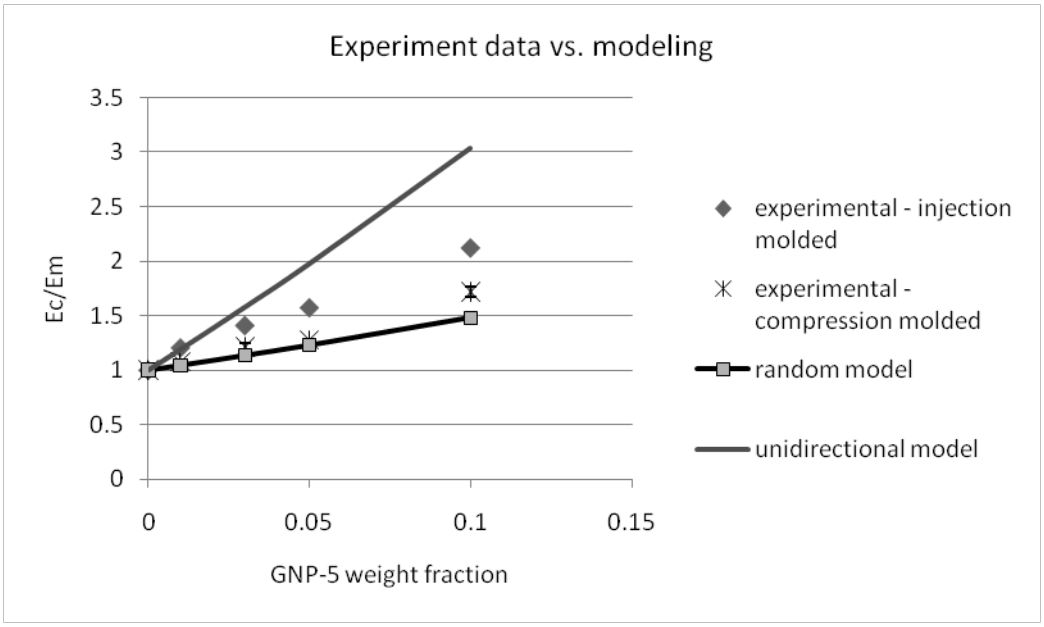

Figure 3.4, Comparison between experimental data (tensile modulus of injection molded samples and flexural modulus of compression molded samples) and Tandon-Weng modeling

Although the reported Poisson's Ratio in literature varies from -0.171 to 4.958, the predicted modulus does not vary significantly using different values due to the small thickness of GNP particles. 0.006 was chosen in model calculation. The aspect ratio of the GNP particles after processing can be determined by the following equation [9]:

$$A_f = \frac{3\phi_{sphere}}{2\phi_{platelet}} \quad (2)$$

Where $\phi_{\text{sphere}} = 0.29$ which is the percolation threshold of spherical-shaped conductive fillers [17]. From Figure 3.1 (a) (b), the electrical percolation takes place around 1wt% for the in-plane direction and 3wt% for the through-plane direction. From equation (2), the actual aspect ratio of the GNP particles should be between 23 and 71. The average value 47 is used in the model.

Interestingly, if we consider the surface area of the GNP prior to processing and the average size of the particles, the expected aspect ratio should be around 300. However, during melt-extrusion, these platelet-shaped particles are reduced in lateral dimension because of the mechanical shearing of the twin-screws,. (Figure 3.4)

From TEM images, a stack of GNP usually contains ~3-5 layers (each layer is a GNP particle consisting of a few graphene sheets with a thickness of ~10nm) with a thickness varying from 30 to 80 nm. The SEM images show an average diameter of GNP particles after processing as 2 micron, which means the aspect ratio of the particles is between 25 and 67. This result is consistent with the result calculated from equation (2).

In Figure 3.4, the random platelet orientation Tandon-Weng equation predictions of the compression molded GNP/PEId composites agree very well at loadings up to 5wt%. However, at 10wt%, the experimental data is higher than predicted. This is because at 10wt%, the distance between particles is very small, resulting in a reduction in the ability of the platelet particles to freely rotate during molding.

Table 3.1, Parameters used in Tandon-Weng equation

Component	Modulus (GPa)	Poisson's Ratio	Density (g/cm^3)
GNP	1060	-0.171~4.958[18]	2.1
PEId	3.3	0.36	1.29

However, for injection molded samples, neither random nor unidirectional model accurately predicts the observed behavior, indicating that a complicated orientation state exists in these samples. To simplify the problem, we only analyze the orientation along the flow direction which is also the direction of tensile testing.

From Figure 3.2(c), the particles close to the surface of the sample tend to orient in the flow direction while the ones at the center of the coupon tend to be randomly oriented. This phenomenon suggests a combination of the unidirectional model and the random model. If we divide the sample coupon into two regions, one considered as unidirectional and the other random, then the modulus of the sample can be expressed as:

$$\frac{E_{11}}{E_m} = x\frac{E_{11,unidirectional}}{E_m} + (1-x)\frac{E_{11,random}}{E_m} \quad (3)$$

where x stands for the volume ratio of unidirectional region. By fitting equation (3) with the experimental data, the values of x at different loadings can be found. (Table 3.2)

Table 3.2, Fit values of the volume ratio of unidirectional region in injection molded coupons

GNP loading	1wt%	3wt^	5wt%	10wt%
x	1	0.62	0.46	0.41

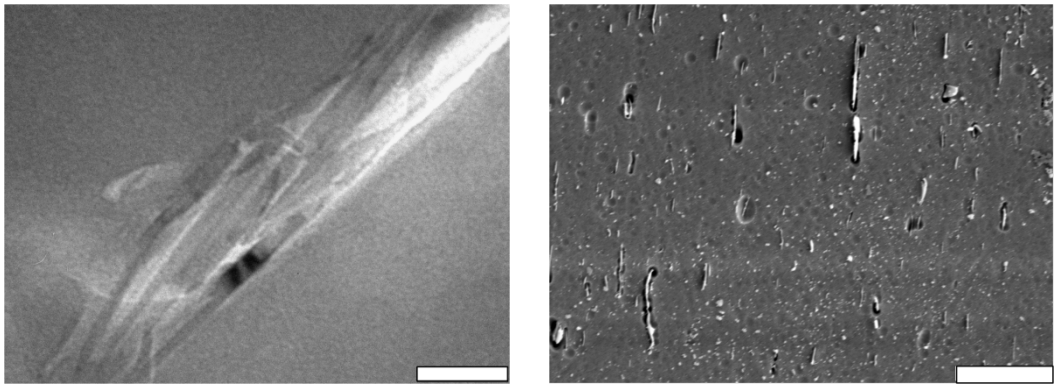

(a) (b)

Figure 3.5, (a) TEM image of GNP particle in PEId matrix after melt-extrusion, showing stacking of layers & (b) SEM image of 1wt% GNP-5/PEId composite made from melt-extrusion, showing reduced particle size (original average size: 3.9 micron in diameter). (scale bars: (a) 50 nm, (b) 5 micron)

To verify this approach, SEM images were taken at the cross-section of flow direction from edge to center (sample thickness: 3.3mm). The SEM images were processed in Image-Pro Plus software (Media Cybernetics, Inc., MD) to calculate the orientation information, a_{11} of the particles:

$$a_{11} =< cos^2\theta > \quad (4)$$

where θ is the angle between the GNP basal plane and the flow direction.

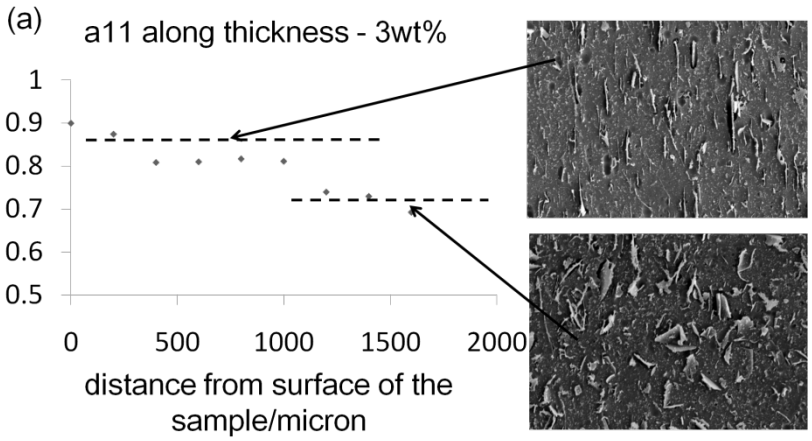

(a)

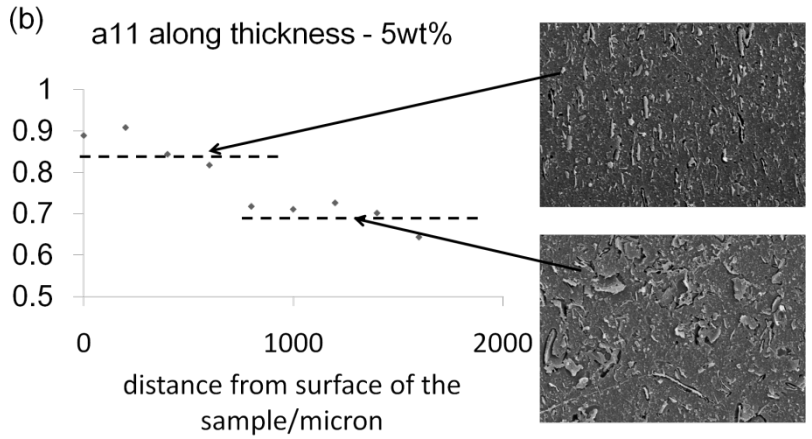

(b)

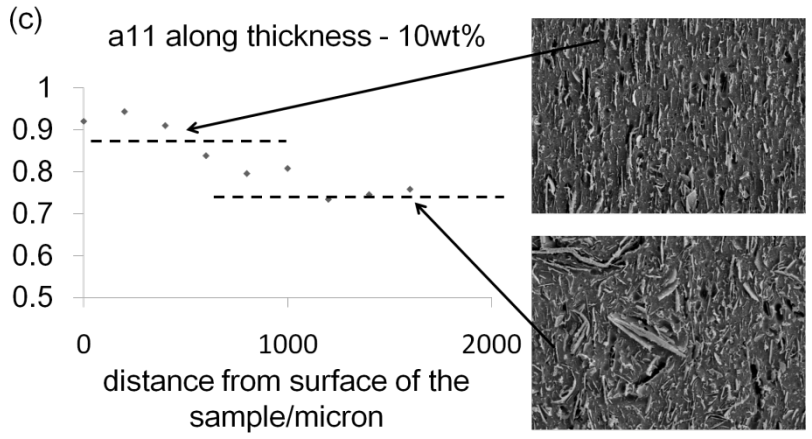

(c)

Figure 3.6, a11 along the thickness direction on the cross-section plane of flow direction (diamond series are a11 values and dash lines indicate the distinguish of two regions) and the representative morphology

Figure 3.6 shows the change of degree of orientation from the surface to the center of the sample. Although none of the points reaches the extreme value for either unidirectional ($a_{11} = 1$) or completely random ($a_{11} = 1/3$), it is clear that the sample can be split into two parts with different levels of orientation. Moreover, for the 3wt% sample, the transition from high to low orientation occurs between 1mm and 1.2mm, indicating the volume ratio of the unidirectional region to be 0.61~0.73. The same procedure can be applied to 5wt% and 10wt% samples, where the volume ratios are 0.36~0.48 and 0.24~0.48 respectively. This result correlates well with the computed values as shown in Table 3.1.

Effect of annealing

It has been shown that the percolation behavior of nanocomposites filled with conductive nanoparticles is influenced by annealing under high temperature (above the melt temperature of the matrix polymer). Similarly during annealing, GNP particles are able to reorient due to polymer chain relaxation and elastic restoring force [12].

From Figure 3.7, the electrical resistivity in the through-plane direction decreases significantly after annealing. The 5wt% GNP-5/PEId composite displays percolation. In the in-plane direction, the decrease in electrical resistivity is less than in the through-plane direction, but is significant. A 1.5 order of magnitude decrease is attained for the 5wt% loading and a 2.5 order of magnitude decrease for the 10wt% loading.

SEM images of the composites taken both before and after annealing document the GNP re-orientation. Figure 3.8 shows the morphology comparison between the composites before and after annealing. It is found that the area that is close to the surface of the tensile bar has a higher degree of orientation (Figure 3.8(a)). However, after annealing, the highly aligned orientation is destroyed as shown in Figure 3.8 (b). As discussed earlier, less oriented particles have a better chance to connect with each other (Figure 3.3) and therefore provide path for electrical conductivity. The fact that the decrease of resistivity in the through-plane direction is larger than that in the in-plane direction indicates that the movement of the particles does not result in their aggregation in the flow direction. The particles rotate at the original position rather than move along the flow direction.

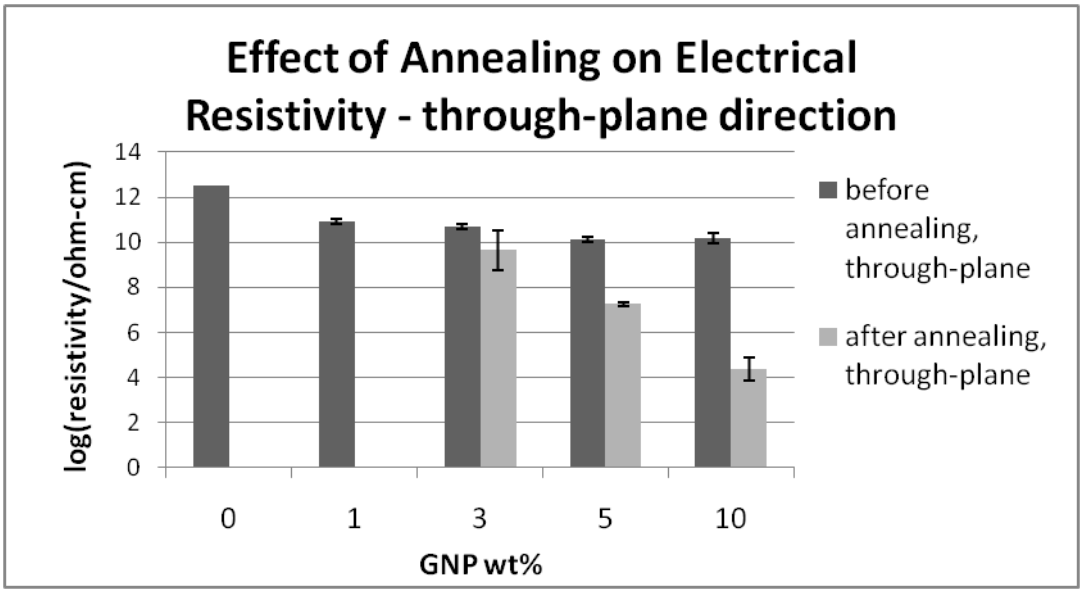

(a)

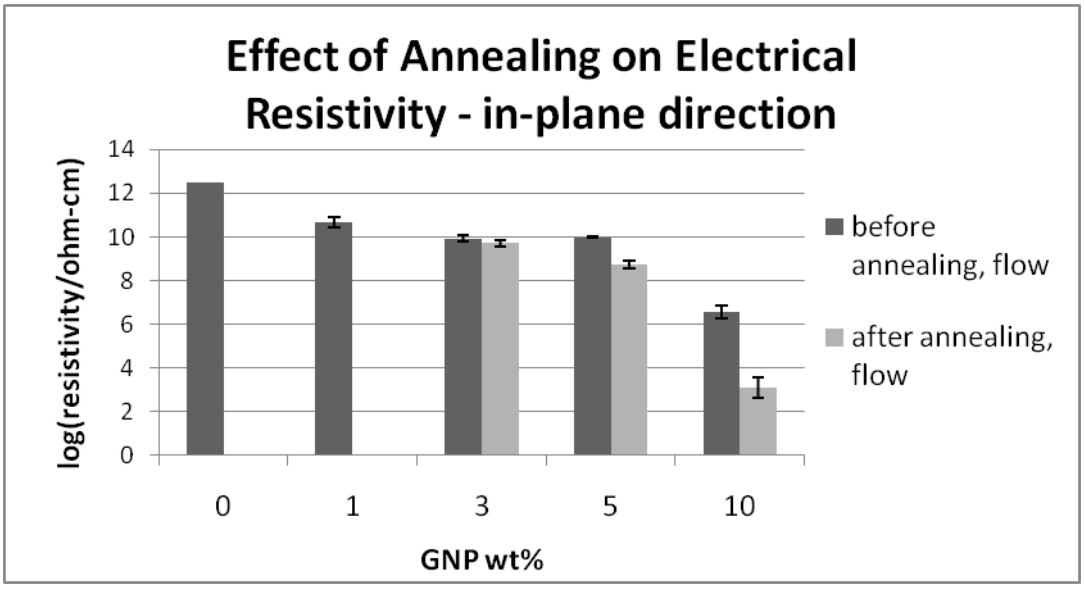

(b)

Figure 3.7, Effect of annealing on electrical resistivity

Figure 3.9 shows the change of electrical resistivity of GNP/PEId composites along with the annealing time. For the 5wt% sample, the minimum time for the effect of annealing to affect the percolation point is between 40 and 60 minutes. For the 10wt% sample, the time is around 10 minutes. With higher GNP loadings, the annealing percolation time decreases. This is due to the smaller distance between GNP

particles in the composites as the concentration increases. Composites with higher loadings of GNP have a shorter distance between particles, requiring less movement of the particles to make contact with each other.

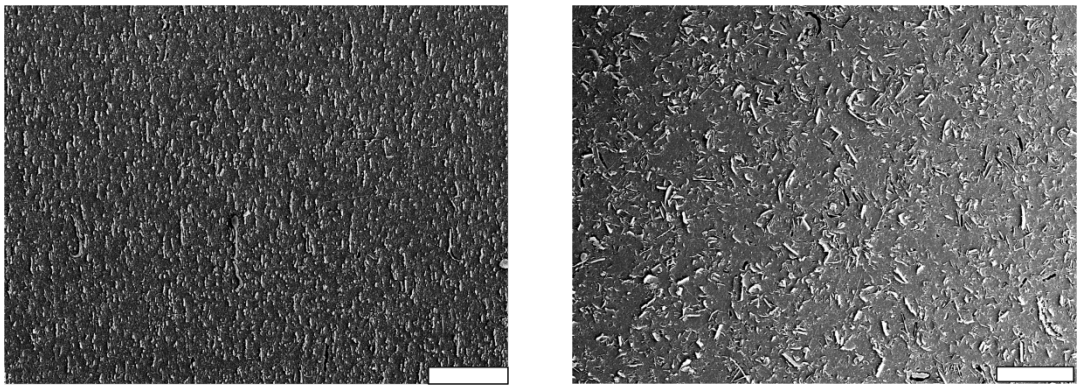

(a) (b)

Figure 3.8, 5wt% GNP-5/PEId composite (a) before annealing and (b) after annealing. Images were taken along the flow direction (as during injection molding), showing the morphology of the near-surface part of the tensile bar coupon (scale bars represent 20 micron)

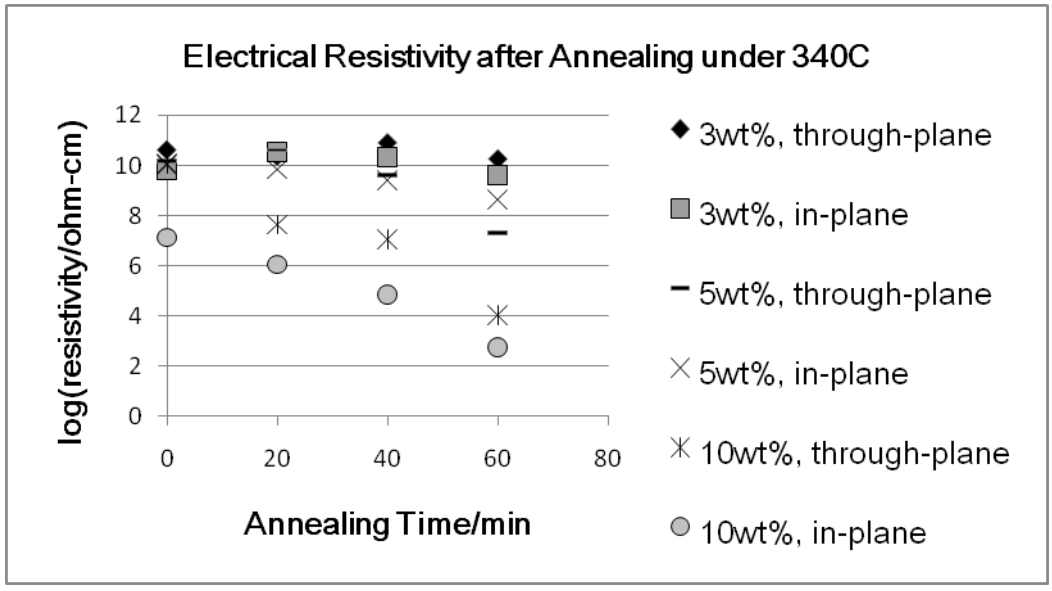

Figure 3.9, Time dependence of the annealing effect

Conclusions

GNP and PEId were compounded by melt-extrusion followed by either injection molding or compression molding. It was found that injection molding leads to better mechanical properties while compression molding results in better electrical conductivity. When the Tandon-Weng equation was applied to predict the modulus of the samples, it was found that the random particle orientation Tandon-Weng equation fits compression molded samples well while a hybrid combination of unidirectional and random model best explains the behavior of injection molded samples. Annealing is found to be effective in overcoming the orientation effects caused by molding and leads to higher electrical conductivity of the GNP/PEId composites as a result of the rotation of GNP particles during the high temperature annealing treatment. SEM images of GNP morphology in the molded coupons confirm the nanoplatelet orientation and annealing effects and support these conclusions.

REFERENCES

REFERENCES

1. Vaia, R.A. and E.P. Giannelis, *Polymer nanocomposites: Status and opportunities.* Mrs Bulletin, 2001. **26**(5): p. 394-401.

2. Huang, J.C., *Carbon black filled conducting polymers and polymer blends.* Advances in Polymer Technology, 2002. **21**(4): p. 299-313.

3. Bauhofer, W. and J.Z. Kovacs, *A review and analysis of electrical percolation in carbon nanotube polymer composites.* Composites Science and Technology, 2009. **69**(10): p. 1486-1498.

4. LeBaron, P.C., Z. Wang, and T.J. Pinnavaia, *Polymer-layered silicate nanocomposites: an overview.* Applied Clay Science, 1999. **15**(1-2): p. 11-29.

5. Kim, J.K., et al., *Moisture barrier characteristics of organoclay-epoxy nanocomposites.* Composites Science and Technology, 2005. **65**(5): p. 805-813.

6. Porter, D., E. Metcalfe, and M.J.K. Thomas, *Nanocomposite fire retardants - A review.* Fire and Materials, 2000. **24**(1): p. 45-52.

7. Schaefer, D.W. and R.S. Justice, *How nano are nanocomposites?* Macromolecules, 2007. **40**(24): p. 8501-8517.

8. Fukushima, H., *Graphite Nanoreinforcements in Polymer Nanocomposites*, in *Department of Chemical Engineering and Materials Science*. 2003, Michigan State University: East Lansing.

9. Kim, H. and C.W. Macosko, *Processing-property relationships of polycarbonate/graphene composites.* Polymer, 2009. **50**(15): p. 3797-3809.

10. Mohanty, A.K., et al., *Effect of process engineering on the performance of natural fiber reinforced cellulose acetate biocomposites.* Composites Part a-Applied Science and Manufacturing, 2004. **35**(3): p. 363-370.

11. Wu, G.Z., et al., *A delay of percolation time in carbon-black-filled conductive polymer composites.* Journal of Applied Physics, 2000. **88**(3): p. 1480-1487.

12. Schmidt, G., et al., *Shear orientation of viscoelastic polymer-clay solutions probed by flow birefringence and SANS.* Macromolecules, 2000. **33**(20): p. 7219-7222.

13. Solomon, M.J., et al., *Rheology of polypropylene/clay hybrid materials.* Macromolecules, 2001. **34**(6): p. 1864-1872.

14. Ren, J.X., et al., *Disorientation kinetics of aligned polymer layered silicate nanocomposites.* Macromolecules, 2003. **36**(11): p. 4188-4194.

15. Tandon, G.P. and G.J. Weng, *THE EFFECT OF ASPECT RATIO OF INCLUSIONS ON THE ELASTIC PROPERTIES OF UNIDIRECTIONALLY ALIGNED COMPOSITES.* Polymer Composites, 1984. **5**(4): p. 327-333.

16. Tandon, G.P. and G.J. Weng, *AVERAGE STRESS IN THE MATRIX AND EFFECTIVE MODULI OF RANDOMLY ORIENTED COMPOSITES.* Composites Science and Technology, 1986. **27**(2): p. 111-132.

17. Shante, V.K.S. and Kirkpatr.S, *INTRODUCTION TO PERCOLATION THEORY.* Advances in Physics, 1971. **20**(85): p. 325-&.

18. Cho, J., J.J. Luo, and I.M. Daniel, *Mechanical characterization of graphite/epoxy nanocomposites by multi-scale analysis.* Composites Science and Technology, 2007. **67**(11-12): p. 2399-2407.

Chapter 4 Effect of Graphite Nanoplatelets on Coefficient of Thermal Expansion of Polyetherimide Composite

Abstract

Thermal expansion is one of the major concerns for polymer composites. In this research, graphite nanoplatelets (GNPs) was added to polyetherimide (PEId) thermoplastic polymer in order to reduce the coefficient of thermal expansion (CTE) of the injection molded composite. First, the coefficient of linear thermal expansion (LTE) was measured in three directions in the anisotropic coupon: 0 degree, 90 degree and the out of plane Z direction. It is found that the GNP particles are very effective in terms of reducing the LTE in 0 degree direction due to high degree of alignment. After annealing above glass transition temperature, significant increase of 0 degree LTE and decrease of Z degree LTE were observed. The bulk CTE was calculated by adding up the LTEs in all three directions and is found to be independent of annealing. Second, several models were applied to predict both CTE and LTE. It is found that Schapery's lower limit model fits the experimental CTE very well. Chow's model was applied for LTEs in three directions. The behavior of GNP-5/PEId composites is explained by the combination of Chow's model and

morphology obtained by scanning electron microscope (SEM).

Introduction

Thermoplastic materials are receiving more and more attention as the matrix to host either continuous fibers or nano-scale particles. Compared to thermoset polymers, thermoplastics are generally tougher and more resistant to chemical decomposition [1]. Moreover, thermoplastics can be processed much faster than thermosets which require a dedicated curing cycle. The thermoplastics also have a much longer shelf life. However, a key factor that has been bothering the thermoset matrices is still not solved by switching to thermoplastics: the expansion and contraction of the polymer due to change in temperature. If used as a structural material, the dimensional change of the polymer due to cyclical (season or location) changes may cause serious deformation. In a composite consisting of continuous fibers, the difference in the coefficient of thermal expansion (CTE) between fiber and matrix would result in significant residual stress in the composite [2-5] which will generate defects [6, 7] and affect matrix-dominated properties such as moisture absorption [8] and glass transition temperature [9].

Many efforts have been made to reduce the CTE of a thermoplastic system. Nano fillers such as carbon nanotubes (CNTs) [10-13], nano clay [14-17] and nano graphite [18] are mostly used in such applications. Although the difference in CTE still exists for nano fillers as compared with their matrices [19], the extremely small size of the filler minimizes the damage especially when the filler is homogeneously dispersed.

Warrier et al [10] incorporated CNTs into carbon fiber (CF)/epoxy composite and succeeded in increasing the glass transition temperature and reducing the CTE, indicating the effectiveness of using nano fillers to minimize the residual stress in a fiber reinforced composite. Similar results are also seen in the work in the Drzal group [Toshiya Kamae, unpublished results].

Nano clay is the most popular filler for reducing CTE of the composites. Gu et al [16] reported a 65% reduction in CTE by adding 3wt% organomontmorillonite in polyimide by a special processing route. This reduction is huge compared to other results [15, 17] where a reduction around 10% is normally found for the same loading. However, the major contributor in Gu's work is the thermal imidization of the matrix instead of the clay. For CNT, the influence is smaller. A 2% reduction is found in 3wt% CNT/epoxy system [11].

A newly-developed nano filler, graphite nanoplatelet (GNP) has already shown great potential to reduce the CTE in the composites. With the same 2D geometry, the GNP can provide a reduction in the CTE of its composite comparable to nano clay. Kalaitzidou et al [18] reported a 25% reduction for 3vol% GNP filled polypropylene. Moreover, the GNP also possesses high thermal and electrical conductivity and can be produced by a scalable, cost-effective process [20], making it the ideal filler for multifunctional composites.

PEId is an engineering thermoplastic that has unique flame-resistance properties and would only generate a very small amount of low density gas when forced to burn, making it well suited and widely used in airplane, aerospace, submarine and

high-floor building applications. However, these applications may also involve dramatic ambient temperature change, which would benefit from a lower CTE. The need of using continuous CF in PEId matrix also would benefit from a reduction in the transverse CTE as a result of adding GNP to the GNP/PEId composite. In this research, the linear coefficient of thermal expansion (LTE) is investigated in injection molded GNP/PEId composites in three dimensions: 0 degree (flow direction), 90 degree and the out-of-plane Z direction. The CTE of the thermally annealed samples are also measured. In addition, models for both LTE and CTE are applied according to the morphology of the GNP/PEId composites.

Experimentation

Materials

Polyetherimide (PEI) was obtained from Sabic-IP (Ultem 1010). GNP-5 (5 micron average diameter, 40m^2/g surface area) was provided by XG-Science Inc. (Lansing, MI).

Melt-extrusion

GNP and PEId were blended by melt-extrusion in a Leistritz twin-screw extruder (MIC27/6L-48D). The screws were operated in the co-rotation setup. Barrel temperatures were set to 310℃, with a melt temperature at 340℃. The die pressure was at around 5.5MPa. Screw speed was set at 150 rpm.

Injection Molding

The composite material was injection molded by a Milacron VSX 85-4.44 (Cincinnati, OH) injection molder with a Master Precision tensile coupon (Type I dog bone) die (Series No. 24157, Greenville, MI). The melt pressure during injection molding was 90MPa.

Coefficient of Thermal Expansion

The CTE of the GNP/PEId composites was measured by Thermal Mechanical Analyzer (TMA, TA Instruments). The central portion was cut from the injection molded tensile coupon. The LTEs were measured under a 10℃/min heating rate on TMA. Three dimensions including 0 degree, 90 degree and Z direction (Figure 4.1) were measured. The CTE was calculated by combining the three LTEs for an individual sample.

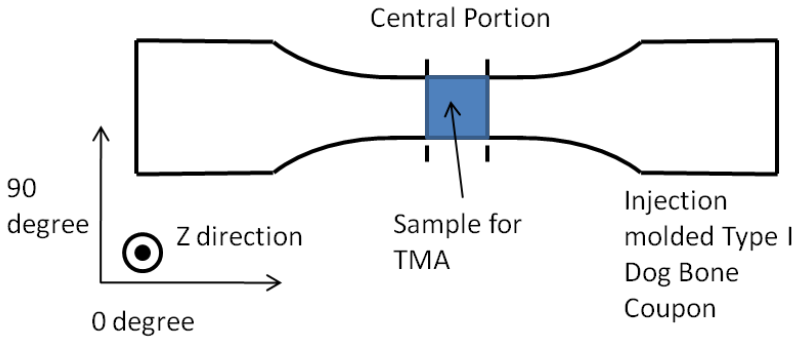

Figure 4.1, Schematics of TMA sample preparation

Annealing

The injection molded samples were annealed in a CARVER Laboratory Press (Model 2731, Fred S. Carver INC.) under 340℃ and 23 MPa. A steel picture-frame mold of

the same size as the dog bone coupon is used to confine the dimensions of the sample. The annealed dog bone coupons were cut and measured by TMA in the same manner as the un-annealed samples.

Results and Discussions

Linear Thermal Expansion

The melt flow during injection molding leads to alignment of GNP particles which causes the composite to behave anisotropically. Figure 4.2 shows the LTEs in 0 degree, 90 degree and Z directions for injection molded coupons of neat PEId and GNP/PEId composites up to 10wt% filler loading.

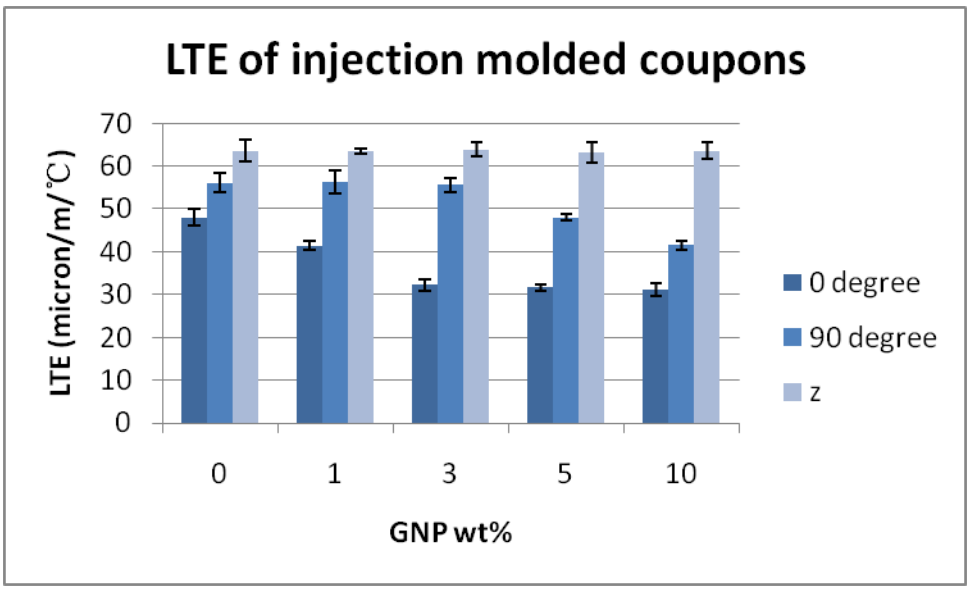

Figure 4.2, LTE of injection molded GNP/PEId composites

With 3wt% GNP particles, the composite shows a reduction of 33% in 0 degree LTE. Additional GNP particles cannot further reduce the LTE in the same direction. Instead, the 90 degree LTE starts to decrease when the GNP loading reaches 5wt% and a

reduction of 26% is recorded at 10wt% loading. Meanwhile, the Z direction LTE remains at the same level regardless of GNP loading.

Interestingly, even the injection molded neat PEId sample shows anisotropic LTEs. This could be due to the fact that the polymer chains are also aligned along the flow direction during injection molding. Generally, higher bond energy leads to lower thermal expansion. Since the 0 degree has more covalent bonds due to chain alignment, its LTE is the smallest among the three directions.

Annealing Effect

In a GNP/PEId composite, the anisotropic behavior in LTEs is significantly larger than in neat PEId sample because of particle alignment. In Chapter 3, annealing is found to allow GNP particle rotation and re-orientation. Although the polymer chain relaxation should be the driving force underneath this phenomenon, no proof is provided.

Now by comparing the LTEs of GNP/PEId samples before and after annealing, it is clear that the polymer chain itself also re-orients during annealing. In Figure 4.3, the annealed neat PEId samples show isotropic LTEs in all three directions, indicating that there is no significant preferential chain alignment.

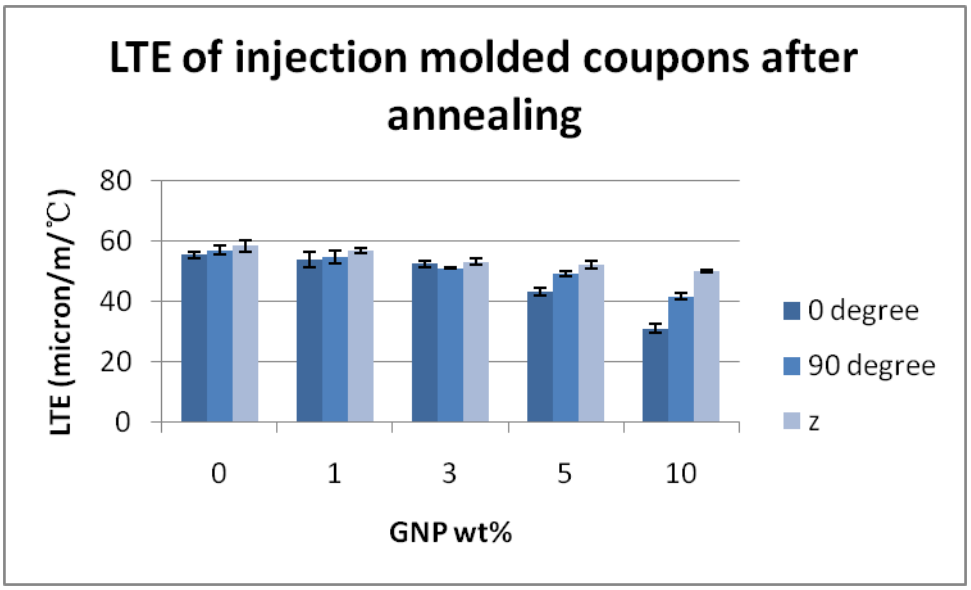

Figure 4.3, LTE of annealed GNP/PEId composites

GNP/PEId composites with up to 3wt% filler loading show isotropic LTEs as well. However, with 5wt% or more filler, anisotropic behavior still exists. This can be regarded to the confinement to GNP particle rotation caused by a dense population of filler particles (Figure 4.4).

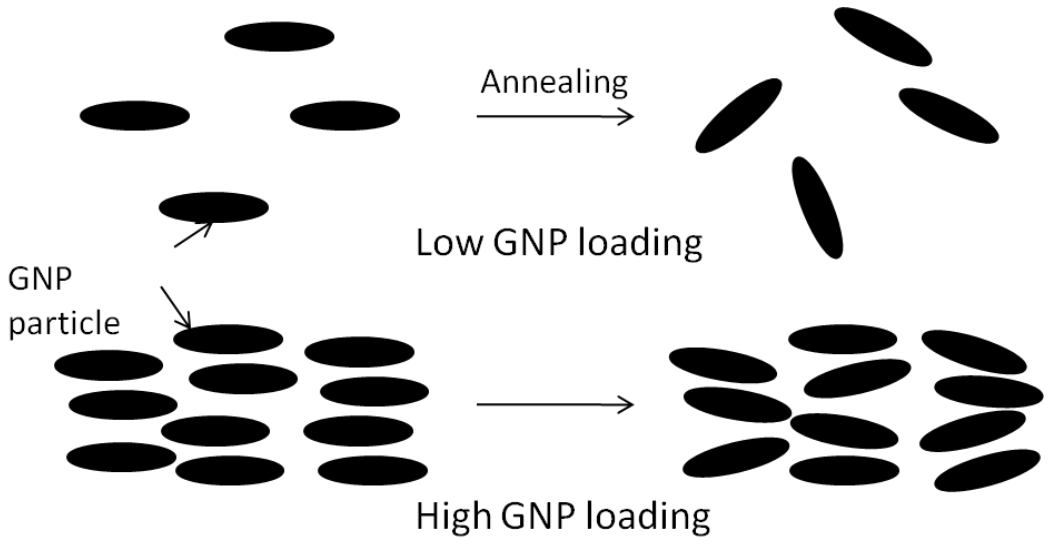

Figure 4.4, Schematics of confinement to GNP particle rotation

The comparison of LTEs before and after annealing is shown in Figure 4.5. In 0 degree

direction, the LTE generally increases significantly after annealing, except for 10wt% loading (Figure 4.5(a)). Below 5wt%, the difference in LTE consists of both polymer chain (16% increase as indicated by neat PEId group) and particle re-orientation (14% increase for 1wt% GNP/PEId, 47% increase for 3wt% GNP/PEId). The fact that the increase of LTE caused by annealing starts to drop from 5wt% loading (20% increase) indicates that the confinement begins to take place. At 10wt%, although the polymer chain re-orientation still exists, the population of the particles is large enough to generate significant interference between particles, resulting in much less rotation of the GNP particles (Figure 4.4). The almost no change in 10wt% sample indicates that the apparent LTE in 0 degree direction is predominated by the GNP particles at this high loading.

After annealing, no significant change of LTE in 90 degree direction can be observed (Figure 4.5(b)). For this specific direction, the two factors, chain and GNP particle re-orientation, actually have opposite effect on LTE. The chain re-orientation will result in more polymer chains aligned in 90 degree compared with before annealing while the rotation of two-dimensional GNP particles results in less orientation. These two opposite effects cancel each other and keep the LTE in 90 degree direction unchanged.

In the Z direction, annealing can reduce LTE (Figure 4.5(c)). Both chain and GNP particle re-orientation benefit the reduction. The fact that there is a significant decrease for 10wt% sample indicates that the polymer chain re-orientation still happens during annealing.

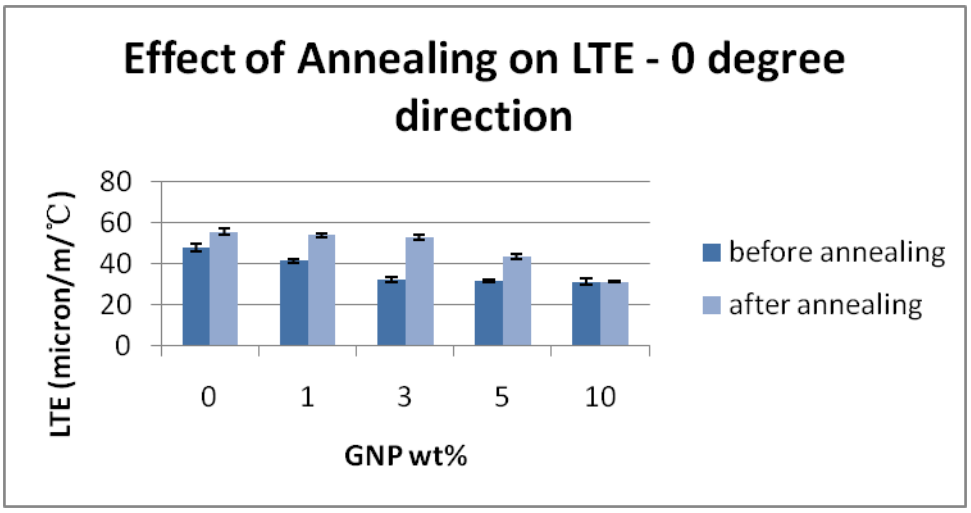

(a)

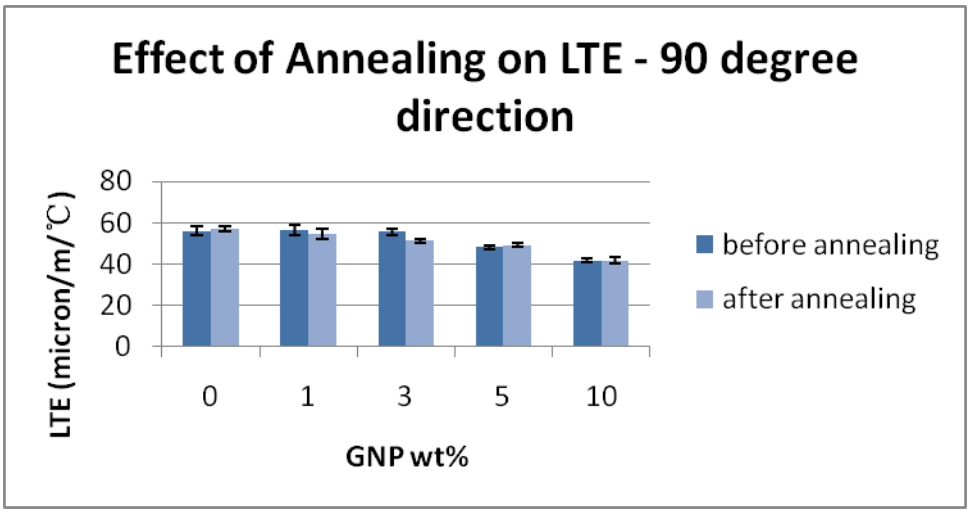

(b)

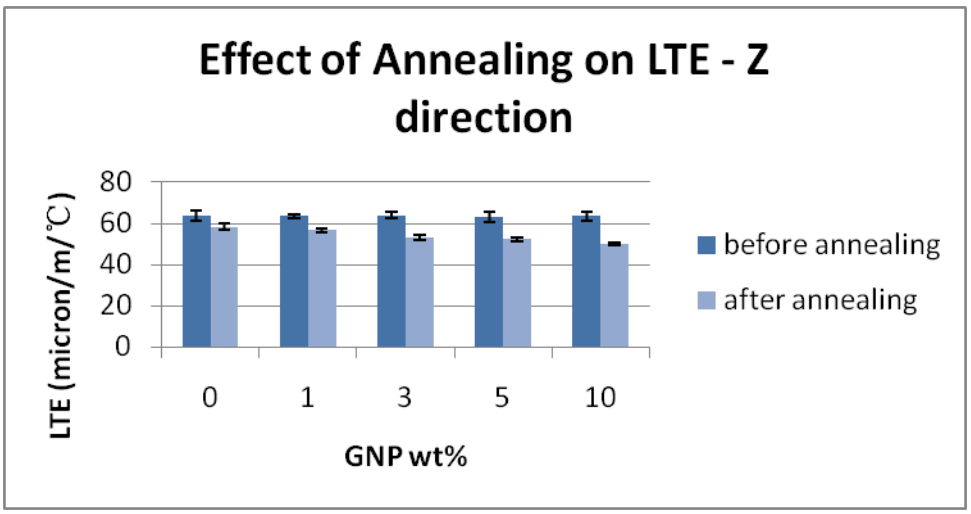

(c)

Figure 4.5, Comparison of LTE: before annealing and after annealing

Bulk thermal expansion (CTE) can be calculated by combining the LTEs in all three directions (Figure 4.6). It can be seen that the CTE of the composites decreases with the increase of GNP-5 loading. Besides, after annealing, most samples retain the same CTE except for 10wt%. This indicates that for most cases, the rotation of the GNP particles and the re-orientation of the polymer chains do not affect the bulk thermal expansion, unless the particle rotation is interfered by the interaction between particles due to high enough GNP concentration (Figure 4.4).

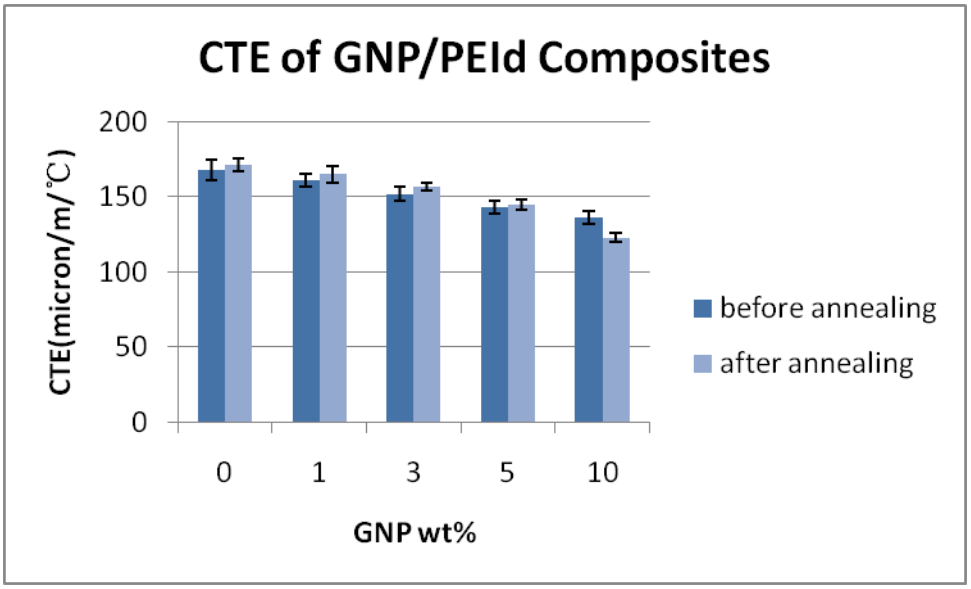

Figure 4.6, CTE of GNP/PEId composites before and after annealing

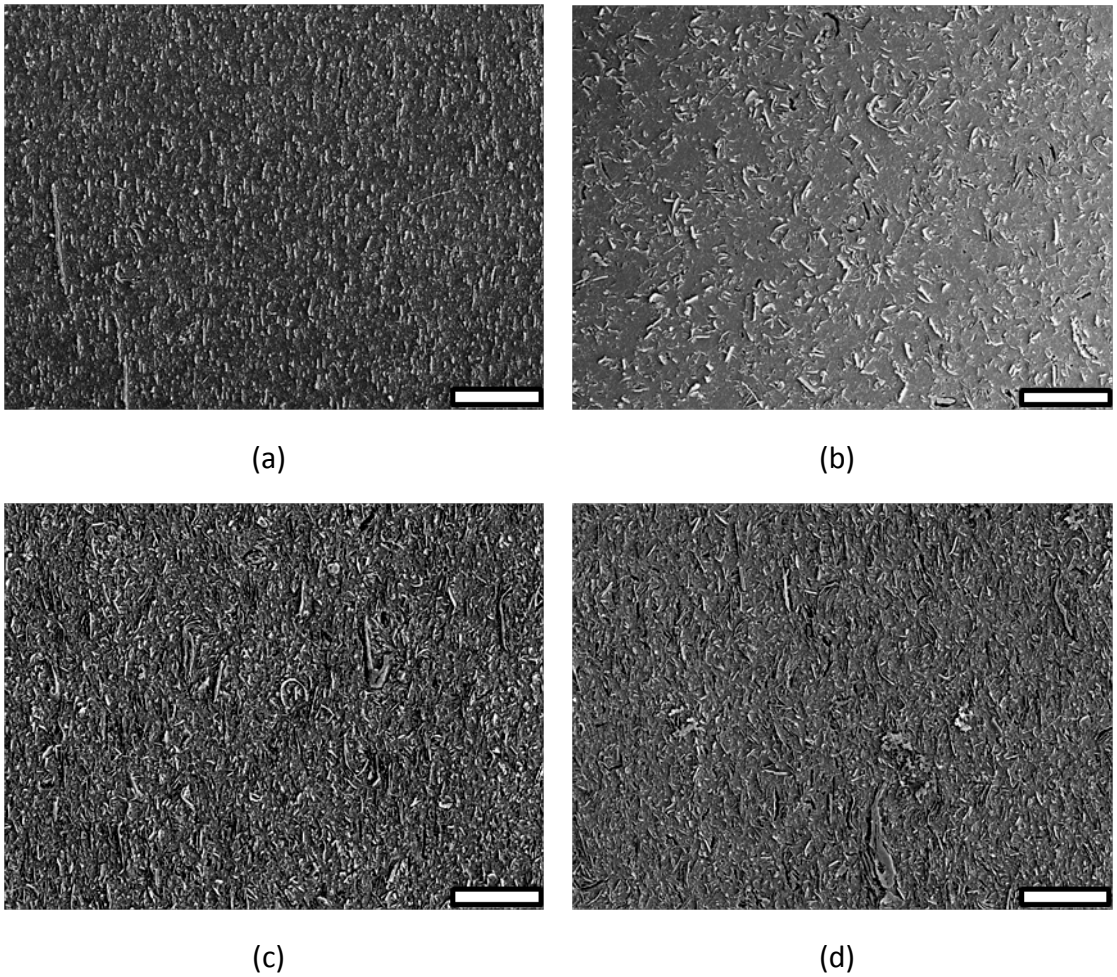

(a) (b)

(c) (d)

Figure 4.7, SEM images of GNP-5/PEId composites: 5wt% injection molded sample, (a) before annealing, (b) after annealing, and 10wt% injection molded sample, (c) before annealing, (d) after annealing. Images are taken at the near-surface part of the tensile bar coupon (see Chapter 3 for details) (scale bars represent 20 micron)

Scanning electron microscope (SEM) images can reveal the rotation of GNP particles after annealing (Figure 4.7). For 5wt%, the rotation is significant. Before annealing, almost all the particles are aligned perfectly while they are randomly oriented after annealing. However, there is not too much difference before and after annealing for 10wt% sample.

Modeling for Coefficient of Thermal Expansion

Bulk Thermal Expansion

Several models have been developed to predict the bulk CTE of the composites [21]. Rule of Mixture [22] gives a first order approximate:

$$\gamma_c = \gamma_f \phi + \gamma_m (1 - \phi) \tag{1}$$

Where γ_c, γ_f, γ_m are the bulk CTE of the composite, filler and matrix respectively and ϕ is the volume fraction of the filler and can be calculated from weight fraction w:

$$\phi = \frac{w}{w + (1-w)\frac{d_f}{d_m}} \tag{2}$$

Where d_m, d_f are the density of the matrix and the filler.

A more sophisticated model proposed by Turner [23] takes into account the interaction between filler and matrix. The equation can be expressed as:

$$\gamma_c = \frac{(1-\phi)k_m\gamma_m/d_m + \phi k_f \gamma_f / d_f}{(1-\phi)k_m/d_m + \phi k_f / d_f} \tag{3}$$

Where k_m, k_f are the bulk modulus of the matrix and the filler respectively and Schapery [24] gives out the upper and lower limit of the CTE of composites:

$$\gamma_c^l = \alpha_m + \frac{k_f}{k_c^u}\frac{(k_m - k_c^u)(\gamma_f - \gamma_m)}{(k_m - k_f)} \tag{4}$$

$$\gamma_c^u = \alpha_m + \frac{k_f}{k_c^l}\frac{(k_m - k_c^l)(\gamma_f - \gamma_m)}{(k_m - k_f)} \tag{5}$$

Where the superscript l and u stand for the lower and upper limit, respectively, and K_c^u, K_c^l are the upper and lower limits of the bulk modulus of the composite and

are provided by Hashin and Shtrikman [25, 26]:

$$k_c^u = k_f + {1-\phi}\Big/{\frac{1}{k_m - k_f} + \frac{3\phi}{(3k_f + 4\mu_f)}} \tag{6}$$

$$k_c^l = k_m + {\phi}\Big/{\frac{1}{k_f - k_m} + \frac{3(1-\phi)}{(3k_m + 4\mu_m)}} \tag{7}$$

Where μ_m and μ_f are the shear modulus of the matrix and the filler, respectively. k and g can be calculated from Young's modulus E and Poisson ratio ν:

$$k = \frac{E}{2(1+\nu)} \text{ and } \mu = \frac{E}{(3-2\nu)} \tag{8}$$

All known parameters are listed in Table 4.1.

Table 4.1, Properties of GNP and PEId

	PEId	GNP
CTE (micron/m/℃)	167.5	23.5 [27]
Young's Modulus (GPa)	3.13	1060
Poisson Ratio	0.36	0.006 [28]
Density (g/cm^3)	1.29	2.1

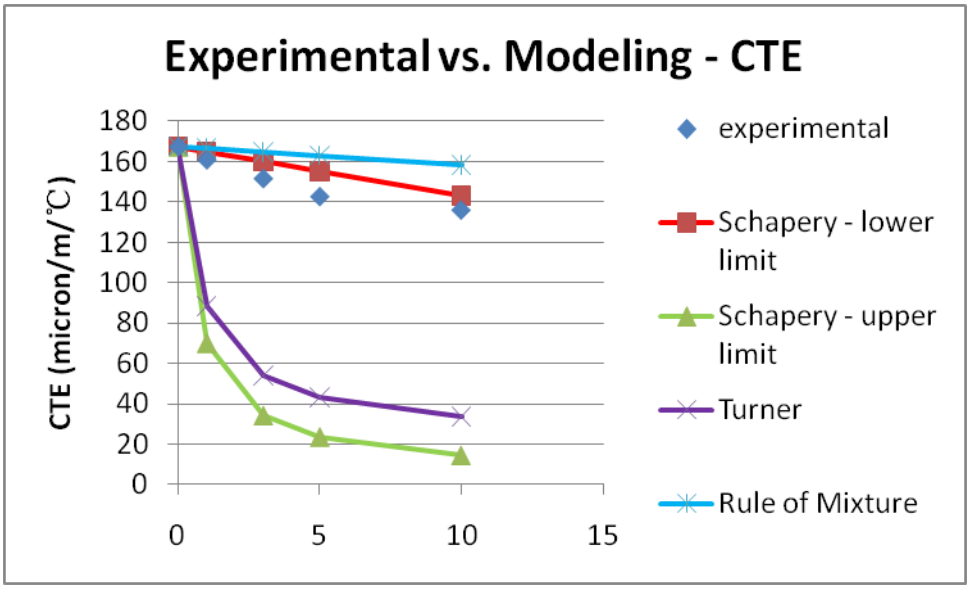

Figure 4.8, Model prediction for CTE of GNP/PEId composites

Among the four models, Schapery's lower limit prediction fits the experimental data best (Figure 4.8). Turner's equation and Schapery's upper limit prediction largely overvalue the effect of GNP particles on the CTE of the composite while Rule of Mixture underestimated the effect.

Linear Thermal Expansion

Based on the Eshelby tensor, Chow et al developed an analytical model for calculating the LTE of the composite filled by perfectly aligned inclusions that can be considered as ellipsoids [29]:

$$\alpha_L = \alpha_m + \frac{k_f}{k_m}\frac{(\gamma_f - \gamma_m)G_1\phi}{2K_1G_3 + G_1K_3} \tag{9}$$

$$\alpha_T = \alpha_m + \frac{k_f}{k_m}\frac{(\gamma_f - \gamma_m)G_3\phi}{2K_1G_3 + G_1K_3} \tag{10}$$

where α_L is the longitudinal LTE of the composite which is in the direction that is parallel with the alignment of the major axis of the ellipsoid (length) and α_T is the LTE of the transverse direction.

In equations (9) and (10), K_i and G_i (i=1, 3) are:

$$K_i = 1 + \left(\frac{k_f}{k_m} - 1\right)[(1-\phi)\alpha_i + \phi] \tag{11}$$

$$G_i = 1 + \left(\frac{\mu_f}{\mu_m} - 1\right)[(1-\phi)\beta_i + \phi] \tag{12}$$

where α_i and β_i are functions of the filler aspect ratio $\rho = length/diameter$, the aspect ratio of the filler A and the Poisson ratio of the matrix ν_m [30].

Similar to nanoclay, GNP can also be considered as ellipsoids with a

thickness/Diameter ratio less than 1 [31]. Note that α_L is actually the LTE of the normal direction of the GNP particle and should be applied for the Z direction, while α_T is the LTE of the radius direction of the GNP particle and should be applied for the 0 degree direction. So equation (9) and (10) become:

$$\alpha_0 = \alpha_{m,0} + \frac{k_f}{k_m}\frac{(\gamma_f - \gamma_m)G_1\phi}{2K_1G_3 + G_1K_3} \tag{13}$$

$$\alpha_Z = \alpha_{m,Z} + \frac{k_f}{k_m}\frac{(\gamma_f - \gamma_m)G_3\phi}{2K_1G_3 + G_1K_3} \tag{14}$$

For 90 degree direction, the situation is more complicated. Due to the geometry of the mold used in injection molding, some of the GNP particles are aligned along the thickness dimension of the coupon while majority of them are aligned along the width dimension (Figure 4.9). This morphology indicates that the overall LTE in 90 degree direction should be a combination of α_L and α_T. Note that the same situation also can be applied to the Z direction. However, during TMA measurement, the testing probe is placed at the center of the sample. Due to the testing sample geometry, the probe cannot detect the dimension change of the edge area (Figure 4.10). On the other hand, for 90 degree direction, the probe is large enough to detect the dimension change caused by the entire sample.

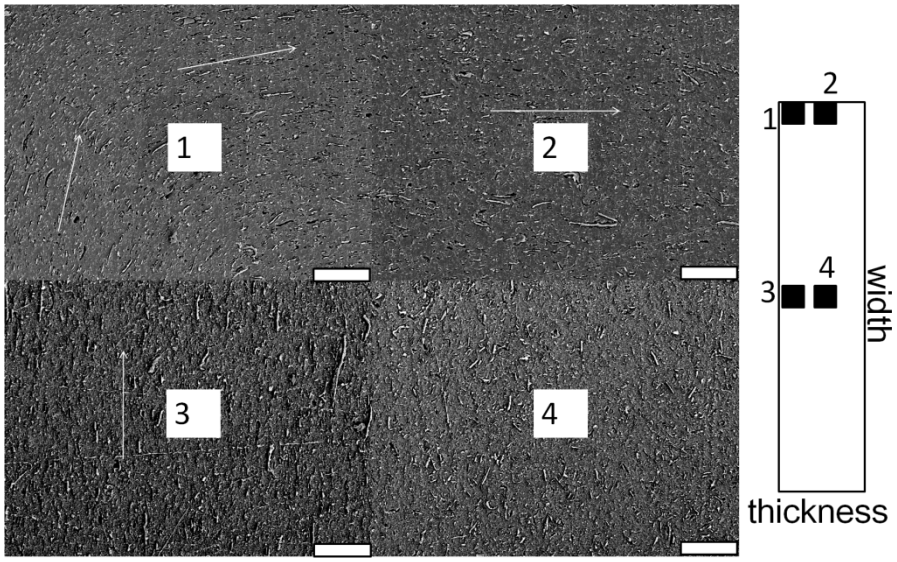

Figure 4.9, SEM images showing orientation of GNP particles observed on the cross-section of an injection molded coupon perpendicular to the flow direction (scale bars represent 20 micron)

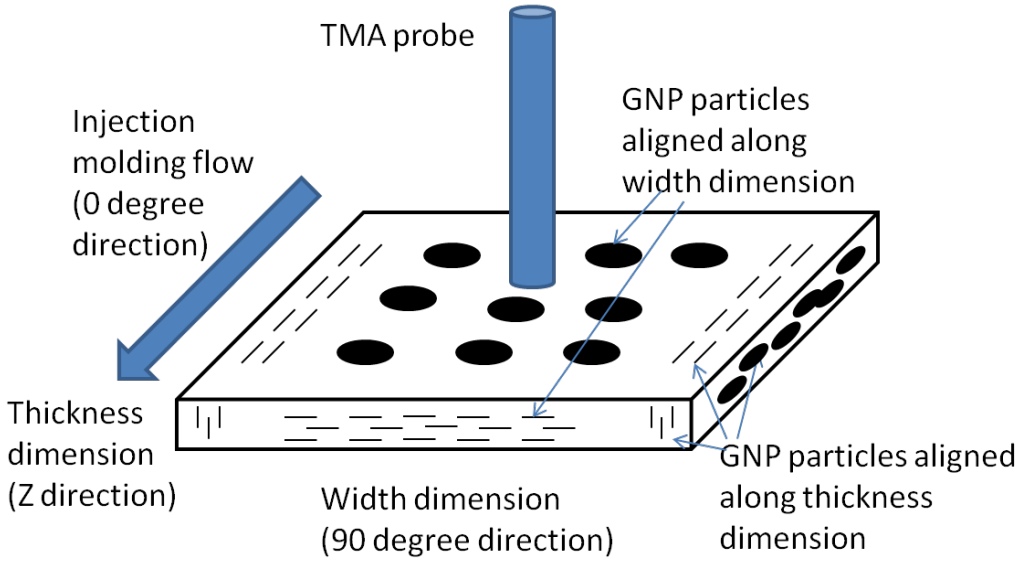

Figure 4.10, Configuration for measuring LTE in Z direction

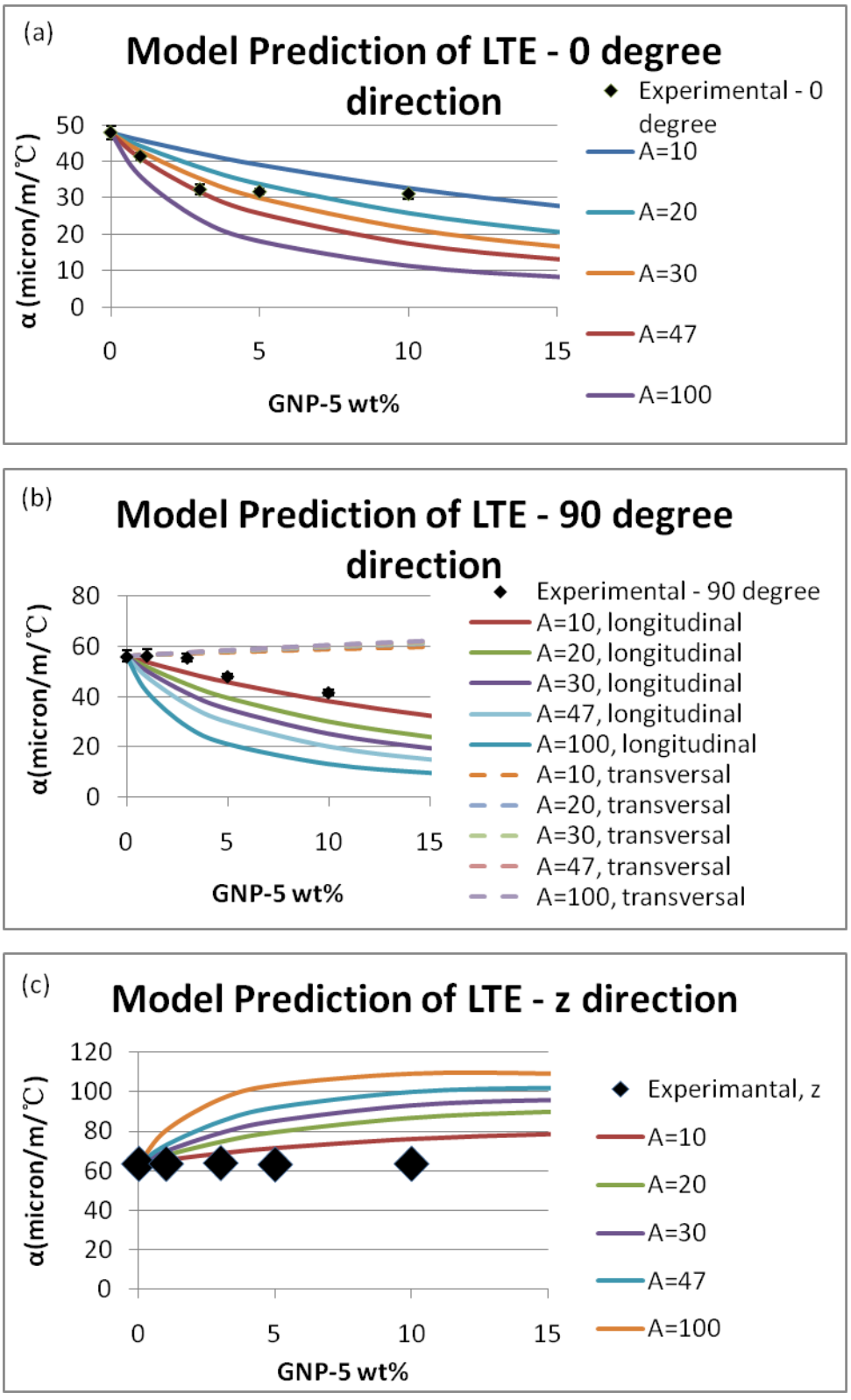

Figure 4.11, Model prediction of LTE in (a) 0 degree direction, (b) 90 degree direction, (c) Z direction

Figure 4.11 shows the prediction of Chow's LTE model calculated with different filler aspect ratio A. For 0 degree direction, the experimental data follow the model with A=47 for loadings not higher than 3wt%. This aspect ratio value is consistent with the result from Chapter 3. From 5wt% and above, the experimental data shift to lower aspect ratio region of the model predictions, indicating either agglomeration of the particles or the decrease of alignment of the particles.

For 90 degree direction, it is clear that with 3wt% loading or less, the experimental data follow the longitudinal model, indicating that the LTE is predominated by the GNP particles with their normal aligned in 90 degree direction. That is to say, the particles that are aligned along the thickness dimension are the major contributor. However, with 5wt% or more GNP added, the LTE in 90 degree direction starts to follow the transverse model, indicating the particles aligned along the width dimension start to be predominant in the composite.

To observe the change of particle alignment that affects 90 degree LTE, SEM images were taken over the entire width-thickness plane of the injection molded coupon. The SEM images were processed in Image-Pro Plus software (Media Cybernetics, Inc., MD) to pick up the orientation information that can calculate a_{11} of the particles:

$$a_{11} =< cos^2\theta > \quad (15)$$

where θ is the angle between a GNP particle and the width dimension of the injection molded coupon.

Then, the a_{11} values can be plotted against the position.

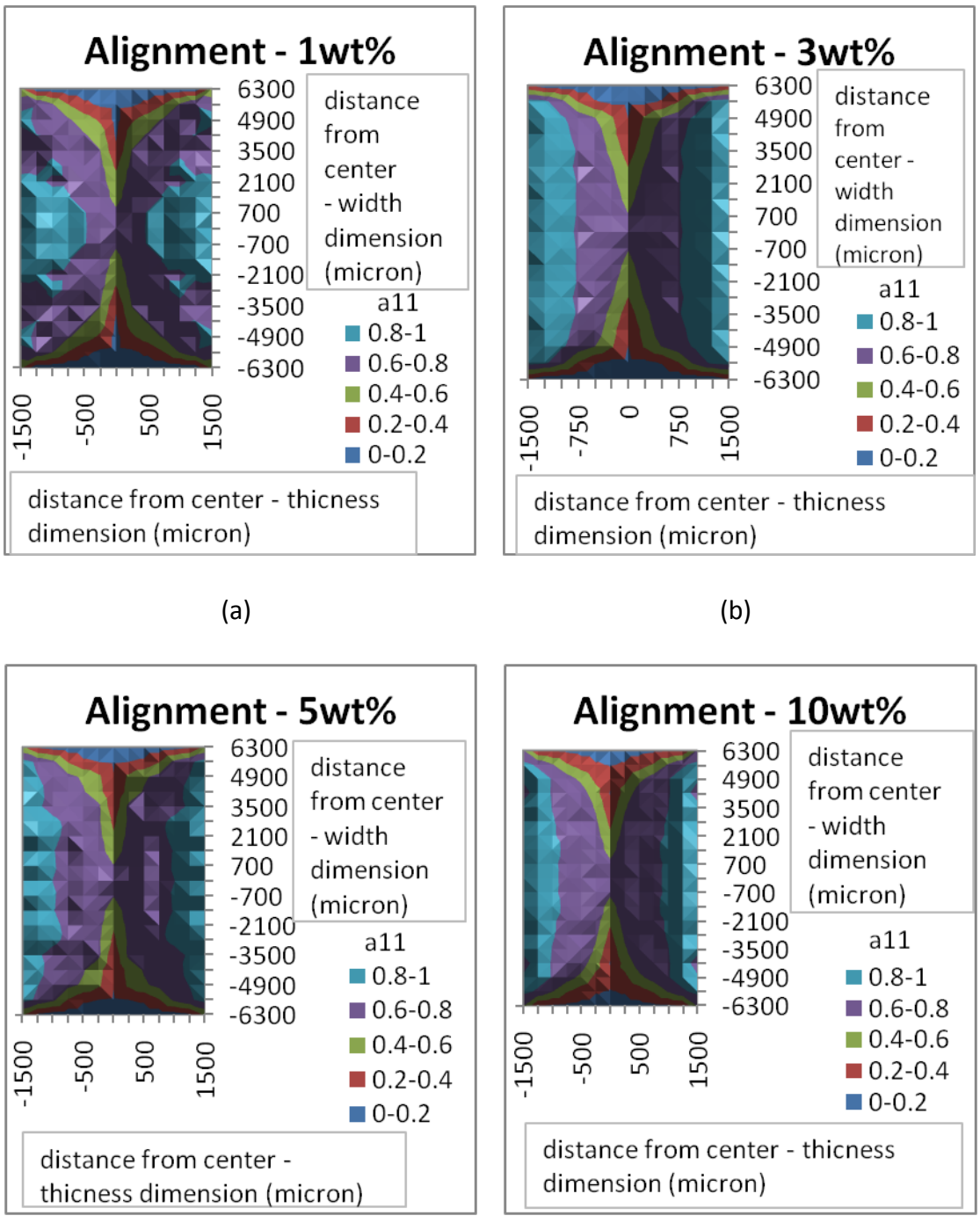

(a) (b)

(c) (d)

Figure 4.12, alignment of GNP particles on thickness-width plane of injection molded coupon

In Figure 4.12, the patterns are significantly different between 1wt% and other loadings, indicating that more particles are aligned along the thickness dimension

other than the width dimension for 1wt% sample. SEM images of representative morphology for different a_{11} values are shown in Figure 4.13.

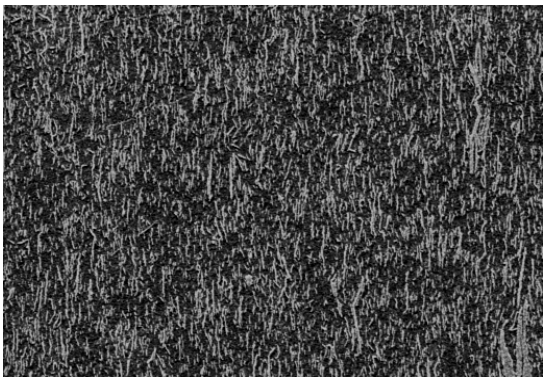

(a)a11 = 0.8~1.0, unidirectionally aligned in width (90 degree) direction

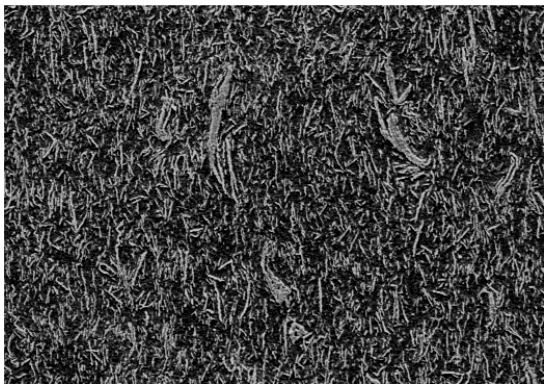

(b)a11 = 0.6~0.8, preferentially aligned in width (90 degree) direction

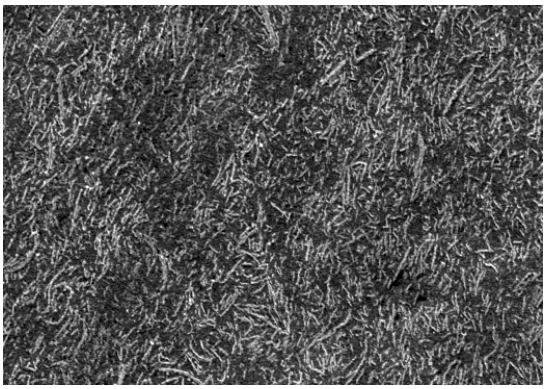

(c)a11 = 0.4~0.6, transition region: aligned in 45 degree direction

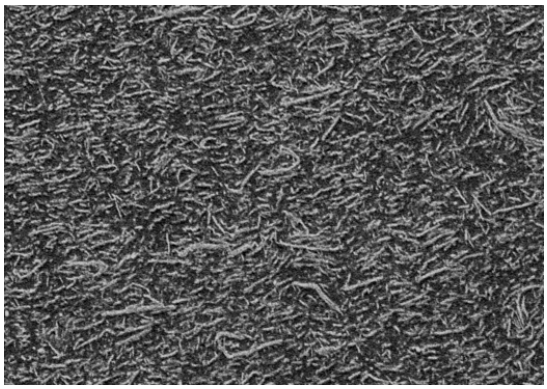

(d)a11 = 0.2~0.4, preferentially aligned in thickness direction (Z direction)

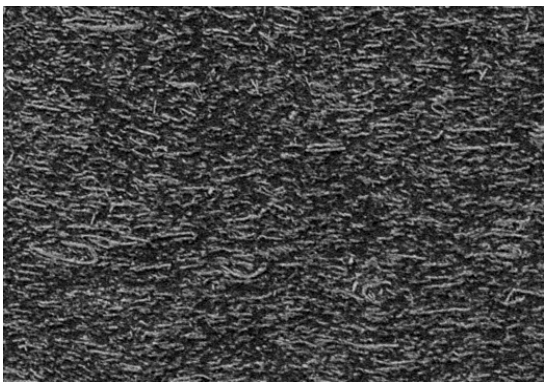

(e)a11 = 0.0~0.2, unidirectionally aligned in thickness direction (Z direction)

Figure 4.13, Morphology for different a11 values, where white lines stand for GNP particles and black part stands for the matrix. The images are taken from 10wt% GNP-5/PEId composite injection molded coupon on the cross-section of flow direction (width-thickness plane)

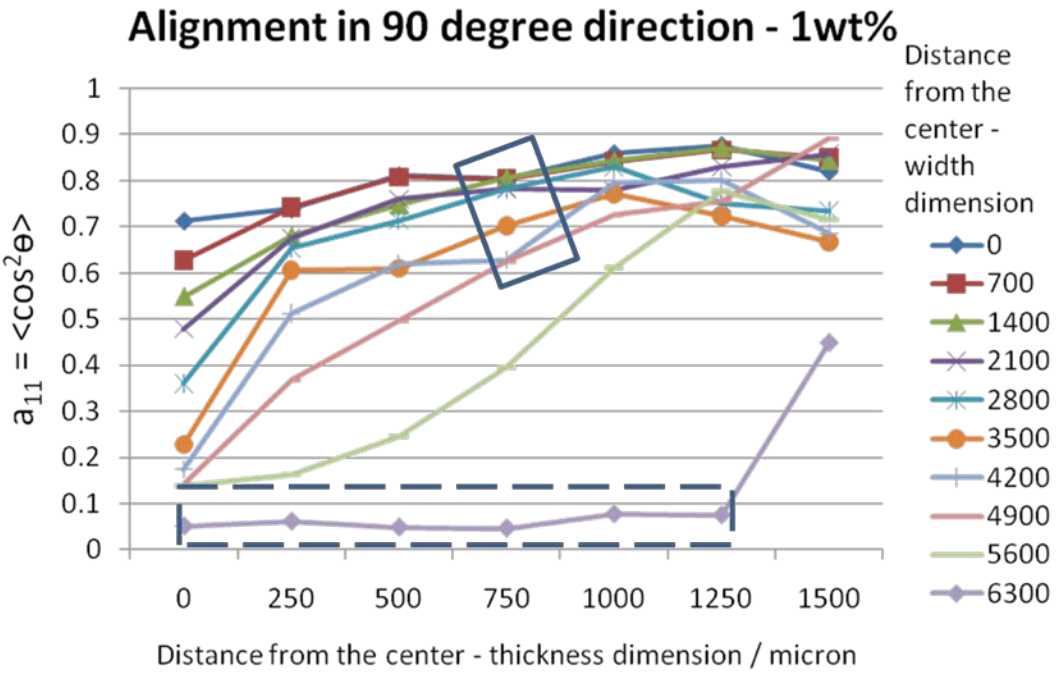

(a)

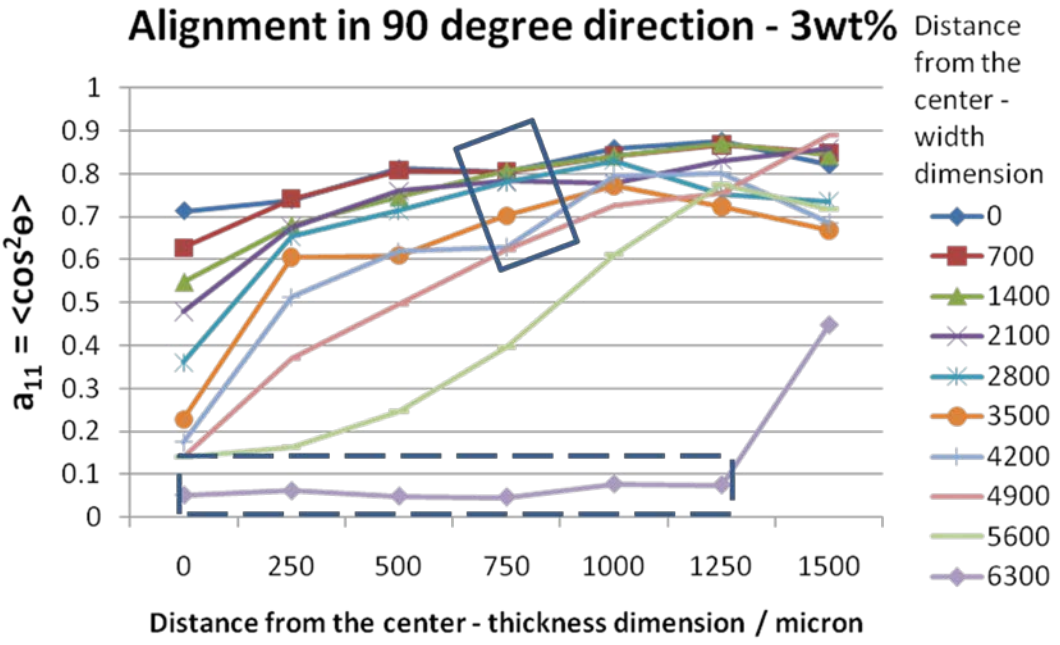

(b)

Figure 4.14, Alignment in 90 degree direction

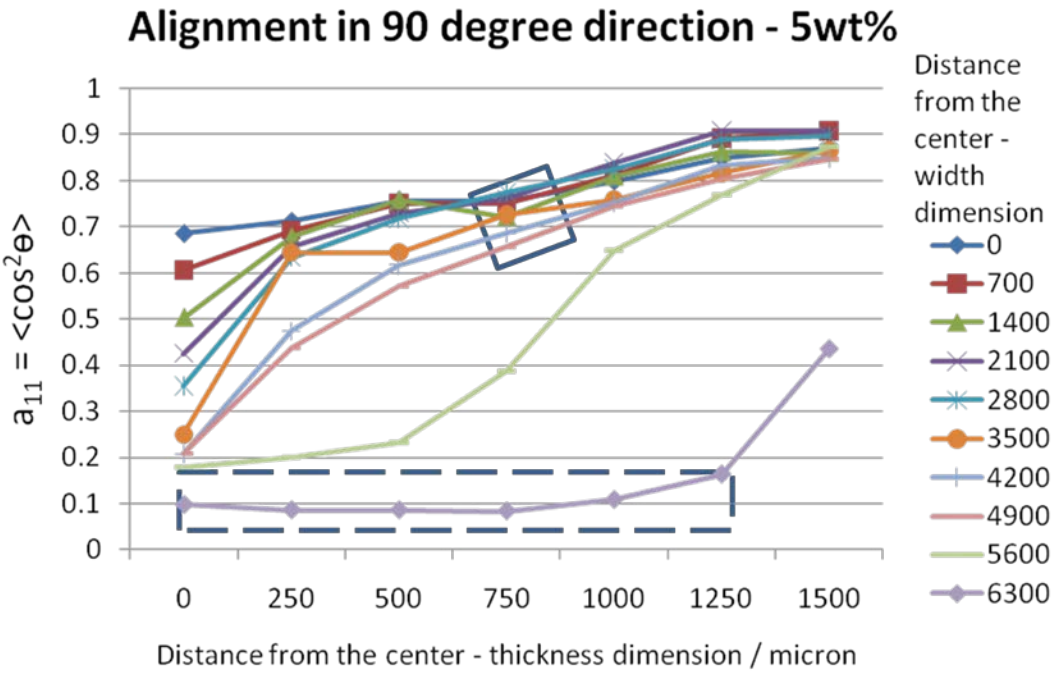

(c)

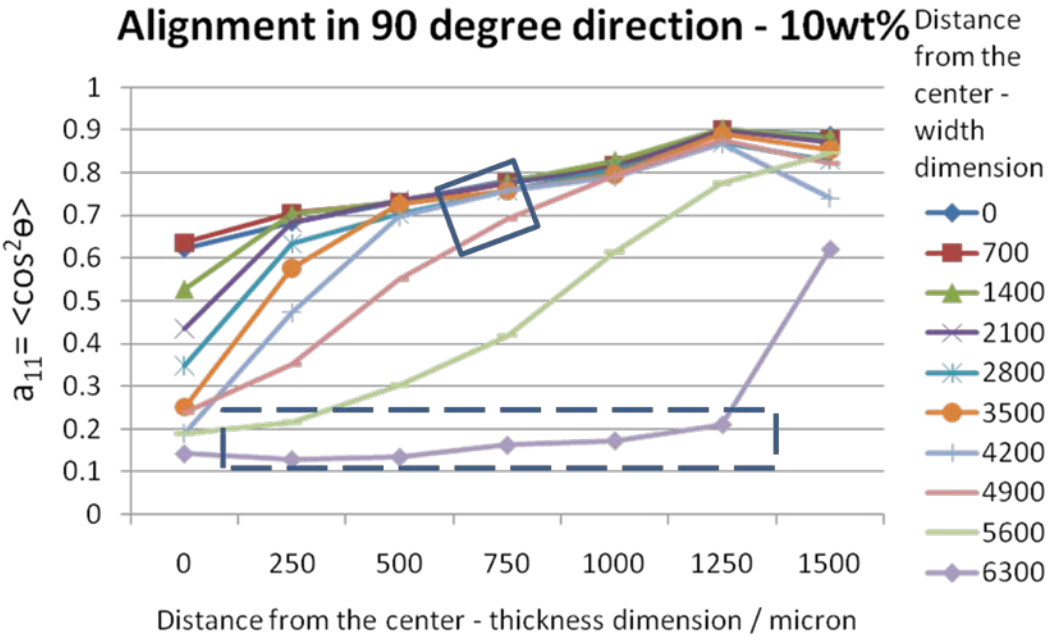

(d)

Figure 4.14, Alignment in 90 degree (cont.)

Figure 4.14 shows more information of the change of alignment with increase of GNP loading. The series that fall into the solid frame stand for the majority of the thickness-width plane. From 1wt% to higher loadings, the size of the frame decrease significantly, indicating that more and more particles are aligned in 90 degree direction with higher GNP loadings. The value of the line which sits in the dash frame (series 6300) keeps increasing with the increase of GNP loading. These two trends are consistent with the experimental data of LTE in 90 degree direction.

Interestingly, the LTE in the Z direction does not follow Chow's model at all (Figure 4.11(c)). While the predicted result indicates that the LTE in the normal direction of platelet particle should increase with the loading of filler, the experimental data of composite stay at the same level as neat polymer no matter how high the loading is.

Conclusions

LTEs of the injection molded GNP-5/PEId composites were measured in the 0 degree, 90 degree and Z direction. It is found that the 0 degree LTE decrease with the increase of GNP-5 loading and can be predicted by Chow's model. The LTE in 90 degree direction also decrease with GNP loading at above 5wt% while the LTE remains the same at lower than 3wt% loadings. This behavior is explained by the morphology of the GNP particles in the cross-section of injection molded coupons which show a development of GNP alignment with an increase of loading. It is also observed that the bulk CTE of GNP/PEId composites can be best predicted by Schapery's lower limit model. Annealing is effective in changing the alignment of

polymer chains and GNP particles, resulting in significant increase of LTE in 0 degree direction and decrease in Z direction. However, the overall bulk CTE is not affected by annealing.

REFERENCES

REFERENCES

1. Johnston, N.J., T.W. Towell, and P.M. Hergenrother, *Physical and mechanical properties of high-performance thermoplastic polymers and their composites*, in *Thermoplastic composite materials*, C. LA, Editor. 1991, Elsevier Science Publishers B.V.: Amsterdam. p. 27-71.

2. Parlevliet, P.P., H.E.N. Bersee, and A. Beukers, *Residual stresses in thermoplastic composites - A study of the literature - Part I: Formation of residual stresses.* Composites Part a-Applied Science and Manufacturing, 2006. **37**(11): p. 1847-1857.

3. Nairn, J.A. and P. Zoller, *MATRIX SOLIDIFICATION AND THE RESULTING RESIDUAL THERMAL-STRESSES IN COMPOSITES.* Journal of Materials Science, 1985. **20**(1): p. 355-367.

4. Barnes, J.A. and G.E. Byerly, *THE FORMATION OF RESIDUAL-STRESSES IN LAMINATED THERMOPLASTIC COMPOSITES.* Composites Science and Technology, 1994. **51**(4): p. 479-494.

5. Chapman, T.J., et al., *PREDICTION OF PROCESS-INDUCED RESIDUAL-STRESSES IN THERMOPLASTIC COMPOSITES.* Journal of Composite Materials, 1990. **24**(6): p. 616-643.

6. Kugler, D. and T.J. Moon, *Identification of the most significant processing parameters on the development of fiber waviness in thin laminates.* Journal of Composite Materials, 2002. **36**(12): p. 1451-1479.

7. Abedian, A. and W. Szyszkowski, *Influence of the free surface on the thermal stresses in unidirectional composites.* Composites Part a-Applied Science and Manufacturing, 1997. **28**(6): p. 573-579.

8. Adams, R.D. and M.M. Singh, *Low temperature transitions in fibre reinforced polymers.* Composites Part a-Applied Science and Manufacturing, 2001. **32**(6): p. 797-814.

9. D'Amore, A., et al., *Long-term behaviour of PEI and PEI-based composites subjected to physical aging.* Composites Science and Technology, 1999. **59**(13): p. 1993-2003.

10. Warrier, A., et al., *The effect of adding carbon nanotubes to glass/epoxy composites in the fibre sizing and/or the matrix.* Composites Part a-Applied Science and Manufacturing, 2010. **41**(4): p. 532-538.

11. Yuen, S.M., et al., *Preparation and thermal, electrical, and morphological properties of multiwalled carbon nanotube and epoxy composites.* Journal of Applied Polymer Science, 2007. **103**(2): p. 1272-1278.

12. Zhang, Y.C. and X. Wang, *Thermal effects on interfacial stress transfer characteristics of carbon nanotubes/polymer composites.* International Journal of Solids and Structures, 2005. **42**(20): p. 5399-5412.

13. Wei, C.Y., D. Srivastava, and K.J. Cho, *Thermal expansion and diffusion coefficients of carbon nanotube-polymer composites.* Nano Letters, 2002. **2**(6): p. 647-650.

14. Agag, T., T. Koga, and T. Takeichi, *Studies on thermal and mechanical properties of polyimide-clay nanocomposites.* Polymer, 2001. **42**(8): p. 3399-3408.

15. Yasmin, A., et al., *Mechanical and thermal behavior of clay/epoxy nanocomposites.* Composites Science and Technology, 2006. **66**(14): p. 2415-2422.

16. Gu, A.J. and F.C. Chang, *A novel preparation of polyimide/clay hybrid films with low coefficient of thermal expansion.* Journal of Applied Polymer Science, 2001. **79**(2): p. 289-294.

17. Asif, A.A., et al., *Surface morphology, thermomechanical and barrier properties of poly(ether sulfone)-toughened epoxy clay ternary nanocomposites.* Polymer International, 2010. **59**(7): p. 986-997.

18. Kalaitzidou, K., H. Fukushima, and L.T. Drzal, *Multifunctional polypropylene composites produced by incorporation of exfoliated graphite nanoplatelets.* Carbon, 2007. **45**(7): p. 1446-1452.

19. Liao, K. and S. Li, *Interfacial characteristics of a carbon nanotube-polystyrene composite system.* Applied Physics Letters, 2001. **79**(25): p. 4225-4227.

20. Drzal, L.T. and H. Fukushima, *Expanded graphite and products produced therefrom*. 2004: US.

21. Wong, C.P. and R.S. Bollampally, *Thermal conductivity, elastic modulus, and coefficient of thermal expansion of polymer composites filled with ceramic particles for electronic packaging.* Journal of Applied Polymer Science, 1999. **74**(14): p. 3396-3403.

22. Orrhede, M., R. Tolani, and K. Salama, *Elastic constants and thermal expansion of aluminum-SiC metal-matrix composites.* Research in Nondestructive Evaluation, 1996. **8**(1): p. 23-37.

23. Turner, P.S., *THERMAL-EXPANSION STRESSES IN REINFORCED PLASTICS.* Journal of Research of the National Bureau of Standards, 1946. **37**(4): p. 239-250.

24. Schapery, R.A., *THERMAL EXPANSION COEFFICIENTS OF COMPOSITE MATERIALS BASED ON ENERGY PRINCIPLES.* Journal of Composite Materials, 1968. **2**(3): p. 380-&.

25. Hashin, Z. and S. Shtrikman, *A VARIATIONAL APPROACH TO THE THEORY OF THE ELASTIC BEHAVIOUR OF MULTIPHASE MATERIALS.* Journal of the Mechanics and Physics of Solids, 1963. **11**(2): p. 127-140.

26. Hashin, Z., *ANALYSIS OF COMPOSITE-MATERIALS - A SURVEY.* Journal of Applied Mechanics-Transactions of the Asme, 1983. **50**(3): p. 481-505.

27. Kirby, R.K., T.A. Hahn, and B.D. Rothrock, in *American Institute of Physics handbook*, D.E. Gray, Editor. 1972, McGraw-Hill: New York. p. 4-119 to 4-142.

28. Cho, J., J.J. Luo, and I.M. Daniel, *Mechanical characterization of graphite/epoxy nanocomposites by multi-scale analysis.* Composites Science and Technology, 2007. **67**(11-12): p. 2399-2407.

29. Chow, T.S., *EFFECT OF PARTICLE SHAPE AT FINITE CONCENTRATION ON THERMAL-EXPANSION OF FILLED POLYMERS.* Journal of Polymer Science Part B-Polymer Physics, 1978. **16**(6): p. 967-970.

30. Chow, T.S., *EFFECT OF PARTICLE SHAPE AT FINITE CONCENTRATION ON ELASTIC-MODULI OF FILLED POLYMERS.* Journal of Polymer Science Part B-Polymer Physics, 1978. **16**(6): p. 959-965.

31. Yoon, P.J., T.D. Fornes, and D.R. Paul, *Thermal expansion behavior of nylon 6 nanocomposites.* Polymer, 2002. **43**(25): p. 6727-6741.

Chapter 5 Highly Aligned Multifunctional Graphite Nanoplatelet-Polyether imide Composite in Film Form

Abstract

The objective of this research is to investigate the effect of adding graphite nanoplatelet (GNP) particles into polyether imide film. Extruded films were produced with various amounts of GNP and different degrees of post-extrusion stretching. A uniform high degree of alignment of the GNP particles along both 0 degree (stretching) direction and 90 degree direction was obtained under high stretching ratios. Tensile properties including tensile modulus, strength and elongation were investigated. O_2 permeability was reduced with the increase of GNP loading and stretching ratio of the film. Bharadwaj's model was applied to predict the permeability. Information of degree of alignment was obtained through analyzing SEM images in image-processing software and used with Bharadwaj's model, resulting in good agreement with experimental data. Annealing of the stretched films under 340℃showed a significant improvement of both electrical and thermal conductivity in the film direction.

Introduction

Polymer nanocomposite films have drawn more and more attention because of their unique multifunctional properties and the possibility to be incorporated into other structural or functional materials. Polyether imide (PEId, Ultem resin, Sabic IP) is a thermoplastic material which has high chemical and thermal resistance, good flame resistance and low smoke generation [1]. Major applications of PEId are as a structural material for confined space, including high-floor office, airplane and submarines. Just like the other thermoplastic based material, PEId can offer lighter and more durable solutions as alternatives to metal and alloys, but falls short in properties like thermal and electrical conductivity and barrier properties to small molecules. Meanwhile, a group of nanofillers such as carbon nanotubes (CNT) [2], nanoclay [3] and nano graphite [4] are considered to be efficient in providing such multifunctionality to their composites. Among those fillers, the graphite nanoplatelet (GNP) combines electrical and thermal conductivity similar to CNT and two-dimensional morphology similar to nanosilicates, resulting in the capability of meeting most of the requirements if incorporated into composites.

In a composite reinforced by anisotropic fillers, the alignment of the filler is usually the key to performance of the composite. Lan et al [5] designed a clay-epoxy thermoset composite with sub-ambient Tg to allow alignment of clay particles under strain. Analogous to this system would be stretching the thermoplastic nanocomposite material above Tg to obtain high alignment such as by a blown film

process. Zenkiewicz et al [6] reported the dependence of blowing ratio on the barrier properties of clay/PLA film. It is found that higher blowing ratio would lead to lower permeability by oxygen, water vapor and carbon dioxide. TEM images shown by the author verified that the particles tend to be more aligned under higher blowing ratio. However, not all the properties can benefit from alignment. Kim et al [7] proposed a schematic that describes electrical conductivity changes due to the transition of graphite particles from the aligned state to the un-aligned state. Similar results are also discussed in Chapter 3. Adequate post-treatment would be necessary to alter the alignment of fillers in order to achieve optimized and balanced performance.

The goal of this research is to fabricate unidirectional-stretched GNP/PEId film through extrusion and film casting. Stretching ratios from low to high were applied to obtain composite film with different degrees of alignment of the GNP particles. Tensile properties, electrical and thermal conductivity and barrier to oxygen transport have been measured. Annealing under high temperature was used to adjust the degree of alignment in order to enhance electrical conductivity.

Experimentation

Materials

Polyetherimide (PEI, Ultem 1010) was provided by Sabic Americas, Inc. (Houston, TX). GNP-5 was provided by XG Sciences Inc. (East Lansing, MI). The GNP particles have an average diameter of 3.9 micron with a specific surface area of 40m^2/g.

Melt-extrusion and film casting

Melt-extrusion was carried on Leistritz twin-screw extruder (MIC27/6L-48D). The screws were in the co-rotation mode. The shearing provided by co-rotating screws can help separate the filler particles and result in a better dispersion than counter-rotation. Barrel temperatures were set to 310℃ with a melt temperature at 340℃. The die pressure was at around 5.5MPa with screw speed set at 150 rpm. GNP was fed at a side feeder at 1/3 screw length away from the main feeder where the polymer was fed. The melt was extruded through a film die and then stretched and collected by a three-roll film collector, whose rolls were heated to 160℃ by oil to get uniform, wrinkle-free film. The stretching ratio is defined as in Figure 5.1:

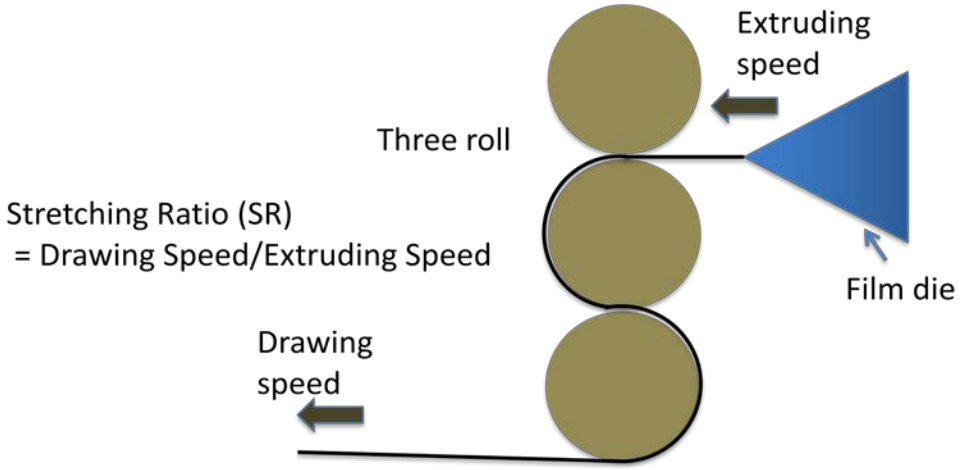

Figure 5.1, Film extrusion, showing stretching ratio

Between the film die opening and the first nip point of the three roll stack, the film is stretched in the melt or rubbery state. The distance between the die and the rolls is an important factor which can affect the shape of the product, such as thickness and width [8]. Also, since the film is exposed in air, a temperature gradient is developed

along the stretching direction as well. For this research, the distance was kept to a minimum in order to get as thin a film as possible. The polymer chains are able to move before reaching the rolls. For a crystalline polymer, this effect will also result in rearrangement of crystalline and amorphous domains resulting in higher crystallinity [9]. For PEId, since it's amorphous, the stretching would only result in the orientation of both chains and GNP particles.

In the experiment setup, the stretching ratio was controlled by fixing the material feeding speed and changing the speed of the three roll stack. The stretching ratio (SR) then is calculated as:

$$\mathrm{SR} = \frac{\text{Die Opening Thickness (DOT)} \times \text{Die Opensing Width (DOW)}}{\text{Film Thickness (FT)} \times \text{Film Width (FW)}}$$

The die opening width was 152 mm and the films were collected at 1, 4, 8 and 16 fpm three-roll speed. Film dimension and SR value are listed in Table 5.1.

Table 5.1, Dimension and stretching ratio of extrusion cast films

Roll speed (fpm)	1	4	8	16
Die Opening (mm)	0.58	0.91	0.91	0.91
Thickness (mm)	0.28±4	0.094±10	0.052±8	0.030±4
Width (mm)	144	136	132	127
SR	2	11	20	34

Annealing of Extrusion Cast Film

The extrusion cast film was also annealed under 340℃ in a hot press. To keep the dimension to the same as the un-annealed sample, a piece of aluminum foil was

used as the mold. A square hole with the same dimension as the GNP/PEId film was cut on the aluminum foil. The foil, along with the sample in the hole, was sandwiched by two sheets of PTFE film and two steel plates. The whole set-up was then placed in the pre-heated 340℃ hot press (CARVER Laboratory Press, Model 2731, Fred S. Carver INC.). A pressure of 23 MPa was applied immediately and held for 1 hour. After that, water cooling was applied to the hot press to cool the sample. The setup of the experiment is shown in Figure 5.2.

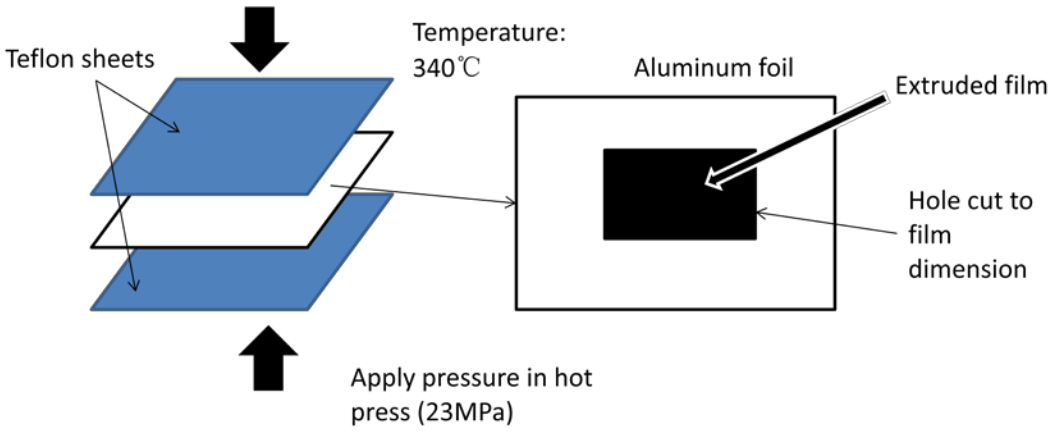

Figure 5.2, Experiment setup of annealing extrusion cast film

The change in thickness dimension after 1 hour annealing is shown in Table 5.2. Note that the samples used for annealing were the central part of the extrusion cast film with all the edges trimmed off, so the thickness is slightly different from Table 5.1.

Table 5.2, Thickness change after annealing for GNP/PEId extrusion cast films

Stretching ratio	11	20	34
Before annealing (μm)	105±5	58±2	34±2
After annealing (μm)	113±8	61±5	36±4

Melt-extrusion and Compression Molding

GNP-5 and PEId were also melt-blended and extruded as strands with the same twin-screw extruder setup as used for film and then cut into pellets. An aluminum foil with a round hole cut in the center was used as mold. The composite pellets were piled at the center of the hole and then compressed into ~150 μm thick films.

Electrical Conductivity Measurement

The resistance of GNP/PEI composite films was measured in two directions: the through-plane direction which is across the thickness of the sample and in-plane direction which is the stretching direction for extrusion cast films and the radius direction for compression molded films (Figure 5.3). The resistance value was then converted into resistivity by taking into account the sample dimensions.

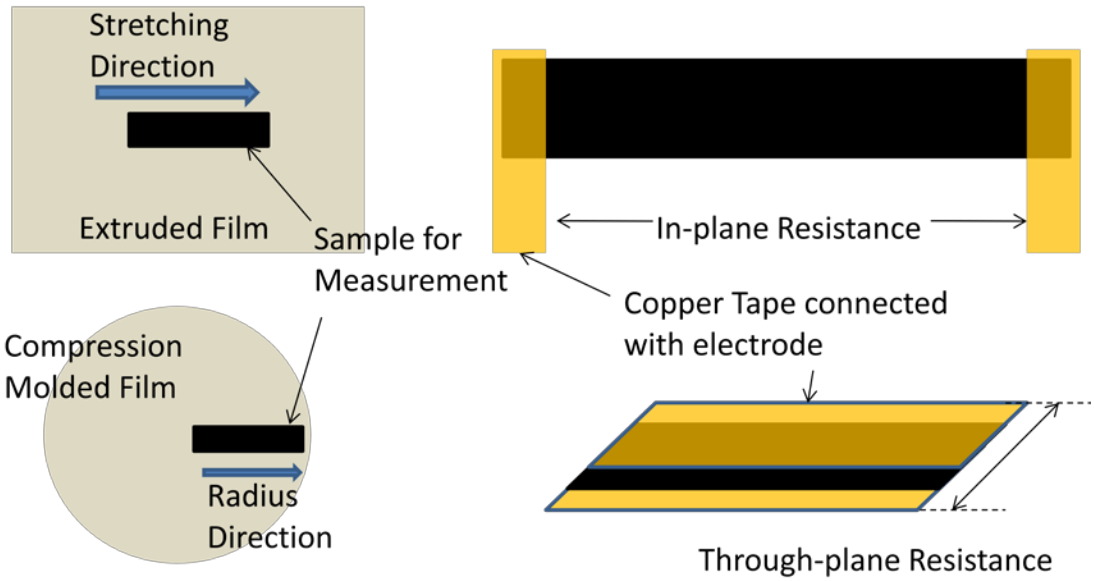

Figure 5.3, Schematic of electrical resistance measurement

Thermal Diffusivity and Thermal Conductivity

Thermal diffusivity of the GNP/PEId composite films was measured by laser flash method (LFA 447 NanoFlash, Netzsch) in through-plane direction. The heat capacity Cp was determined by Differential Scanning Calorimetry (DSC, TA Instruments) and the density of the samples was calculated by the rule of mixtures. Thermal conductivity was calculated by multiplying thermal diffusivity by Cp and density.

Scanning Electron Microscope (SEM) Observation

SEM was used to observe the morphology of the samples at high vacuum mode. The composite film samples were cut and mounted in a cast epoxy holder (manufacture: LECO, St. Joseph, MI). Then the surface was polished with #4000 grit finish, 1 micron alumina powder/water slurry on a LECO LP20 polisher and then 0.05 micron alumina powder/water slurry on a Buehler Vibromet polisher (Lake Bluff, IL) for 2h. The

polished surface was etched by plasma in a chamber filled with O_2 at room temperature and 0.283 torr. A 10nm gold layer was also sputter coated to the surface for observation. For extrusion cast films, cross-sections of both stretching direction (0 degree) and 90 degree direction were observed (Figure 5.4).

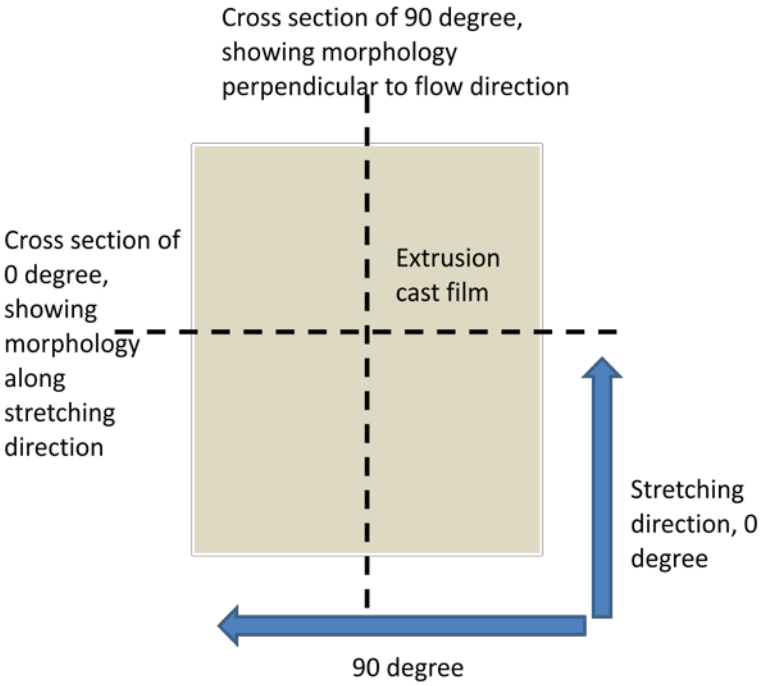

Figure 5.4, Cross-sections that were observed by SEM. Dash-line indicates the direction in which the film was cut.

Tensile Properties

Tensile properties including modulus, strength and elongation were tested under ASTM D638 with a stretching rate of 0.1 in/in/min. A UTS SFM-20 machine (United Calibration Corp.) was used for the testing. The extrusion cast films were cut into Type V specimens with the geometry dimensions shown in Figure 5.5. Samples were cut along both 0 degree and 90 degree directions.

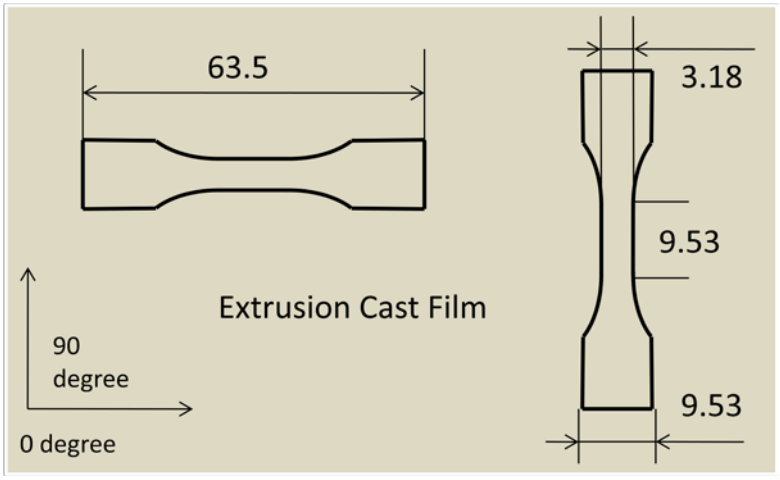

Figure 5.5, Sample preparation for tensile modulus and strength testing

O_2 Permeability

O_2 permeability was measured by MOCON OXTRAN 2/20 model (MOCON, Inc.). The composite film was sandwiched by two pieces of aluminum masks with a 1 cm^2 opening at the center. Permeation of O_2 was measured under a pressure of 30 psi and recorded with a unit of cc/m^2/day. A testing cycle included the following steps: (1) the O_2 detector was re-zeroed at the beginning of each cycle for 30 min with purge of H_2/N_2 mixture, (2) the O_2 detector was connected with testing cell A for 30 min, (3) the O_2 detector was connected with testing cell B for 30 min. Two cells were tested alternatively in a single experiment. Multiple cycles with a typically 12-hour total testing time was applied to all the samples in order to saturate the sample and reach equilibrium state. Typical testing curve is shown in Figure 5.6. The permeability p was then calculated by:

$$p = \frac{\text{Permeation} \times \text{Film Thickness}}{\text{Pressure}}$$

The unit used in this article is cc-m/m^2/day/Pa.

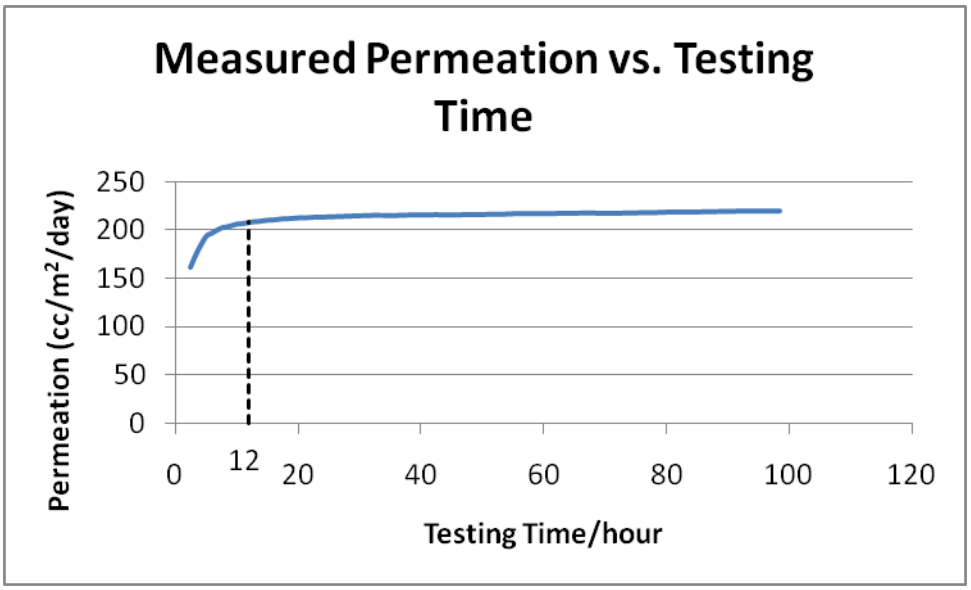

Figure 5.6, Measured permeation vs. testing time for compression molded neat PEId film, showing the plateau after about 12 hours

Results and Discussions

Morphology of Extrusion Cast Films

The properties of the nanocomposites are highly dependent on the morphology, especially for the composites filled by anisotropic fillers. Tandon and Weng used an analytical model to demonstrate the difference in elastic modulus between composites with randomly-oriented fillers and uni-directionally-oriented fillers [10, 11]. In Chapter 3, it was discussed that the injection molded GNP-5/PEId coupon had a tensile modulus in between of Tandon-Weng's unidirectional model and the random model and SEM images showed that the GNP particles were aligned at the near surface region but randomly oriented at the center of the coupon. One major goal of fabricating extrusion cast film is to achieve a more uniform alignment through the entire thickness of the sample, as can be seen in GNP/PEId composite films by

SEM observation (Figure 5.7).

Figure 5.8 shows the change of the particle alignment after annealing for GNP/PEId extrusion cast films. All the films showed significant change in degree of alignment after annealing. Image-Pro Plus software (Media Cybernetics, Inc.) was used to gather information of the angle θ between GNP particle and 0 or 90 degree directions, depending on different cross-sections. For example, in the cross-section of 0 degree direction, the alignment along the 90 degree direction is revealed, with θ the angle between a GNP particle and the 90 degree direction. On the other hand, in the cross-section of the 90 degree direction, the alignment along 0 degree direction is revealed, with θ being the angle between a GNP particle and the 0 degree direction. The degree of alignment was characterized by:

$$a_{11} =< cos^2\theta >$$

Values of a_{11} along different directions are shown in Figure 8. It can be observed that with the increase of stretching ratio, the GNP particles are more aligned in the PEId matrix. However, the alignment appears to reach a maximum at SR=20. Higher stretching ratio (SR=34) cannot further align the particles. After 1 hour annealing, most of the samples showed the same degree of alignment in both 0 and 90 degree directions.

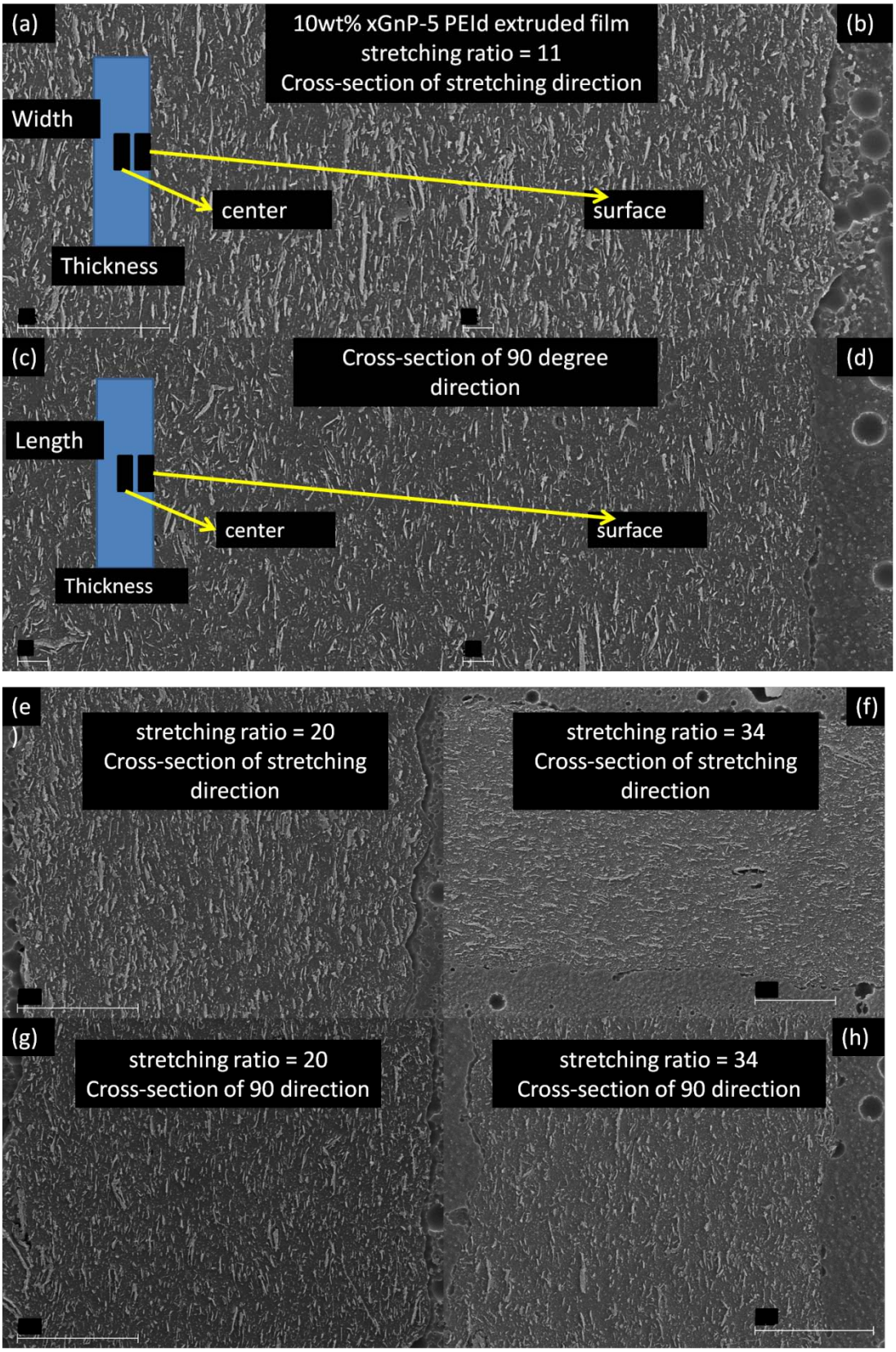

Figure 5.7, SEM images of cross-sections of extrusion cast film, showing GNP particle alignment. The bubbles in the images are on the epoxy putty region, not a feature of the film sample. (scale bars: (a)(e)~(h): 10 micron, (b)~(d): 2 micron)

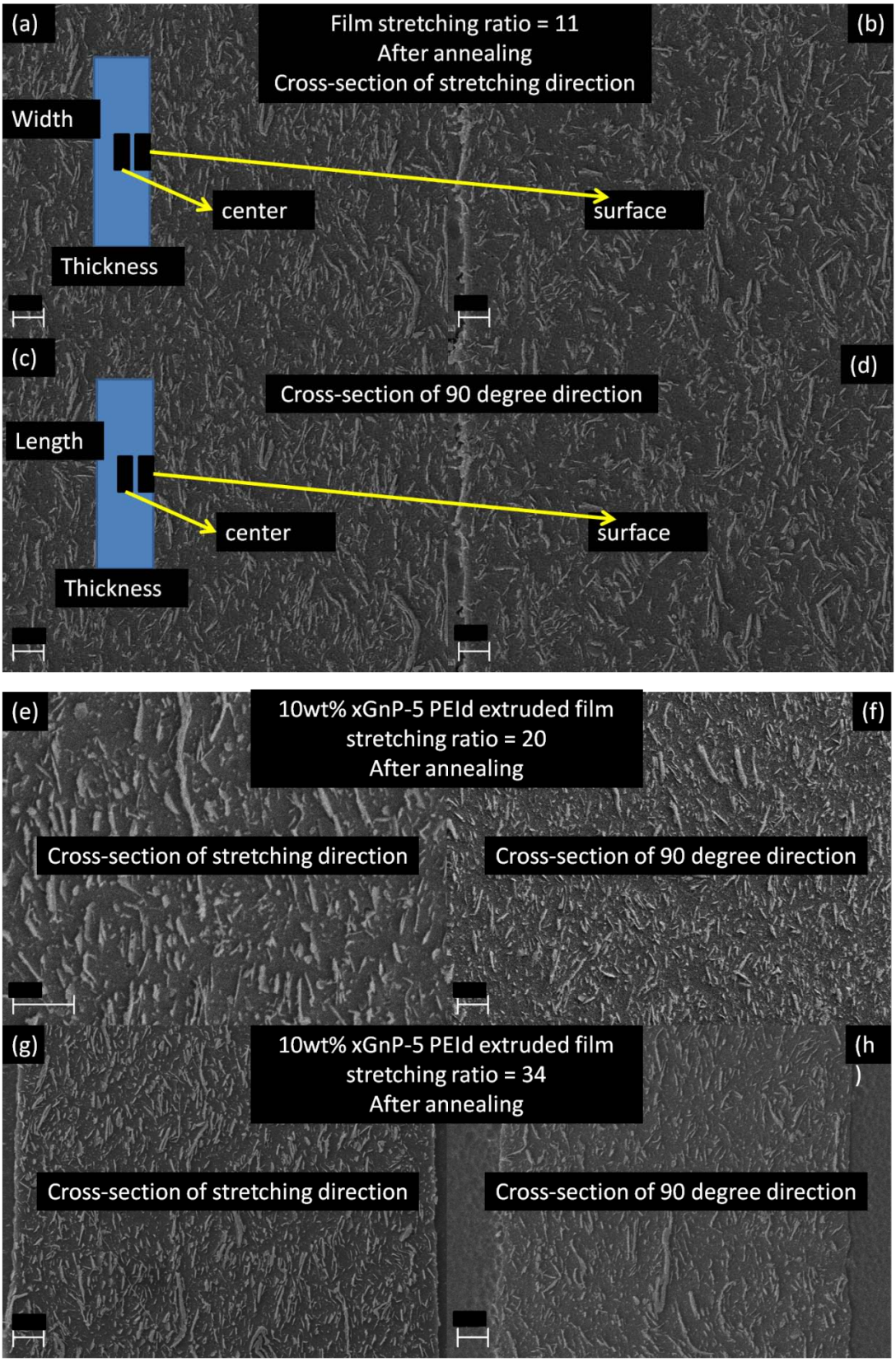

Figure 5.8, SEM images of cross-sections of annealed extrusion cast film, showing the change in GNP particle alignment (scale bars represent 2 micron)

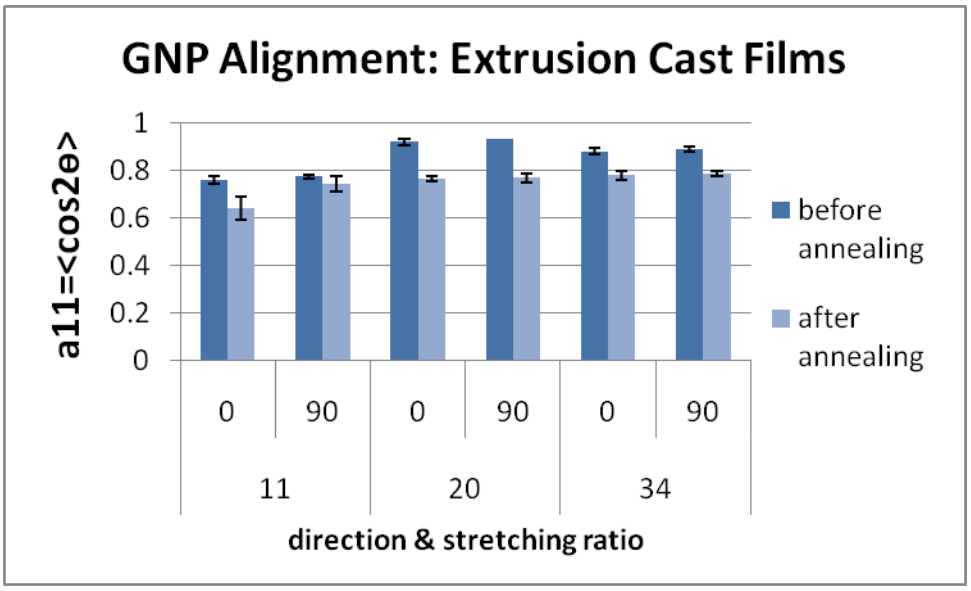

Figure 5.9, Degree of alignment of GNP particles in extrusion cast films

For the film with SR=11, the comparison between Figure 5.7(a)(b) and Figure 5.8(a)(b) indicates that the re-orientation of the particles happens more significantly at close to film surface than the center. This phenomenon implies that the particles close to the surface can rotate more freely than the ones at the center of the film. It is noticed that the re-oriented particles can connect with each other, although the change in degree of alignment is not dramatic, from 0.9 to around 0.75 which can still be considered as preferential alignment (Figure 5.9).

Tensile Properties

Polymer material can be categorized into two types: ductile polymer and brittle polymer. The former would exhibit necking behavior after yielding while the latter would fail before yielding. Neat PEId film shows typical ductile behavior with generation of necking phenomenon and undergoes a long cold draw before failing (Figure 5.10(a), Figure 5.12(a)). With the presence of GNP particles, the composite

film exhibits more like brittle material, which fails without necking. Interestingly, in Figure 5.10(b), it seems that the sample reached yielding but failed immediately. Other tested samples showed similar behavior for SR=11 and SR=20 composite films, indicating that the yielding of the polymer results in the failure of the sample, and no necking probably means that the confinement of the polymer chains by the GNP restricts polymer chain re-arrangement. The failure of the film might be initiated by the GNP particles that are not perfectly aligned or well bonded to the matrix.

However, when the stretching ratio is 34, the film performs as a ductile material in the 0 degree direction. In Figure 5.12, the elongation at break of SR=34 film is significantly higher than its yield elongation and the elongation of other samples. The stress in Figure 5.10(c) reaches a maximum at around 3.7% strain and decreased slightly afterwards, but remains close to the maximum until fracture. This indicates that the presence of GNP particles results in enhanced strength of the composite after the yielding of the matrix. However, such behavior was not observed in the 90 degree direction. The film broke at the same time of yielding, just like SR=11 and SR=20 films (Figure 5.12(b)).

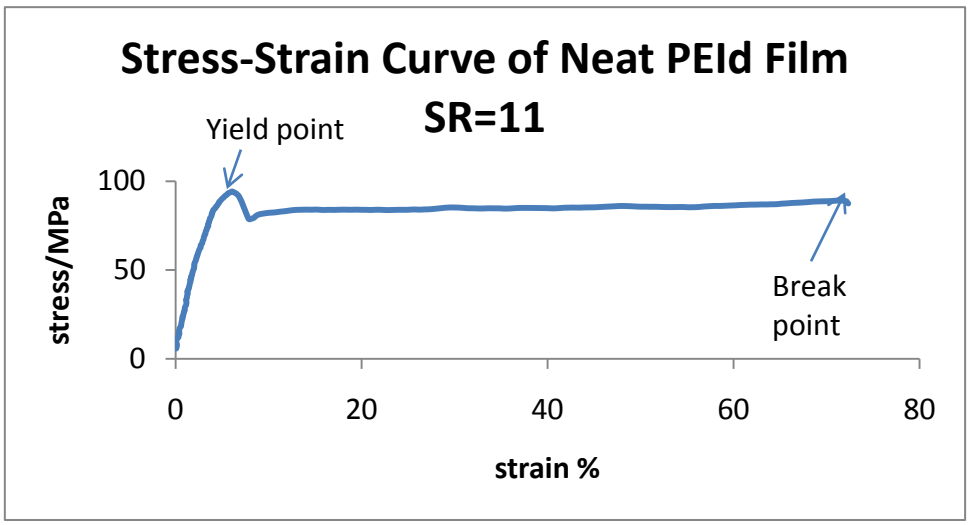

(a)

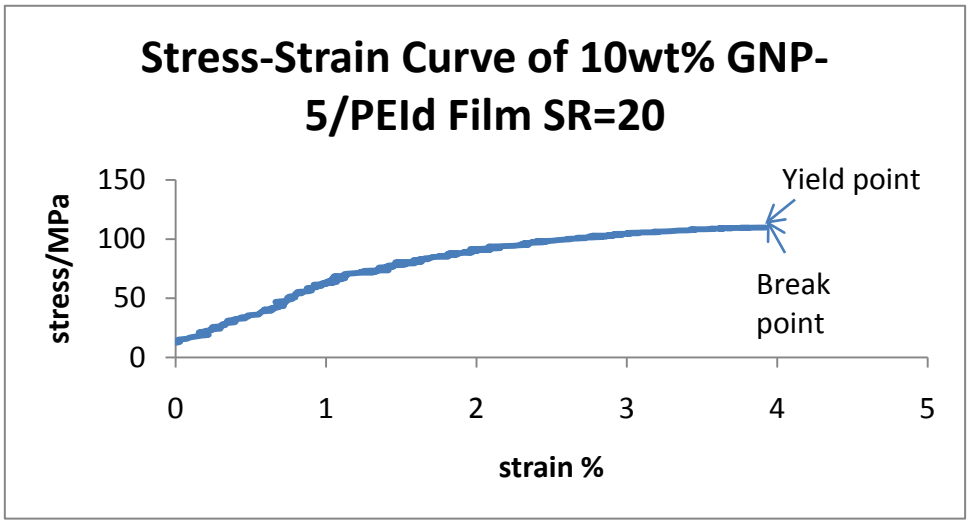

(b)

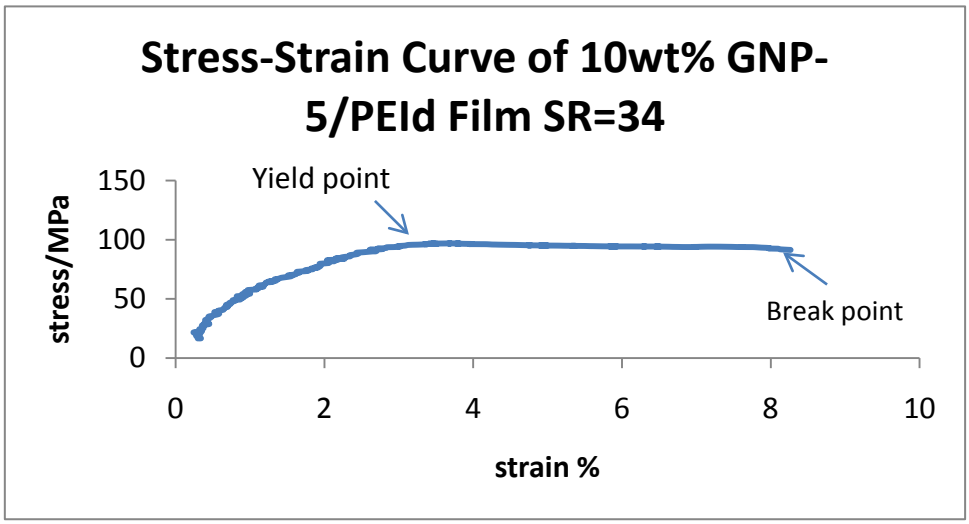

(c)

Figure 5.10, Typical stress-strain curve for extrusion cast films

From the morphology study, it can be observed that the alignment of GNP particles is very uniform in the composite film. Meanwhile, since the film was stretched under relatively high temperature, the amorphous polymer chain can also align along the stretching direction, making the neat polymer to perform like fiber with transverse isotropic properties [12, 13].

Figure 5.11 shows the tensile modulus and strength of GNP-5/PEId films. Both modulus and strength show anisotropic behavior in 0 and 90 degree directions. For modulus, the difference is not obvious for neat PEId film but very significant for composite films. For strength, the difference becomes more significant with the increase in stretching ratio. The highest stretching ratio results in lower modulus and strength, especially for SR=34, which indicates that the film samples might have been over-stretched during the film casting process. Figure 5.12(b) also implies over-stretching with high stretching ratio, showing that the elongation at yield decreases with the increase of the stretching ratio.

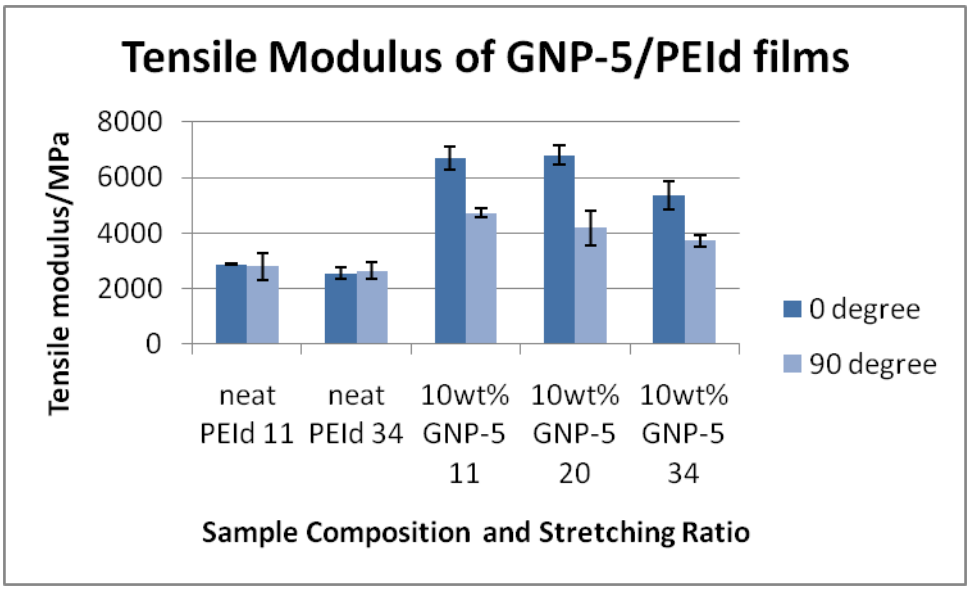

(a)

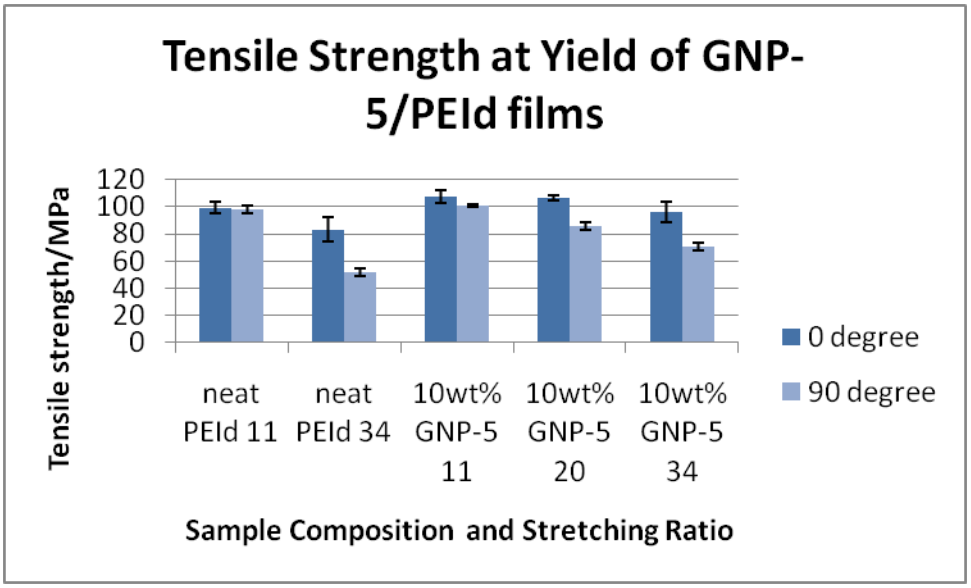

(b)

Figure 5.11, (a) Tensile modulus (b) tensile strength of GNP-5/PEId composites films. According to Figure 10, the strength value shown here is the strength as yield

For 10wt% GNP-5/PEId film with an SR=11, a 134% improvement in modulus and a 9% increase in strength were recorded in the 0 degree direction while the improvement in 90 degree direction were 79% and 3% respectively. Since the degree of alignment for the GNP particles is the same in both directions (Figure 5.9), the cause of the

difference can be attributed to the polymer chain alignment. Considering that the neat polymer did not exhibit such large difference in the two directions, the presence of GNP might also increase the extent that the polymer chains get aligned.

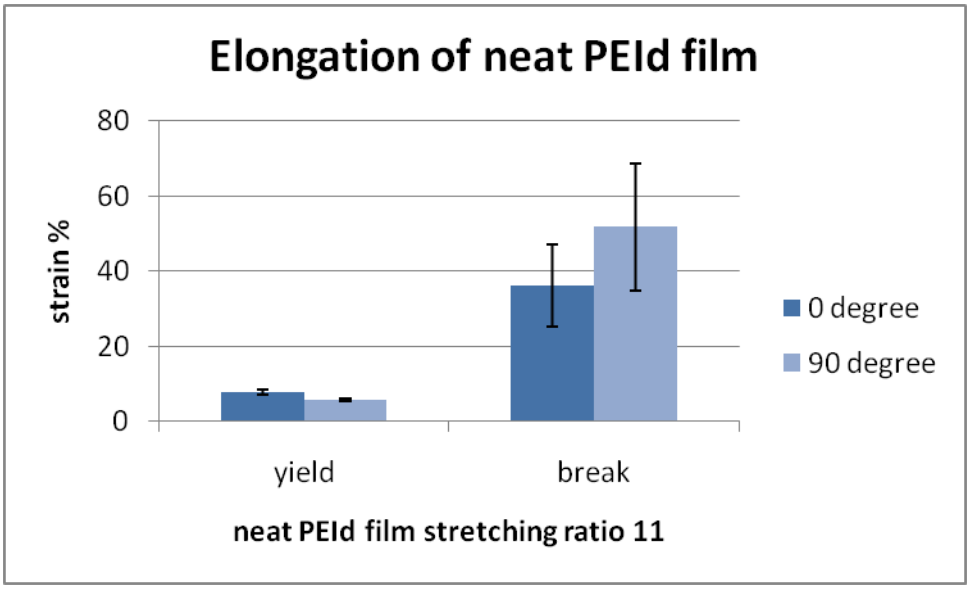

(a)

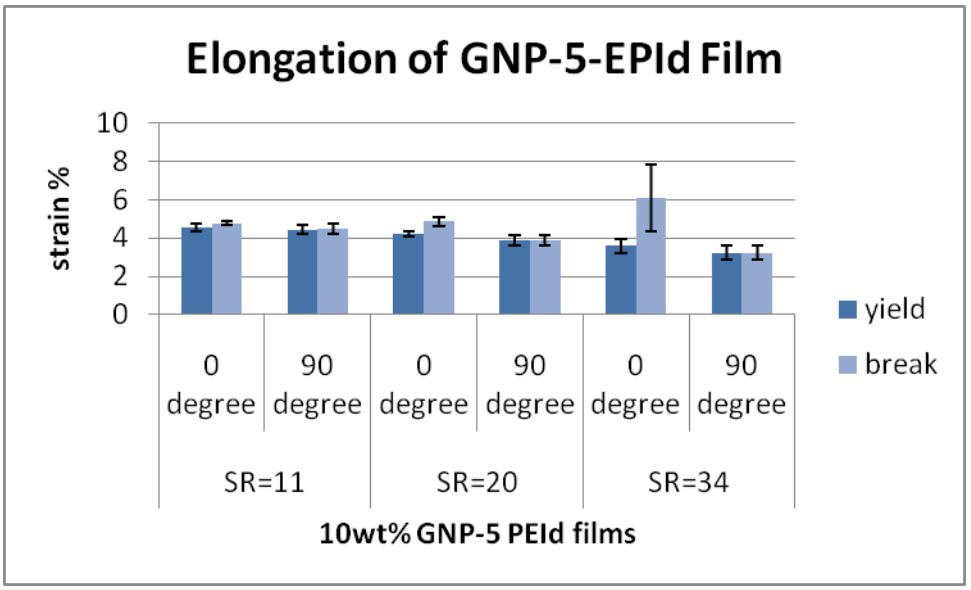

(b)

Figure 5.12, Elongation of film during tensile testing (a) neat PEId film (b) GNP-5/PEId composite film

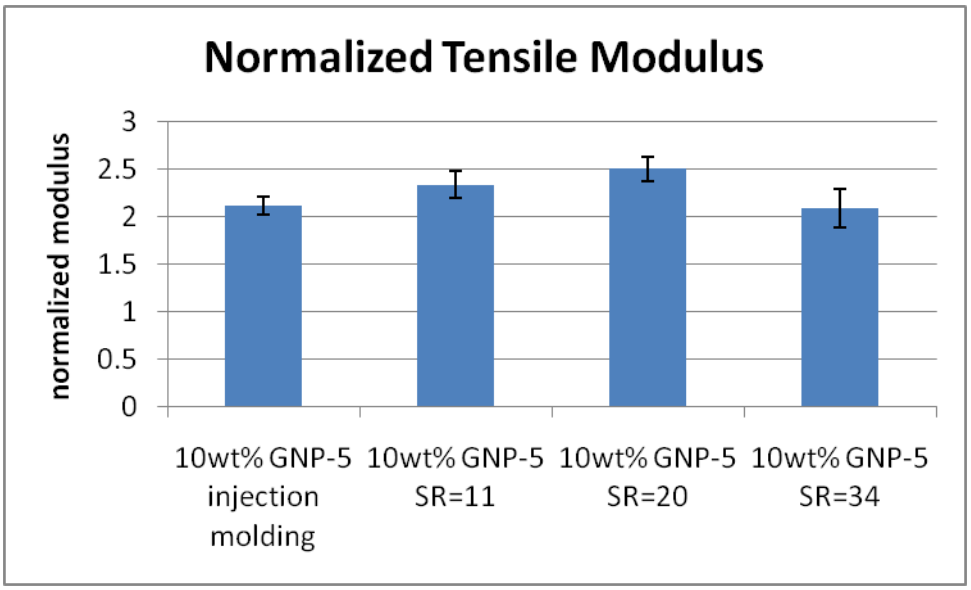

(a)

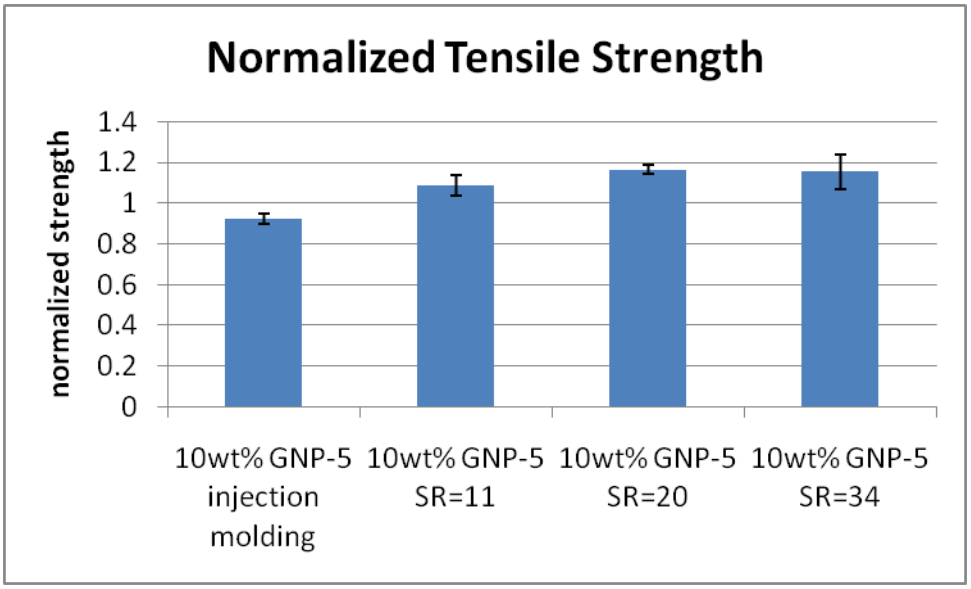

(b)

Figure 5.13, Normalized tensile modulus and tensile strength, showing comparison between injection molded coupon and films made from various stretching ratios (a) modulus (b) Strength

When compared to injection molded composite coupons (Chapter 3), the stretched films show higher modulus and strength due to better alignment. Due to the fact that the injection molded coupon and the film were measured with different sample dimensions, the values are normalized by the modulus and strength of the neat samples that were fabricated under the same condition. An ascending trend can be

observed from injection molded samples to films with higher stretching ratio for both modulus and strength, except for SR=34 films possibly due to severe overstretching (Figure 5.13). This trend indicates the benefit of particle alignment on both tensile modulus and tensile strength.

O_2 Permeability

Polymer and composite membranes have been widely used as either barrier to small molecules or selective separator for gases [14-16]. The morphology of the filler is the deciding factor for the change of the permeability. Unless specially modified to enhance the bonding between filler and matrix, spherical particles like silica would actually enlarge the permeability due to poor interface between filler and matrix and can be used as gas separators due to selectivity to gas types [17-19]. However, Amino silane-modified clay resulted in reduced permeability to gases for the same matrix because of chemical coupling between filler and matrix [18, 20]. Nunes [20], Takahashi [17, 18] and Kim [19] suggested that the dispersion state of the nanoparticles is the key to the barrier properties. For platelet-shaped fillers such as layered-silicate and graphite, the gas permeability of their composites is usually reduced, due to the tortuous zigzag path forced by impenetrable platelet fillers [15, 21]. The alignment and aspect ratio of the filler are two major factors for the permeability of the composites as indicated by Bharadwaj's model [22]:

$$\frac{p_c}{p_m} = \frac{1-\phi}{1+\frac{\rho}{2}\phi<cos^2\theta>} \quad (1)$$

Where p_c and p_m are the permeability of composite and neat matrix polymer respectively. The ratio between is determined by filler volume fraction ϕ, the aspect ratio of the filler ρ and the degree of alignment $a =< cos^2\theta >$. It can be seen from Equation (1) that the higher aspect ratio and alignment lead to lower permeability of the composite.

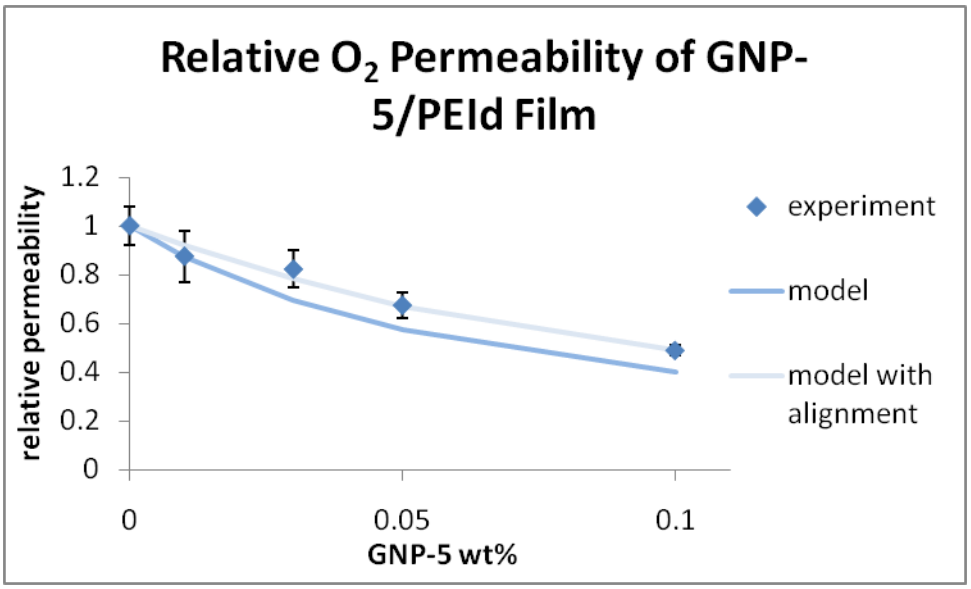

Figure 5.14, Relative O_2 Permeability of compression molded GNP-5/PEId film. Series "model" was calculated by assuming perfect alignment $a = 1$. Series "model with alignment" was calculated using the a value shown in Figure 5.15.

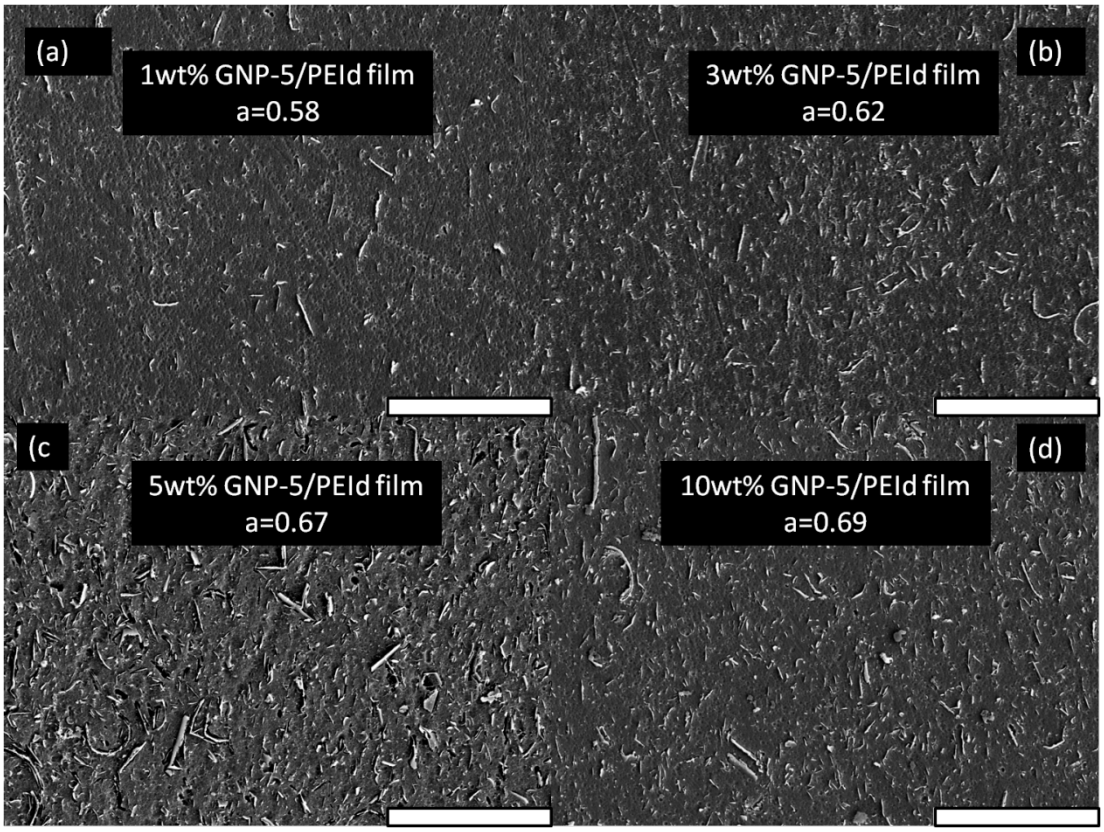

Figure 5.15, SEM images of compression molded GNP-5/PEId film, showing alignment of GNP particles. The a values shown in the images are averages from images taken at different position of the sample (Scale bars represent 20 micron)

Figure 5.14 indicates that the O_2 permeability decreases with the increase of GNP-5 content. With 10wt% GNP-5 added, the permeability of the composite film is reduced to about 50% of that of the neat polymer. The aspect ratio of the GNP-5 particles is set to 47 according to Chapter 3. In Figure 5.14, if perfect alignment is assumed, the model prediction is over-estimating the effect of the filler. Figure 5.15 shows the SEM images of the cross-section of compression molded films. The degree of alignment is used in equation (1) and the corresponding predicted value is shown in Figure 5.14 as “model with alignment”. It can be seen that this model correlates with the experimental data very well.

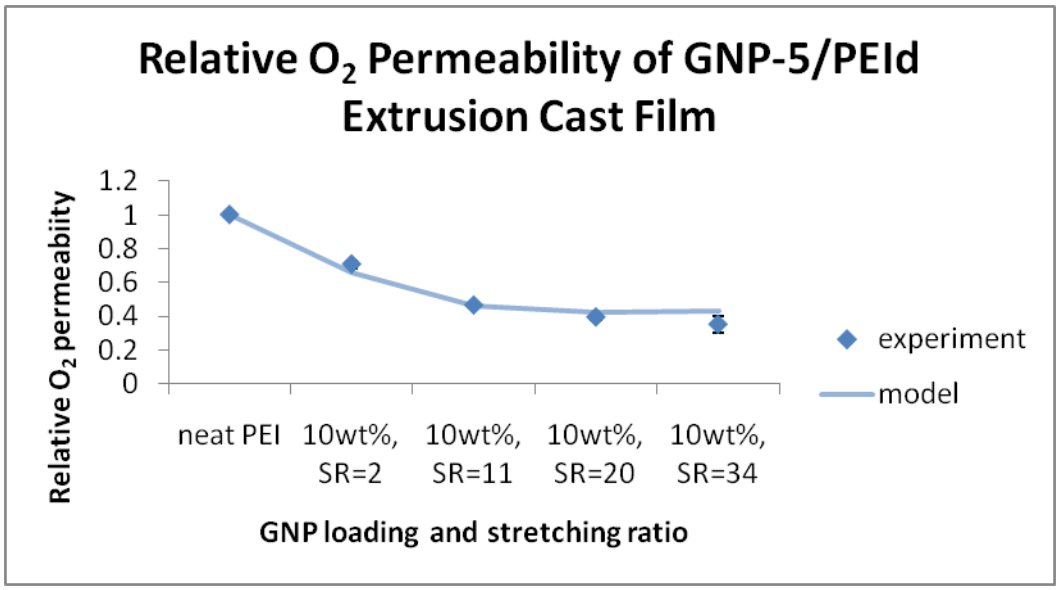

Figure 5.16, Relative O_2 permeability of GNP-5/PEId extrusion cast film

Figure 5.16 shows the relative O2 permeability of extrusion cast film with various stretching ratios. With the increase of stretching ratio, the permeability decreases. About 65% decrease is observed for the film with SR=34. The series "model" is calculated from Equation (1) with an aspect ratio of 47 and α values in Figure 5.9. It can be observed that the model proposed by Bharadwaj predicts the behavior of the stretched GNP/PEId films very well.

Effect of Annealing

Figure 5.8 and Figure 5.9 show the change of GNP particle alignment after 1 hour 340℃ annealing. The re-arrangement of the GNP orientation helps the connection between particles thus enhance both electrical and thermal conductivity for the composite.

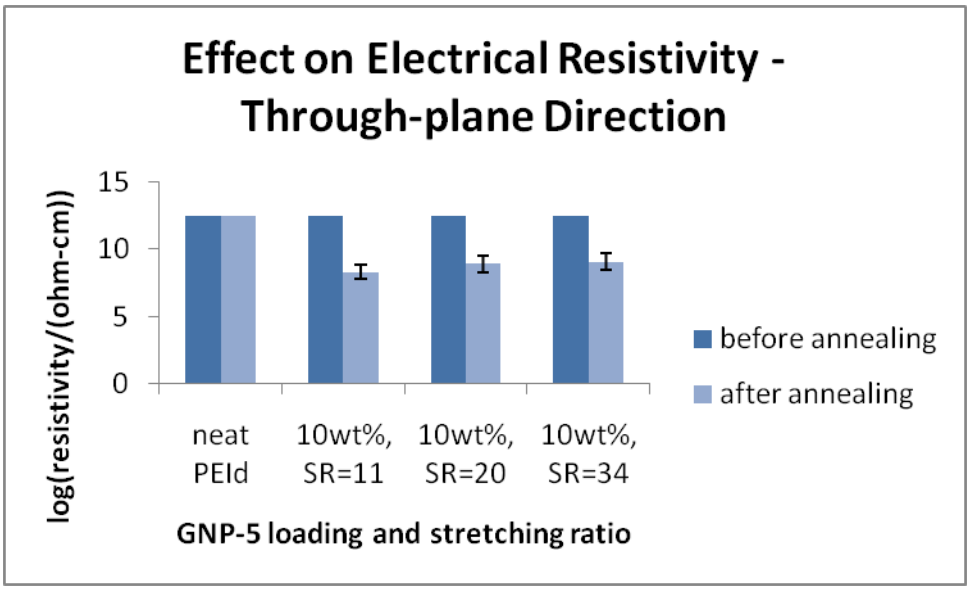

(a)

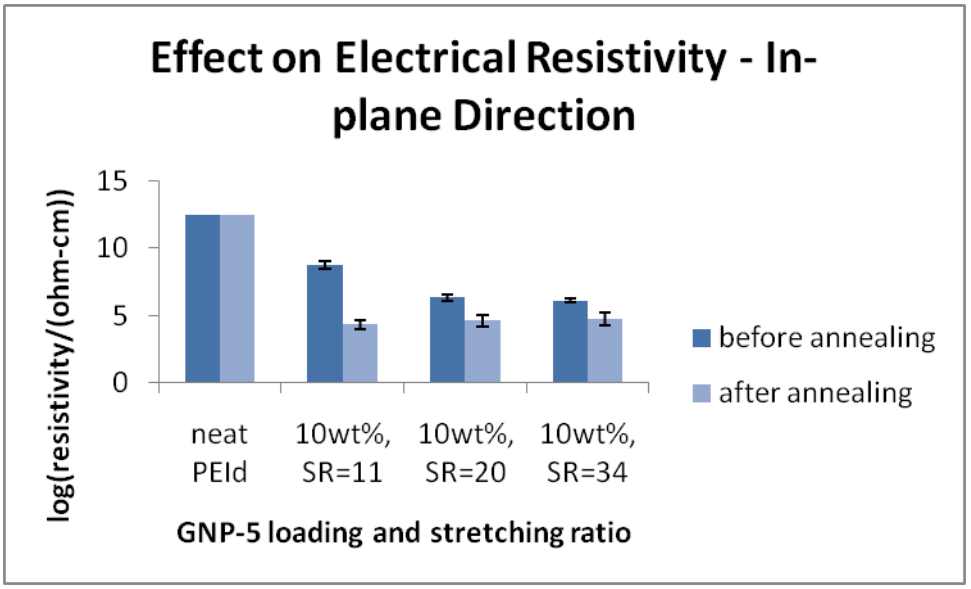

(b)

Figure 5.17, Effect of annealing on electrical resistivity of GNP-5/PEId extrusion cast films (a) through-plane direction (b) in-plane direction

Figure 5.17 indicates that 1 hour annealing would reduce the resistivity of the composite film significantly in both through-plane and in-plane directions. About 4 orders of magnitude decrease was observed for all samples.

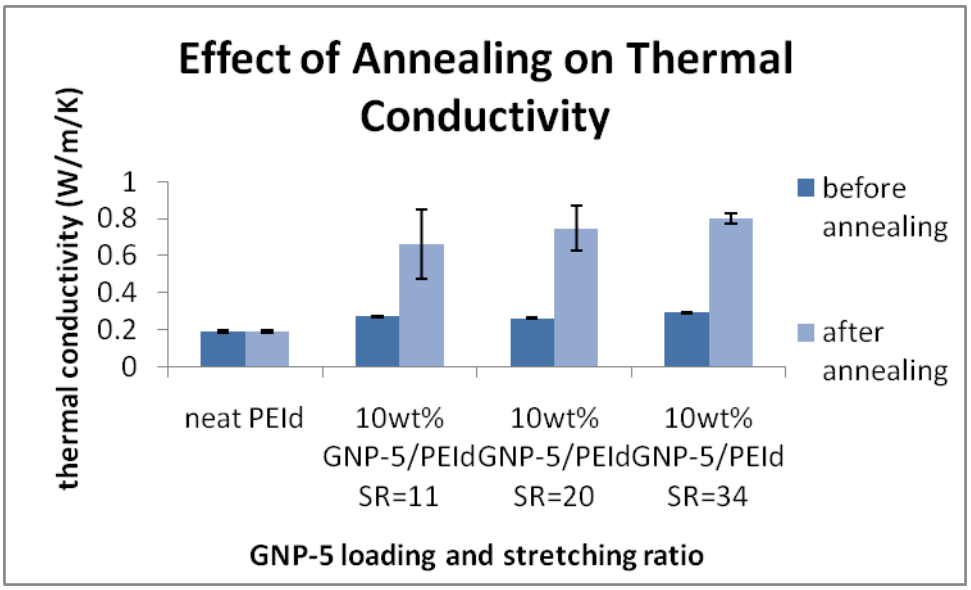

Figure 5.18, Effect of annealing on thermal conductivity of GNP-5/PEId extrusion cast film

The same effect can also be observed for thermal conductivity. Figure 5.18 shows a increase of 173% in the through-plane thermal conductivity for 10wt% composite films. The reason of the improvement is that the GNP particles re-oriented after annealing (Figure 5.8, 5.9). Figure 5.8 clearly shows that the particles are less aligned in the in-plane direction after annealing, acting as better heat conductors in the through-plane direction for the film. Figure 5.9 shows significant decrease of degree of alignment in the in-plane direction, which means an increase of that in the through-plane direction. Since the GNP particle has very high anisotropic thermal conductivity (high in-plane, low through-plane), the alignment change resulted in significant improvement in through-plane conductivity after annealing.

Conclusions

Neat PEId and GNP-5/PEId films have been successfully fabricated via extrusion cast

and unidirectional stretching. The alignment of the GNP particles formed by extrusion cast fabrication benefited the modulus and strength as compared with injection molded coupons. The addition of GNP particles changed the polymer from ductile to brittle type material. However, with SR=34, the composite exhibited ductile behavior during tensile testing with less strength drop after yielding during necking process. The unidirectional stretched film behaved anisotropically. For the 10wt% GNP-5/PEId film with SR=11, a 134% improvement in modulus and a 9% increase in strength were recorded in the 0 degree direction while the improvement in the 90 degree direction was 79% and 3% respectively. A 50% decrease of O2 permeability has been observed for compression molded 10wt% GNP-5/PEId film while a 65% decrease was recorded for extrusion cast film at the same loading. It was found that Bharadwaj's model can predict the permeability for GNP-5/PEId system very well if incorporated with the alignment information of GNP particles obtained by SEM observation. Annealing was effective to re-orient the GNP particles and provide connection between them, resulting in improved electrical and thermal conductivity. However, permeability may also be increased due to less aligned particles after annealing as indicated by Bharadwaj's model (Equation 1). SEM images showed that the degree of alignment dropped from around 0.9 to around 0.76. Due to the good barrier property and improved electrical and thermal conductivity, the GNP film has high potential for use where multifunctional properties are required.

REFERENCES

REFERENCES

1. http://www.sabic-ip.com. Last visited: March 2011

2. Bauhofer, W. and J.Z. Kovacs, *A review and analysis of electrical percolation in carbon nanotube polymer composites.* Composites Science and Technology, 2009. **69**(10): p. 1486-1498.

3. Choudalakis, G. and A.D. Gotsis, *Permeability of polymer/clay nanocomposites: A review.* European Polymer Journal, 2009. **45**(4): p. 967-984.

4. Kalaitzidou, K., H. Fukushima, and L.T. Drzal, *Multifunctional polypropylene composites produced by incorporation of exfoliated graphite nanoplatelets.* Carbon, 2007. **45**(7): p. 1446-1452.

5. Lan, T. and T.J. Pinnavaia, *CLAY-REINFORCED EPOXY NANOCOMPOSITES.* Chemistry of Materials, 1994. **6**(12): p. 2216-2219.

6. Zenkiewicz, M., J. Richert, and A. Rozanski, *Effect of blow moulding ratio on barrier properties of polylactide nanocomposite films.* Polymer Testing, 2010. **29**(2): p. 251-257.

7. Kim, H. and C.W. Macosko, *Processing-property relationships of polycarbonate/graphene composites.* Polymer, 2009. **50**(15): p. 3797-3809.

8. Shiromoto, S., et al., *A Neck-in Model in Extrusion Lamination Process.* Polymer Engineering and Science, 2010. **50**(1): p. 22-31.

9. Lee, S.Y., S.Y. Park, and H.S. Song, *Lamellar crystalline structure of hard elastic HDPE films and its influence on microporous membrane formation.* Polymer, 2006. **47**(10): p. 3540-3547.

10. Tandon, G.P. and G.J. Weng, *THE EFFECT OF ASPECT RATIO OF INCLUSIONS ON THE ELASTIC PROPERTIES OF UNIDIRECTIONALLY ALIGNED COMPOSITES.* Polymer Composites, 1984. **5**(4): p. 327-333.

11. Tandon, G.P. and G.J. Weng, *AVERAGE STRESS IN THE MATRIX AND EFFECTIVE MODULI OF RANDOMLY ORIENTED COMPOSITES.* Composites Science and Technology, 1986. **27**(2): p. 111-132.

12. Murakami, S., et al., *A STUDY ON THE STRUCTURAL-CHANGES DURING UNIAXIAL DRAWING AND OR HEATING OF POLY(ETHYLENE NAPHTHALENE-2,6-DICARBOXYLATE) FILMS.* Polymer, 1995. **36**(2): p. 291-297.

13. Matsuo, M., et al., *Characteristics of ultradrawn polyethylene films as a function of temperature estimated by the positron annihilation lifetime method.* Macromolecules, 2002. **35**(8): p. 3059-3065.

14. Stern, S.A., *POLYMERS FOR GAS SEPARATIONS - THE NEXT DECADE.* Journal of Membrane Science, 1994. **94**: p. 1-65.

15. LeBaron, P.C., Z. Wang, and T.J. Pinnavaia, *Polymer-layered silicate nanocomposites: an overview.* Applied Clay Science, 1999. **15**(1-2): p. 11-29.

16. Giannelis, E.P., *Polymer-layered silicate nanocomposites: Synthesis, properties and applications.* Applied Organometallic Chemistry, 1998. **12**(10-11): p. 675-680.

17. Takahashi, S. and D.R. Paul, *Gas permeation in poly(ether imide) nanocomposite membranes based on surface-treated silica. Part 1: Without chemical coupling to matrix.* Polymer, 2006. **47**(21): p. 7519-7534.

18. Takahashi, S. and D.R. Paul, *Gas permeation in poly(ether imide) nanocomposite membranes based on surface-treated silica. Part 2: With chemical coupling to matrix.* Polymer, 2006. **47**(21): p. 7535-7547.

19. Kim, J.H. and Y.M. Lee, *Gas permeation properties of poly(amide-6-b-ethylene oxide)-silica hybrid membranes.* Journal of Membrane Science, 2001. **193**(2): p. 209-225.

20. Nunes, S.P., et al., *Membranes of poly(ether imide) and nanodispersed silica.* Journal of Membrane Science, 1999. **157**(2): p. 219-226.

21. Yano, K., et al., *SYNTHESIS AND PROPERTIES OF POLYIMIDE CLAY HYBRID.* Journal of Polymer Science Part a-Polymer Chemistry, 1993. **31**(10): p. 2493-2498.

22. Bharadwaj, R.K., *Modeling the barrier properties of polymer-layered silicate nanocomposites.* Macromolecules, 2001. **34**(26): p. 9189-9192.

Chapter 6 Dispersion Optimization of Exfoliated Graphene Nanoplatelet in Polyetherimide Nanocomposites: Extrusion vs. Pre-Coating vs. Solid State Ball Milling

Abstract

Polyetherimide (PEId) nanocomposites reinforced with high stiffness and electrically conductive exfoliated graphite (graphene) nanoplatelets (GNP, ~10nm thick and ~1-15 microns in diameter) were fabricated by various processing methods to achieve good dispersion including: melt-extrusion, pre-coating of the polymer powder with GNP , solid state ball milling as well as combinations of these methods. GNP compounded with PEId by melt extrusion have a high percolation threshold (~10wt%). In order to lower the percolation threshold, a pre-coating method using a non-solvent was used, in which the GNP particles are coated onto the PEId polymer powder surface by surface deposition from a non-solvent. As a result of this processing approach, the electrical conductivity is greatly increased with a percolation threshold as low as 2wt%. However, the electrical conductivity improvement comes at the expense of only a very small increase in flexural modulus

and a reduction in flexural strength to a value lower than the neat polymer. Solid state ball milling (SSBM) was investigated as an alternative process to enhance dispersion, adhesion and to reduce GNP size. High electrical conductivity and improved modulus were achieved by this approach along with better mechanical properties. Further improvements to the mechanical properties could be made by combining the extrusion and SSBM approaches. Examination of the nanocomposite morphology explains the effect of these combined compounding approaches on GNP particle dispersion and their relation to the improved GNP/PEId nanocomposite performance.

Introduction

Nanocomposites are defined as composite materials with at least one Gibbsian solid phase where at least one dimension is in the nanometer range (1-100 nm) [1]. Graphene based nanoparticles, which combine good electrical and thermal properties similar to CNTs and the two-dimensional morphology similar to silica-alumina layered clays, are considered to be potentially excellent multifunctional nanoparticles. The process of generating thin graphene nanoplatelets consisting of several layers of graphene sheets is relatively simple and cost-effective. Usually, three steps are involved in fabricating these nanoparticles from natural graphite: (i) intercalation, where both electron-donor agents and electron acceptors can be intercalated in between graphene layers; (ii) exfoliation, where a large amount of heat is applied to expand the intercalated agents; (iii) pulverization, where

the exfoliated graphite is down-sized to smaller platelets. As demonstrated by Drzal's group [2, 3], exfoliated graphite nanoplatelets (GNP) can be fabricated from acid intercalation, microwave heating and ultra-sonic pulverization. Cost-effective industrial scale manufacturing can be attained by this route (XG Sciences, Inc., www.xgsciences,com, East Lansing, MI). The GNP nanoplatelet lateral width is controllable during fabrication. Typical sizes of the nanoplatelets include 1 micron, 5 micron, and 15 micron in diameter and usually notated as GNP-1, GNP-5 and GNP-15 respectively.

The properties of a nanocomposite are highly affected by its compounding method which may alter the distribution, separation and orientation of the nanoparticles. Typical compounding methods for thermoplastic matrix include [4]: (1) melt compounding, such as high density polyethylene (HDPE) and exfoliated graphite mixed in a Brabender mixer [5, 6] or twin-screw extrusion [7]; (2) solution mixing, where a solvent is used to dissolve the polymer and then the graphite is added and dispersed [8, 9]; (3) in-situ polymerization, where monomers are usually intercalated in between graphite layers followed by polymerization which at the same time exfoliates the graphite [10, 11].

While it is convenient in industrial application, melt-extrusion falls short of attaining the electrical conductivity at low percolation threshold of the resulting composite [4, 12]. Solution mixing is capable of separating and dispersing nanoparticles which results in lower percolation threshold [13], but the use and recovery solvent is problematic from an environmental and cost perspective. In-situ polymerization can

only be applied to a limited category of polymers. Efforts have been made to find a practical and efficient way to disperse the graphene nanoplatelets in order to achieve lower percolation threshold. Some researchers used unsaturated polyester resin (UPR) to modify expanded graphite [14] followed by melt-extrusion which resulted in a percolation threshold at 5.7wt%, instead of 22.2wt% for composites with conventional graphite. Recently, Drzal's group[4] developed a 'pre-coating' method to achieve low percolation threshold where a non-solvent of the polymer is used to disperse GNP particles. After adding polymer powder into this suspension, the GNP particles can deposit on the polymer surface resulting in a controllable, continuous coating on the surface of the polymer powder. Subsequent compression molding results in deformation and consolidation of the polymer but the continuous GNP phase remains intact after the molding process forming a low concentration percolated network.

The main purpose of this research is to find an alternative compounding method for adding GNP to amorphous high temperature thermoplastics, such as polyetherimide (PEId) which has a high glass transition temperature, extremely good chemical resistance and excellent thermal stability, in order to achieve better nanocomposite mechanical properties and a low percolation threshold. Three compounding methods were used and compared. First, the GNP/PEId nanocomposites were fabricated from melt-extrusion. The flexural modulus and strength were measured along with electrical resistivity and the percolation threshold. To further improve electrical conductivity and lower the percolation threshold, the pre-coating method

using a non-solvent (acetone) was used. The third method, solid state ball milling (SSBM) of the dry mixture of PEId and GNP was investigated, where the GNP and PEId are combined in a mill along with metal balls in a vibrating chamber at room temperature (far below the Tg of the PEId), as an alternative process to enhance the adhesion between PEId and GNP particles and at the same time to reduce particle size. This solvent-free method is believed to be a simple, cost-effective method having advantages over the pre-coating method to fabricate composites with low percolation threshold.

Experimentation

Materials

Polyetherimide (PEId) was obtained from GE Plastics (Ultem 1010, in two forms: pellet and powder). GNP-1 (particles with a diameter of 1 micron) and GNP-15 (particles with a diameter of 15 micron) were prepared in our lab [2].

Melt-extrusion

Melt-extrusion was carried on Leistritz twin-screw extruder (MIC27/6L-48D). The screws were operating in the counter-rotation mode. Barrel temperatures were set to 330℃, with a melt temperature at 340℃. The die pressure was at around 5.5MPa. Screw speed was set at 100 rpm. The pellet product obtained from melt-extrusion was pulverized into powder by a cryogenic mill.

Pre-coating

GNP was first dispersed in acetone under ultrasonication. PEId powder (~300 microns in diameter) was then added into the suspension while stirring. Acetone was then evaporated. The mixture was further mixed in a Speed Mixer (Flextec Corporation). The sample was dried in a vacuum oven at 120℃.

Solid State Ball Milling (SSBM)

SSBM was carried out in SPEX SamplePrep 80000 Dual Mixer/Mill. 10 gram sample (PEId and GNP) was placed in a cylindrical hardened steel vial (5.7 cm diameter, 7.62 cm long) with four 6.35 mm and two 12.7 mm steel balls. During processing, two vials were vibrated at high frequency in the device. The processing time was 200 minutes. Both neat polymer powder and extrusion-compounded composite powder were used in the vial with or without additional GNP. The resulting material after SSBM is in flake-like shape with a typical size of 150 micron in diameter and a few microns in thickness (Figure 6.1). The particle shown in Figure 1 consists of several smaller particles sitting on a larger plate, indicating a wide size distribution and some extend of re-agglomeration of the particles.

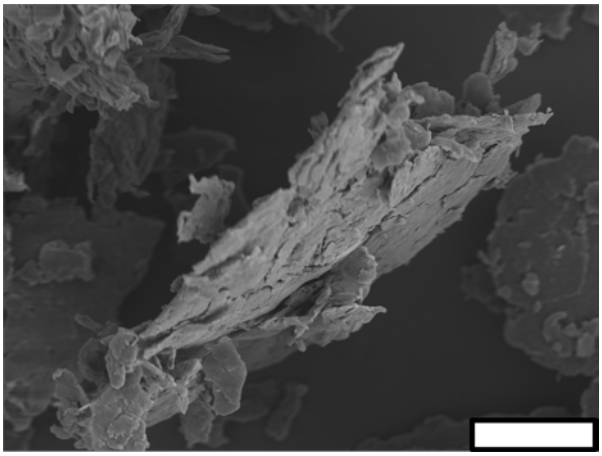

Figure 6.1, SEM image of GNP-PEId composite after SSBM, showing geometry of the particles (Scale bar represents 50 micron)

Compression Molding

After compounding, the composite material was compression molded in a CARVER Laboratory Press (Model 2731, Fred S. Carver INC.). A picture-framed mold was used with a dimension of 76mm × 76mm × 3mm. The material was heated to 340℃ and held for 15 min. A compression pressure of 20MPa was applied to the material and was held for 45 min in order to achieve better consolidation. After that, the press was cooled by water.

Electrical Resistivity Measurement

The resistance of GNP/PEId composites was measured in two directions: the through-plane direction (thickness direction) which was the same direction as the applied pressure in compression molding and the in-plane direction which was perpendicular to pressure. The resistance value was then converted into resistivity by taking into account the sample dimensions.

Flexural Strength and Modulus Testing

Flexural strength and modulus were tested under ASTM 790 standard on a UTS SFM-20 machine (United Calibration Corp.) at room temperature. The test was performed at a flexural rate of 0.03 in/min. Maximum force, instead of force at 5% strain, was used to calculate the strength of the composite.

Scanning Electron Microscope (SEM) Observation

A JEOL JSM-6400 (Tokyo, Japan) SEM was used to observe the morphology of the samples. The powder form samples were observed directly with a 10nm gold layer that was sputter coated. The composite flex bar samples were cut and mounted in a cast epoxy holder (manufacture: LECO, St. Joseph, MI). Then the surface was polished with #4000 grit finish, 1 micron alumina powder/water slurry on a LECO LP20 polisher and then 0.05 micron alumina powder/water slurry on a Buehler Vibromet polisher (Lake Bluff, IL) for 2h. The polished surface was etched by plasma in a chamber filled with O_2 at room temperature and 0.283 torr. A 10nm gold layer was also sputter coated to the surface for observation.

Results and Discussions

Electrical Conductivity

Figure 6.2 shows the electrical resistivity of the GNP/PEId composites. The resistivity in the in-plane direction is always lower than that in the through-plane direction due

to the particle anisotropy and alignment during compression molding (Figure 6.3 (a)). The percolation threshold of melt-extrusion processed nanocomposites is higher than 10wt% (about 5 vol%). This is mainly because during melt-extrusion the high polymer melt viscosity prevents the nanoparticles from forming a percolated network (Figure 6.3 (b)). While the GNP particles were homogeneously distributed into the polymer matrix during melt-extrusion, the stacked layers of graphene formed by the platelet-shape nature could not be separated efficiently during extrusion, reducing the number of effective nanoparticles. The size reduction during melt-extrusion (Figure 6.3 (b)) also affects electrical conductivity because of the decrease of aspect ratio. Encapsulation of the GNP by the polymer matrix prevents the GNP particles from touching each other resulting in a lower conductivity [15].

Mixing the GNP and PEId in a solvent (dichloromethane) resulted in improved conductivity and reduced the percolation threshold ~5wt%. One possible explanation is that in a solvent system, the viscosity is much lower than in a melt system, so the polymer chains move freely and are able to permeate into the graphite layers, preventing the graphene sheets which are separated by ultrasonication from re-stacking. The net result is that the concentration of effective particles would then be much more than in melt-extrusion.

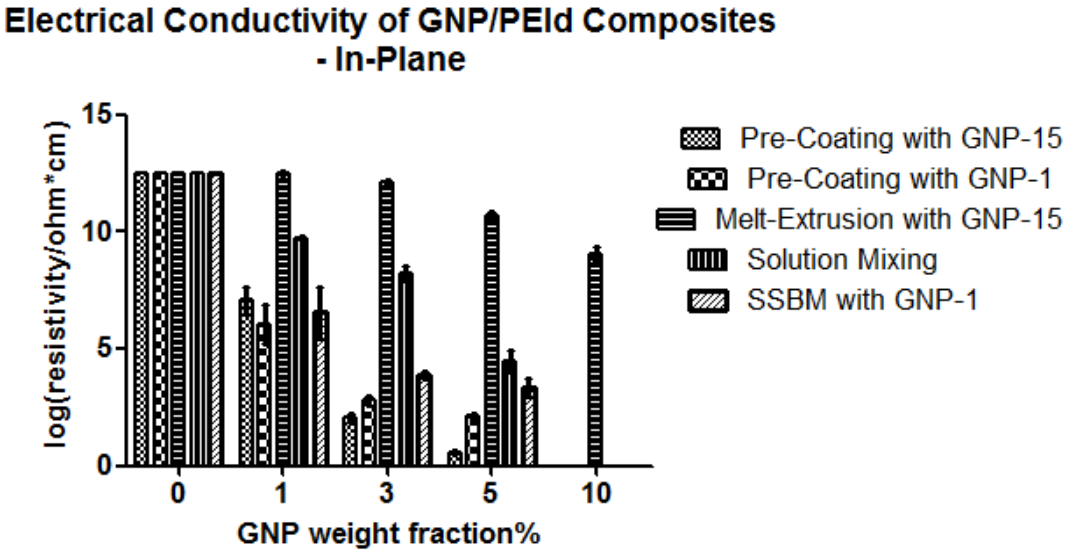

(a)

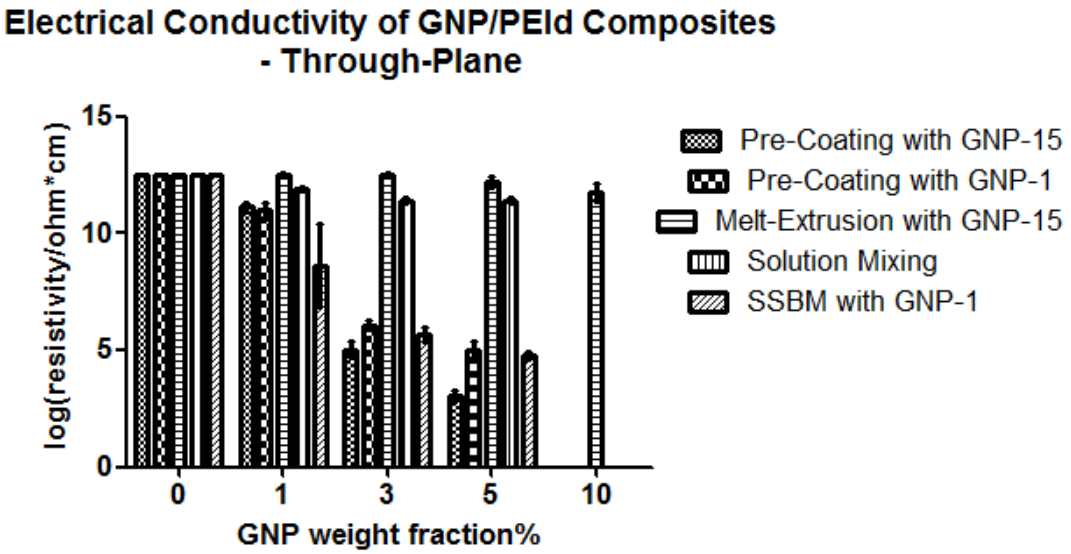

(b)

Figure 6.2, Comparison of electrical resistivity of GNP/PEId composites from different compounding methods: (a) in-plane direction (b) through-plane direction.

Pre-coating compounding and SSBM both produce nanocomposites with a low percolation threshold at lower than 3wt%. Composites from SSBM show the lowest percolation threshold at 1wt% (the relatively larger error bar is due to that the 1wt% loading is just around percolation threshold where a little variation inside the sample

can result in a large difference in electrical resistivity), the electrical conductivity of which is greater that the nanocomposites produced by pre-coating in the through-plane direction but falls short in the in-plane direction at higher loadings.

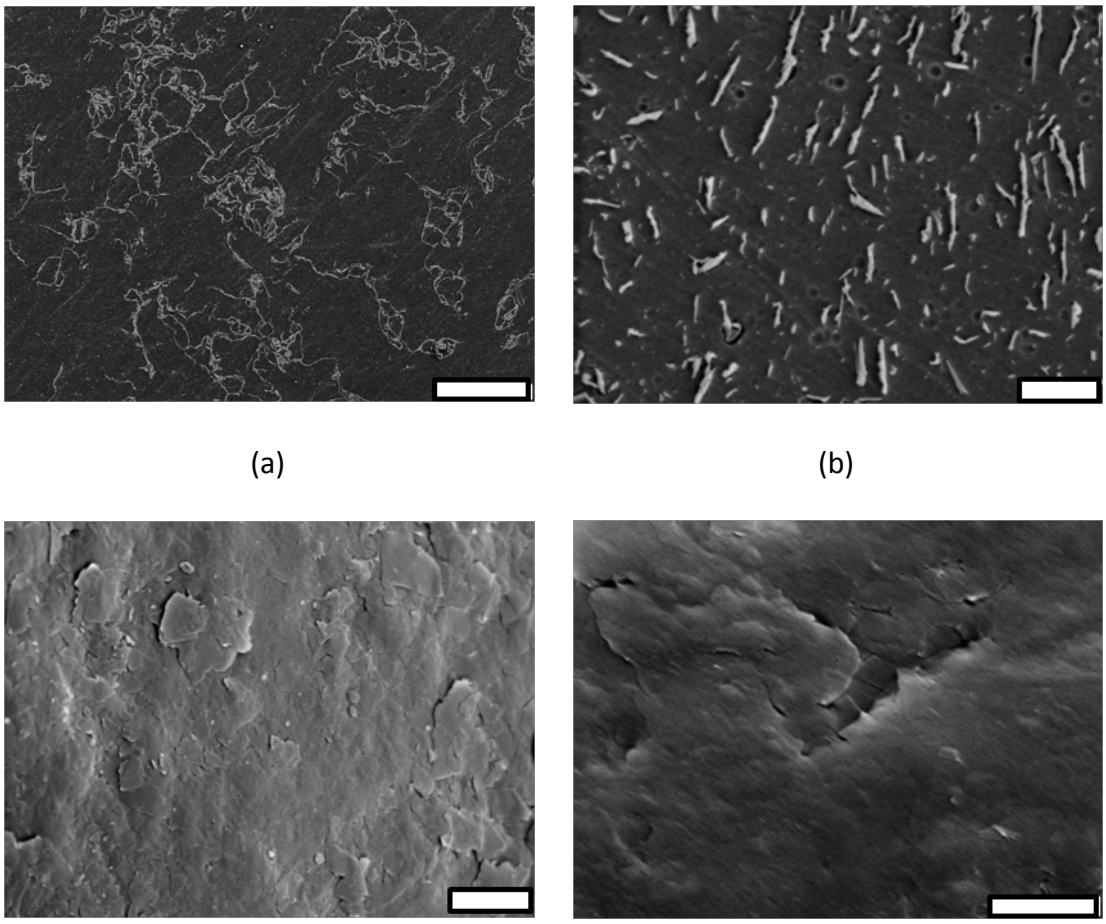

(a) (b)

(c) (d)

Figure 6.3, SEM images of GNP/PEId composites (a) polished surface of the cross section of 3wt% GNP-1/PEId composite from pre-coating compounding, showing orientation and long continuous graphite phase (white lines) (b) 3wt% GNP-15/PEId composite from melt-extrusion compounding, showing size reduction and distribution of GNP particles (c) polymer powder surface after pre-coating with 3wt% GNP-1 (d) polymer powder surface after SSBM with 3wt% GNP-1. (scale bars: (a) 50 micron, (b)~(d): 2 micron)

This result indicates that the SSBM process has a similar effect on forming a continuous conductive phase in the polymer matrix by forming a complete

continuous coating of GNP on the polymer powder surface (Figure 6.3 (c)(d)). A few shiny edges in the SEM image indicate a thick and uniform coating of GNP particles has been produced. Composites with GNP-15 show better conductivity after percolation because the nanoparticle higher aspect ratio provides a continuous conductive phase with fewer contact points and lower contact resistance.

Flexural Properties

The flexural modulus and strength of GNP/PEId nanocomposites made by pre-coating and melt-extrusion compounding are shown in Figure 6.4 and Figure 6.5, respectively. 5wt% GNP-15/PEId composite made by melt-extrusion shows a 30% increase in flexural modulus while the same loading composite made by pre-coating compounding only shows an improvement of 13% in modulus. This indicates that during pre-coating, GNP-15 particles wrapped around the polymer powder particles form a thick layer of graphite. Due to the large aspect ratio, the particles tend to overlap each other. The polymer cannot flow into the graphite layers in the following compression molding process, resulting in fewer effective GNP particles available to increase the matrix modulus. Composites with GNP-1 from the same pre-coating process show slightly better modulus than the ones made with GNP-15 because of less overlapping of the nanoparticle particles.

Flexural strength is highly dependent on the defects in the sample. Melt-extrusion separates and surrounds GNP particles from each other with polymer and provides the composite with the highest strength which reaches a maximum at 3wt%. The

strength starts to drop at higher than 3wt% because of the increase of the number and the size of defects created by agglomerates of GNP. Also, due to the confinement of GNP particles, the polymer matrix cannot elongate to the intrinsic strain limit of the neat polymer. Note that the maximum force in flexural testing was used here to calculate the strength, instead of the force at 5% strain which is suggested by ASTM 790. The reason is, composites made from pre-coating or SSBM are usually brittle and could not reach 5% strain. Pre-coating results in very poor strength because of the continuous phase of graphite acts as a weak point in the composite. The graphite-rich area fails at low loads more easily than the polymer matrix.

With the same amount of GNP-1, SSBM composites always show a higher modulus and strength than the pre-coated GNP nanocomposites. SEM images (Figure 6.3 (c)(d)) indicate that the powder from SSBM process has a surface morphology where GNP particles are embedded into the polymer powder which results in better adhesion between polymer matrix and GNP during the compression molding process. This is due to the fierce high energy generated during SSBM from the collisions resulting in partial melting of the polymer. SSBM is also very efficient in reducing the size of the polymer powder. Smaller-sized polymer powder means a larger surface area for the same amount of material, resulting in thinner graphite layers on each polymer powder particle surface and better dispersion.

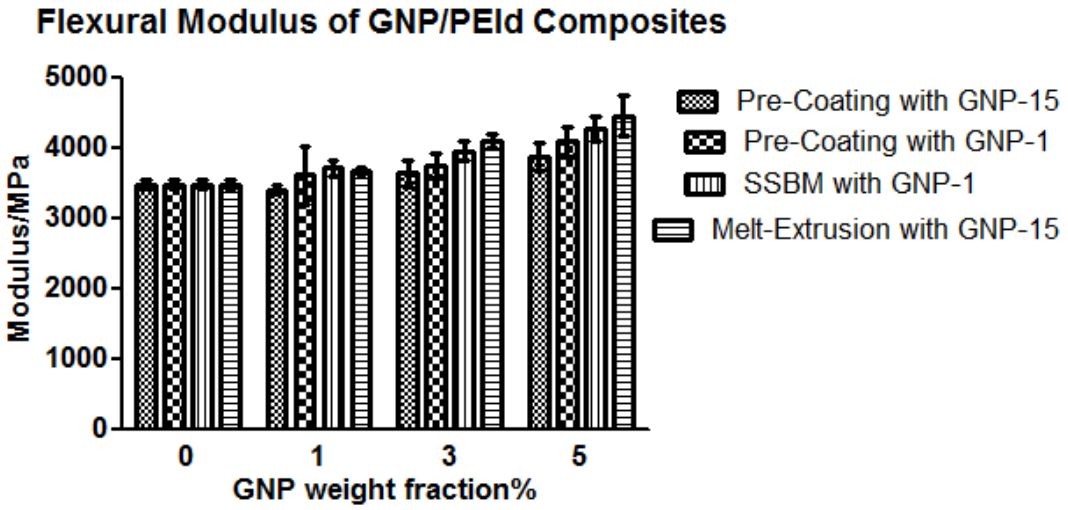

Figure 6.4, Flexural modulus of GNP/PEId composites

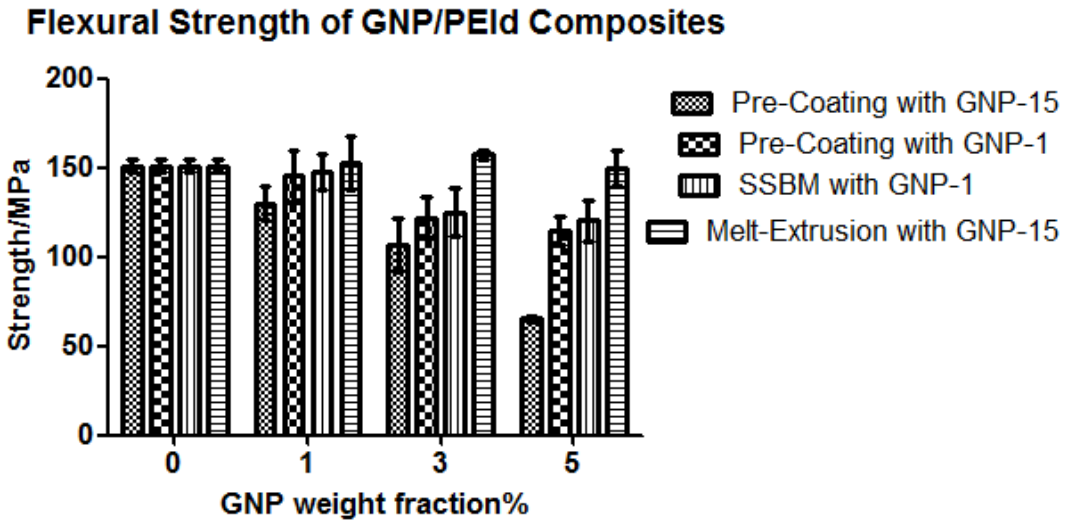

Figure 6.5, Flexural Strength of GNP/PEId composites

Combining Melt-Extrusion with SSBM

Melt-extrusion distributes the GNP particles very well in order to achieve high flexural properties but it is not a sufficient way to prevent the particles from re-stacking. However, very small amounts of GNP added in the SSBM process are able to achieve electrical percolation in the nanocomposite. Figure 6.6 shows the electrical resistance, flexural modulus and strength for the composites produced by

the two-step compounding approach, combining melt-extrusion and SSBM. The x-axis in Figure 6.6 indicates the amount of GNP-15 used in melt-extrusion step, while the three series with different patterns indicate the difference in the SSBM step. With 1wt% additional GNP-1 added in the SSBM step, all the composites produced by melt-extrusion compounding all percolated with a higher modulus and a much smaller drop of strength as compared to the neat polymer than the composites with similar resistivity made from pre-coating or SSBM compounding approaches.

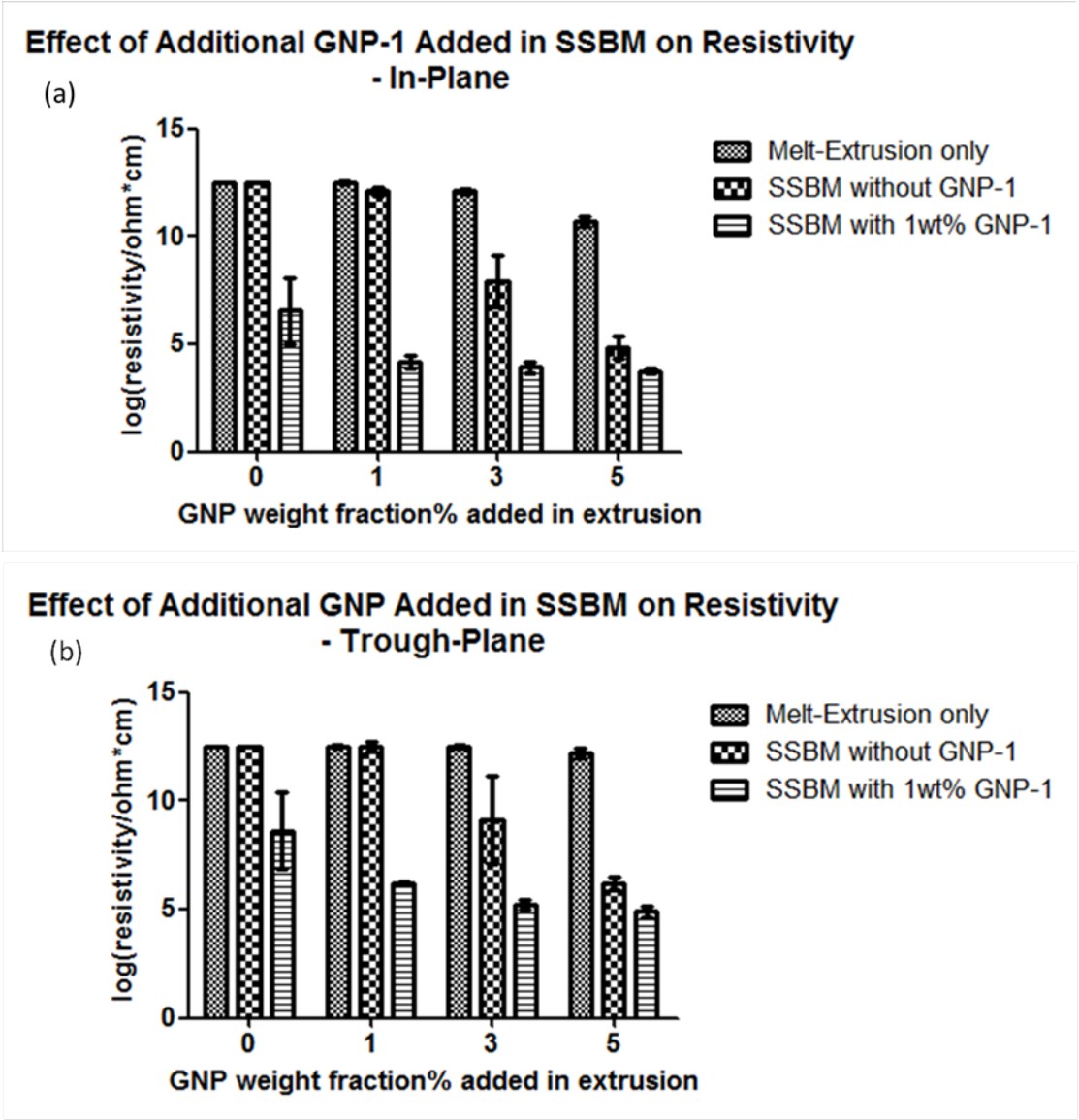

Figure 6.6, Properties of GNP/PEId composites from two-step compounding

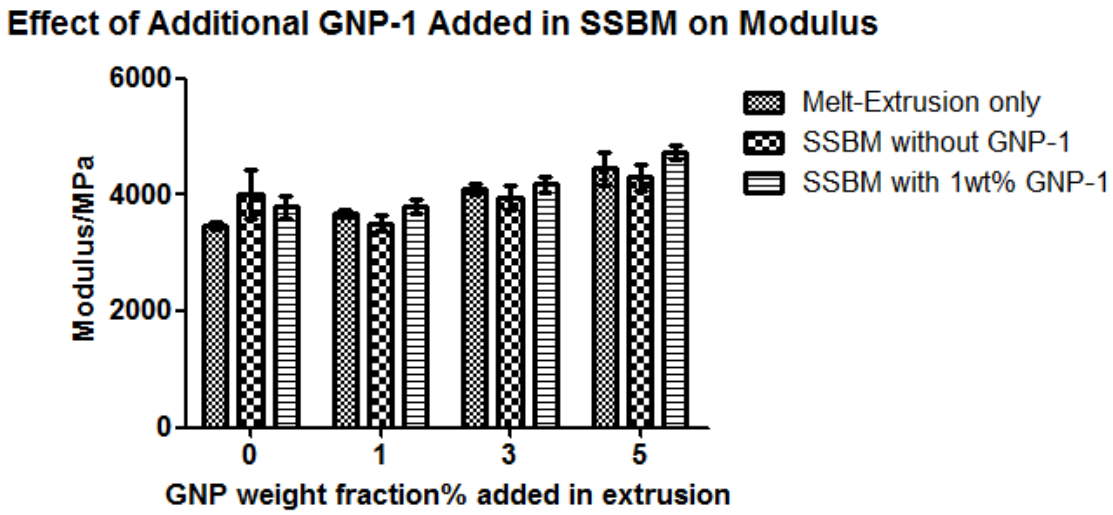

(c)

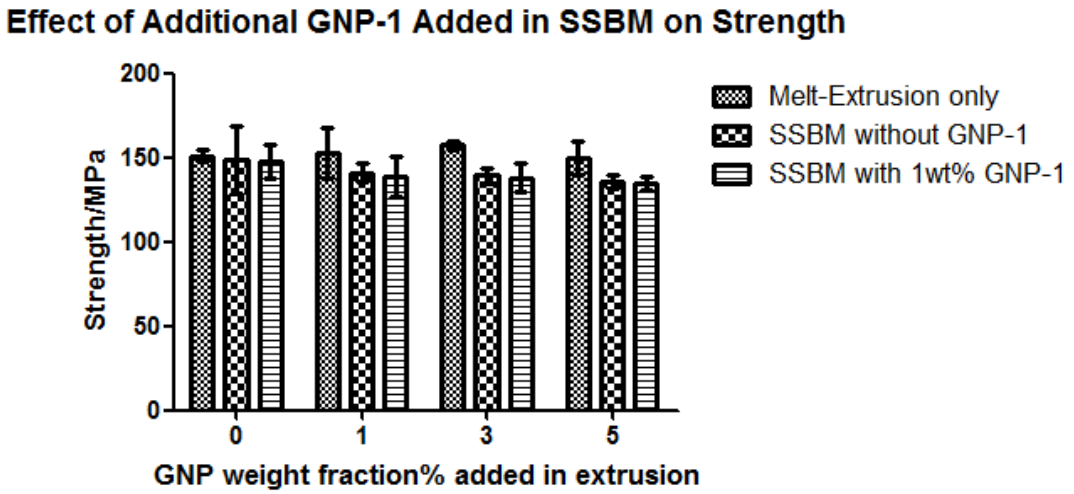

(d)

Figure 6.7, Properties of GNP/PEId composites from two-step compounding (cont.): melt-extrusion with GNP-15 then SSBM with GNP-1: (a) in-plane electrical resistivity (b) through-plane electrical resistivity (c) flexural modulus (d) flexural strength

Figure 6.7 shows the combined morphology of this kind of composite. The right side of the image is typical morphology of the extrusion compounded nanocomposite. The GNP particles are distributed homogeneously in the bulk while separated by polymer matrix. This morphology is beneficial for mechanical properties. The left side of the image shows the coating morphology. The relatively smooth surface indicates

a uniform coating layer of GNP particles. The boundary between the left and right side is a layer of graphite phase formed by coating. This kind of coating morphology also indicates a continuous phase for the conductive nanoparticles formed during SSSB process where the GNP particles were coated on the polymer powder surface. The composite made from this process can attain percolation at lower concentrations because of the continuous conductive phase.

Besides coating of higher concentrations of GNP-1 particles, GNP and PEId size reduction during SSBM also aids melt-extrusion-compounding achieve lower percolation in the nanocomposite. Areas containing higher amounts of fragile GNP agglomerates can be broken down to individual particles during collision of polymer powder particles in SSBM resulting in better separation and dispersion of GNP. Also, with the size reduction, the GNP particles that are encapsulated in polymer matrix are now exposed to the surface. (Figure 6.8) After SSBM, the anisotropic composite particles usually have a diameter of around 150 microns with a thickness of about 10 microns (Figure 6.1) which is close to the size of GNP-15. The GNP exposed on the surface during SSBM will form a continuous conductive phase, resulting in a percolated GNP-PEId nanocomposite.

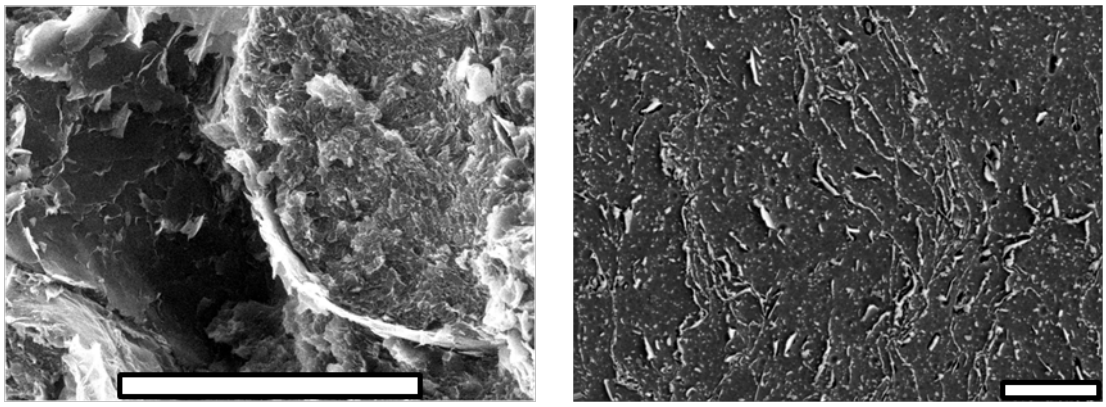

(a) (b)

Figure 6.8, SEM image of 3wt% GNP/PEId extrusion compounded + 1wt% GNP-1 in SSBM step, showing two kinds of morphology: extrusion compounded GNP particles embedded in polymer matrix and SSBM coated GNP particles lying on the surface: (a) liquid nitrogen fractured cross-section, left side showing coating morphology while right side showing extrusion morphology (b) polished cross-section, discrete particles showing extrusion morphology while continues line showing coating morphology (Scale bars: (a) 100 micron, (b) 5 micron)

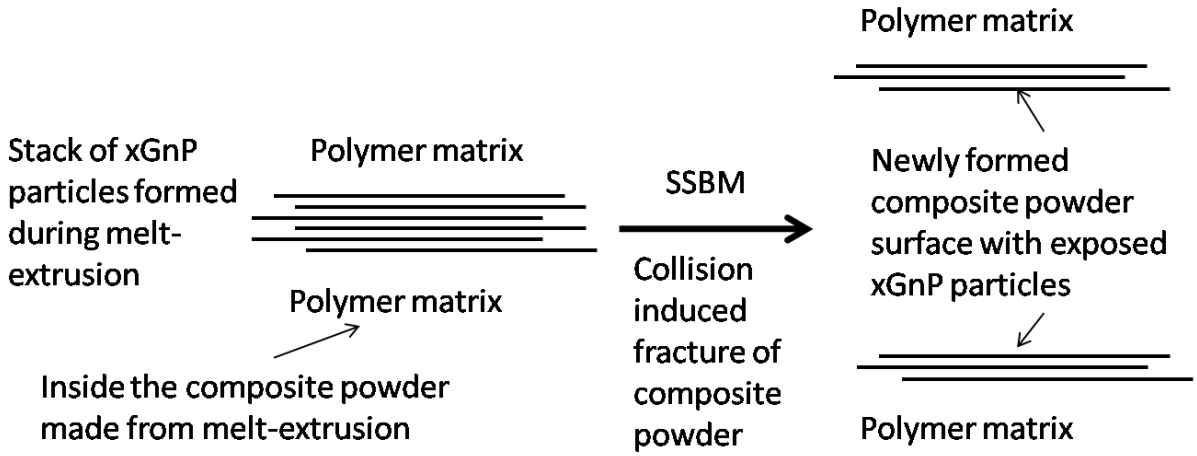

Figure 6.9, Schematics of the effect of SSBM on the composite powder made from melt-extrusion

Conclusions

A new efficient, solventless compounding method, solid state ball milling, has been identified as a viable new processing method for nanocomposites. This method

succeeds in simultaneously lowering the percolation threshold by forming a continuous GNP coating on the surface of size-reduced polymer powder with good adhesion and achieves excellent mechanical properties. Composites fabricated with the SSBM approach showed percolation threshold similar to pre-coating but with better mechanical properties and without using solvent. The morphology of the GNP-PEId nanocomposites identified the results of different compounding methods. While melt-extrusion tends to form discrete GNP phases by separating and reducing the size of the GNP particles, pre-coating and SSBM succeed in forming a continuous phase of the conductive GNP nanoparticles.

REFERENCES

REFERENCES

1. Komarneni, S., NANOCOMPOSITES. Journal of Materials Chemistry, 1992. **2**(12): p. 1219-1230.

2. Fukushima, H., Graphite Nanoreinforcements in Polymer Nanocomposites, in Department of Chemical Engineering and Materials Science. 2003, Michigan State University: East Lansing.

3. Kalaitzidou, K., Exfoliated Graphite Nanoplatelets as Reinforcement for Multifunctional Polypropylene Nanocomposites, in Department of Chemical Engineering and Materials Science. 2006, Michigan State University: East Lansing.

4. Wang, Y.S., M.A. Ogurkis, and J.T. Lindt, ELECTRICAL-PROPERTIES OF EXFOLIATED-GRAPHITE FILLED POLYETHYLENE COMPOSITES. Polymer Composites, 1986. **7**(5): p. 349-354.

5. Krupa, I. and I. Chodak, Physical properties of thermoplastic/graphite composites. European Polymer Journal, 2001. **37**(11): p. 2159-2168.

6. Zheng, W., X.H. Lu, and S.C. Wong, Electrical and mechanical properties of expanded graphite-reinforced high-density polyethylene. Journal of Applied Polymer Science, 2004. **91**(5): p. 2781-2788.

7. Zheng, W.G., S.C. Wong, and H.J. Sue, Transport behavior of PMMA/expanded graphite nanocomposites. Polymer, 2002. **43**(25): p. 6767-6773.

8. Zheng, W. and S.C. Wong, Electrical conductivity and dielectric properties of PMMA/expanded graphite composites. Composites Science and Technology, 2003. **63**(2): p. 225-235.

9. Pan, Y.X., et al., A new process of fabricating electrically conducting nylon 6/graphite nanocomposites via intercalation polymerization. Journal of Polymer Science Part B-Polymer Physics, 2000. **38**(12): p. 1626-1633.

10. Zou, J.F., et al., Conductive mechanism of polymer/graphite conducting composites with low percolation threshold. Journal of Polymer Science Part B-Polymer Physics, 2002. **40**(10): p. 954-963.

11. Kalaitzidou, K., H. Fukushima, and L.T. Drzal, A new compounding method for exfoliated graphite-polypropylene nanocomposites with enhanced flexural properties and lower percolation threshold. Composites Science and

Technology, 2007. **67**(10): p. 2045-2051.

12. Kim, S., I. Do, and L.T. Drzal, Multifunctional xGnP/LLDPE Nanocomposites Prepared by Solution Compounding Using Various Screw Rotating Systems. Macromolecular Materials and Engineering, 2009. **294**(3): p. 196-205.

13. Ansari, S. and E.P. Giannelis, Functionalized Graphene Sheet-Poly(vinylidene fluoride) Conductive Nanocomposites. Journal of Polymer Science Part B-Polymer Physics, 2009. **47**(9): p. 888-897.

14. She, Y.H., G.H. Chen, and D.J. Wu, Fabrication of polyethylene/graphite nanocomposite from modified expanded graphite. Polymer International, 2007. **56**(5): p. 679-685.

15. Yu, J., et al., Conductivity of polyolefins filled with high-structure carbon black. Journal of Applied Polymer Science, 2005. **98**(4): p. 1799-1805.

Chapter 7 Effect of Particle size on the Thermal and Electrical Conductivity of Graphite Nanoplatelet/Polyetherimide Composites

Abstract

Graphite nanoplatelets (GNPs) with different sizes were compounded with polyetherimide (PEId) by melt-blending and pre-coating in order to investigate their effect on the electrical and thermal conductivity of the composites. Pre-coating compounding successfully created a percolated GNP network with an electrical percolation threshold at 1wt%, while melt-blended samples required concentrations over 5wt% to achieve percolation. The pre-coated samples also show higher thermal conductivity than the melt-blended ones. Smaller GNP particle size results in lower thermal conductivity. An improvement of 1600% in thermal conductivity was recorded for pre-coated 10wt% GNP-15/PEId composite as compared to the neat polymer and a polynomial dependence on GNP concentration was found to predict thermal conductivity.

Introduction

Polymer and polymer composite materials are considered to be a viable substitute for metal alloys and are being widely used because of their light weight and good chemical resistance. However, the lack of thermal conductivity of neat polymers or polymer blends limits some of the potential applications of this lightweight material in certain areas, such as bi-polar plates for fuel cells, engine shields, packaging of electronic devices, and so on. To overcome this problem, conductive fillers such as metal powder [1-5], ceramic particles [6-8], carbon nanotubes [9-13] and graphene-based nanofillers [14-17] have been introduced into polymer matrices. Table 7.1 gives the thermal conductivity, coefficient of thermal expansion (CTE) and density of various materials that are commonly used as fillers in composites.

Table 7.1, Thermal conductivity, coefficient of thermal expansion and density of fillers[18]

Material	Thermal Conductivity (W/m^oK)	Linear CTE ($10^{-6}/℃$)	Density (g/cm^3)
Copper	398	17	8.9
Silver	429	18	10.49
Aluminum	247	23	2.7
Tungsten	155	4.5	19.3
Kovar	17	5.1	8.39
Beryllium oxide	260	6	3
Aluminum nitride	320	4.5	3.3
Silicon carbide	270	3.7	3.3
Graphite (in-plane)	2000	-2.0 [19]	2.1
Graphene & CNT	1750-5800 [20, 21]	-0.9 [22]	2.1

Copper metal and metal alloys are a common thermal conductor. Copper possesses a thermal conductivity of 398 W/mK. However, its CTE is as high as $17\times10^{-6}/℃$. High

CTE causes the material to deform significantly with a change in temperature which is usually a problem for materials used as conductors. In addition, a density of 8.9g/cm^3 prevents copper from being used in weight-sensitive applications including aerospace. Aluminum has a lower density compared to copper and is widely used for aircraft electronics and laptops, but its CTE is even higher. In order to lower the CTE, various ceramic particles are developed by adding a low CTE material into metal matrix, forming materials such as aluminum nitride and silicon carbide. The best thermal conductor would be diamond, which has a thermal conductivity of 3000 W/mK and a CTE as low as 0.9×10^{-6}/℃. However, the extremely high cost of diamond prevents it to be widely used.

Although graphite has a thermal conductivity close to diamond and a very low CTE and density, it is not very practical to be used as a bulk material due to brittleness and difficulty in machining. Carbon nanotubes (CNTs), for example, can be considered as rolled up0 sheets of graphene. Researchers [21] have found out that the thermal conductivity of single-wall CNTs (SWCNTs) ranges from 1750-5800 W/mK. An epoxy matrix filled with 3wt% (~1.5vol%) CNT achieves a 300% improvement in thermal conductivity as compared to the neat epoxy resin [11]. As a comparison, around 8.75vol% silver particles are required to have the same improvement [1]. However, similar to diamond, the high cost of CNTs makes them impractical for composites.

Another form of graphitic materials, graphene or graphite nanoplatelets, have the potential for composites applications. Generally, natural graphite can be exfoliated or

expanded into very thin layers, forming a thin (3-7 nm) platelet morphology (diameters ranging from sub micron to 200 microns) while maintaining good in-plane properties. Two typical methods are usually used including the graphite oxide (GO) [14] route and the graphite intercalation compound (GIC) [23] route. The GIC route is considered to be able to best preserve the properties of pristine graphite since the basal plane of sp^2 carbon atoms are not disrupted during the process. A novel process consisting of acid intercalation, microwave exfoliation and ultrasonication pulverization has been developed in the Drzal group to deliver exceptional electrical, thermal and mechanical properties in the exfoliated graphite nanoplatelet (GNP) material with a surface area up to 300 m^2/g, a thickness as thin as 3 nm, and a lateral dimension up to 200 μm [24]. This scalable process has proved its potential to provide cost-effective conductive fillers for nanocomposites applications.

Unlike the electrical conductivity of polymer composites, the percolation phenomena and filler aspect ratio dependence have not been explicitly explained for thermal conductivity. Mamunya et al [25] discovered a non-monotonous dependence of thermal conductivity on the volume content of CNT filler. The minimum of conductivity happens at the same volume percentage as the electrical percolation threshold. However, the difference is very small with large overlapping error bars. No “percolation” behavior is found in thermal conductivity dependence on particle loading. Moreover, the aspect ratio of the filler always takes an important role in electrical percolation and conductivity [26, 27], while the importance fades for thermal conductivity. Devpura et al [6] used modeling to predict the size effect on

metal powder/polymer systems below electrical percolation threshold and found that the larger filler particles exhibit higher thermal conductivity in composites. The authors hypothesize that the effect was the result of thermal boundary resistance between particle and matrix. However, the effect of the particle size above the percolation threshold was not discussed.

One possible reason for the difficulty of investigating percolation phenomena and filler aspect ratio dependence for thermal conductivity is that the two factors are usually coupled: larger aspect ratio normally results in lower percolation threshold. To compare composites with percolated and non-percolated network at the same loadings, two sets of GNP/polyetherimide (PEId) composites were fabricated, one of which was melt-blended by a twin-screw extruder and the other one made through a pre-coating process where the GNP particles are coated onto polymer powder surfaces and then compression molded in order to create a continuous GNP phase [28] [Chapter 6]. The aim of this research is to investigate the importance of particle percolation and particle size on the thermal conductivity of polymer composites.

Experimental Materials and Methods

Materials

Polyether imide (PEId) was obtained from Sabic-IP (Ultem 1010, in two forms: pellet and powder). GNP-1 (particles with an average diameter of 1 micron, 100m^2/g surface area) and GNP-15 (particles with a diameter of 15 micron, 40m^2/g surface

area) were prepared in the lab [24]. GNP-5 (5 micron average diameter, 40m^2/g surface area) was provided by XG-Science Inc. (Lansing, MI).

Melt-extrusion

Melt-extrusion was carried on Leistritz twin-screw extruder (MIC27/6L-48D). The screws were operated in the co-rotation mode. Barrel temperatures were set to 310℃, with a melt temperature at 340℃. The die pressure was at around 5.5MPa. Screw speed was set at 150 rpm.

Pre-coating

GNP was first dispersed in acetone under ultrasonication. PEId powder (~300 microns in diameter) was then added into the suspension while stirring. After evaporation of the acetone, the mixture was further mixed in a Speed Mixer (Flextec Corporation). The sample was dried in a vacuum oven at 120℃.

Compression Molding

After compounding, the composite material was compression molded in a CARVER Laboratory Press (Model 2731, Fred S. Carver INC.). A picture-frame mold was used with a diameter of 2.56 cm and a thickness of 3 mm. The composite material was heated up to 340℃ and held for 15 min. A compression pressure of 20MPa was applied to the material and was the mold remained closed for 45 min in order to achieve consolidation. After that, the press was cooled by water while the pressure

was maintained.

Electrical Resistivity Measurement

The resistance of GNP/PEId composites is measured by 2-point AC impedance method. The resistance value was then converted into resistivity by taking into account of the sample dimensions.

Thermal Diffusivity and Thermal Conductivity

Thermal diffusivity of the GNP/PEI composites is measured by laser flash method (LFA 447 NanoFlash, Netzsch) in both in-plane and through-plane directions. The heat capacity Cp is determined by Differential Scanning Calorimetry (DSC, TA Instruments) and the density of the samples is calculated by the rule of mixture. Thermal conductivity was then calculated by multiplying diffusivity by Cp and density.

Results and Discussion

Electrical conductivity

The electrical conductivity of the GNP/PEI composites is shown in Figure 7.1. All the pre-coated samples percolate at 1wt% while the melt-blended ones percolate after 5 wt% loading although some percolation behavior starts at around 3 wt%. Figure 7.2 shows the internal morphology of the well formed network of GNP fillers in the pre-coated 3wt% GNP-1/PEI composite.

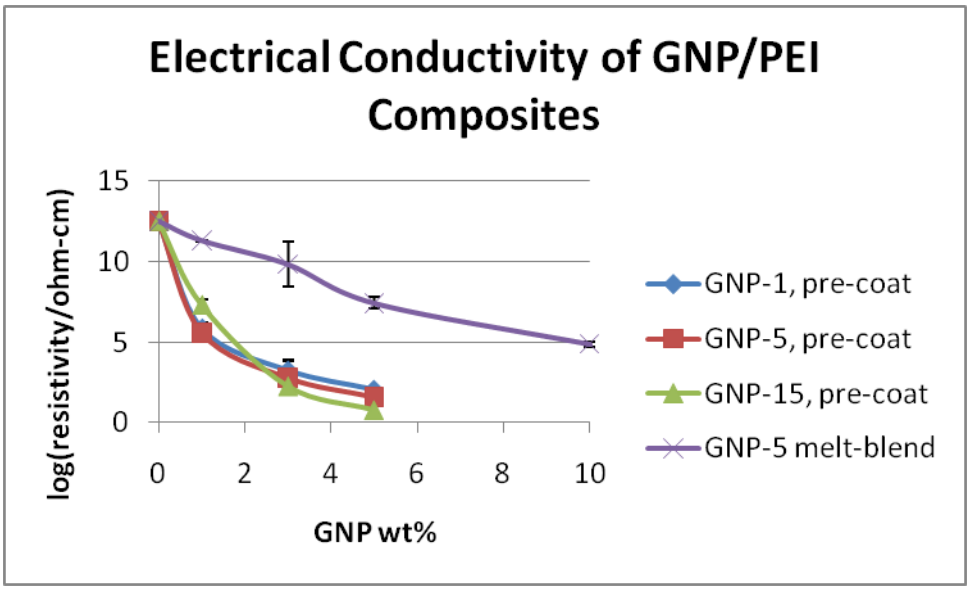

Figure 7.1, Electrical conductivity of GNP/PEI composites

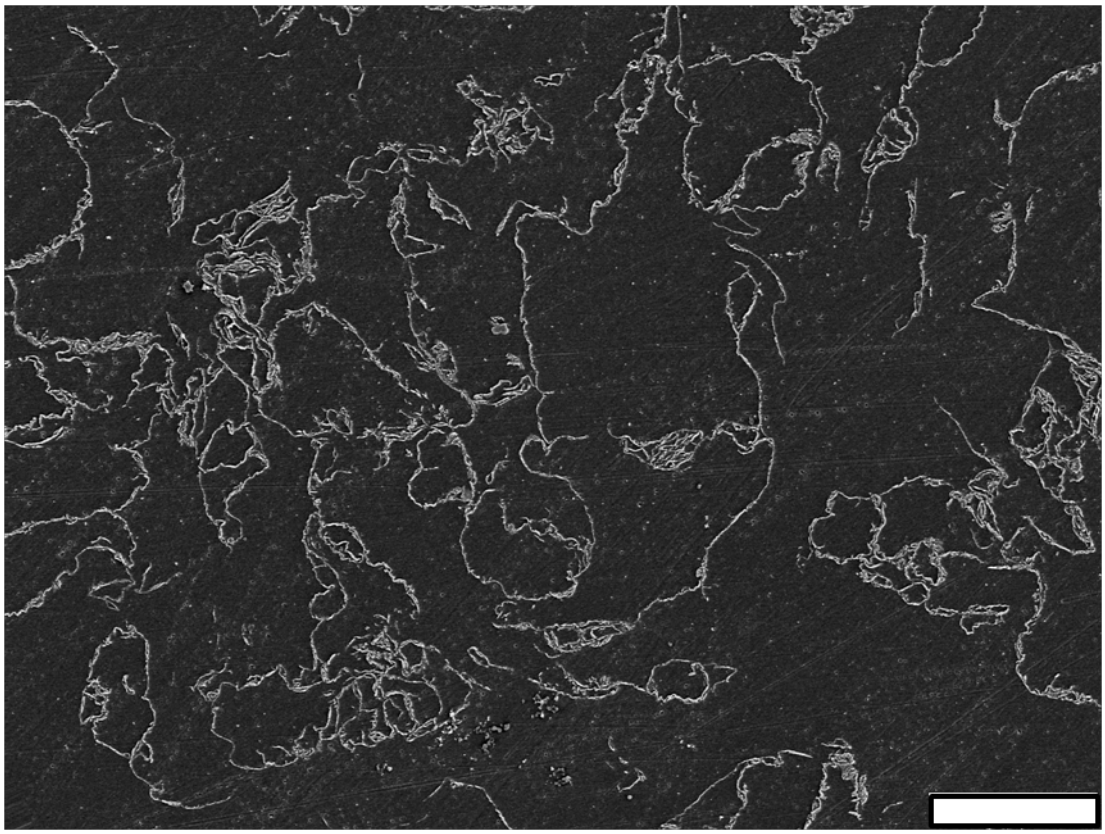

Figure 7.2, SEM image of pre-coated 3wt% GNP-1/PEI composite showing continuous phase created by pre-coating. The white lines indicate GNP phase while the dark part indicates the PEI matrix. The observed surface is prepared by polishing and plasma etching as explained elsewhere. (Scale bar: 20 micron)

Thermal Conductivity

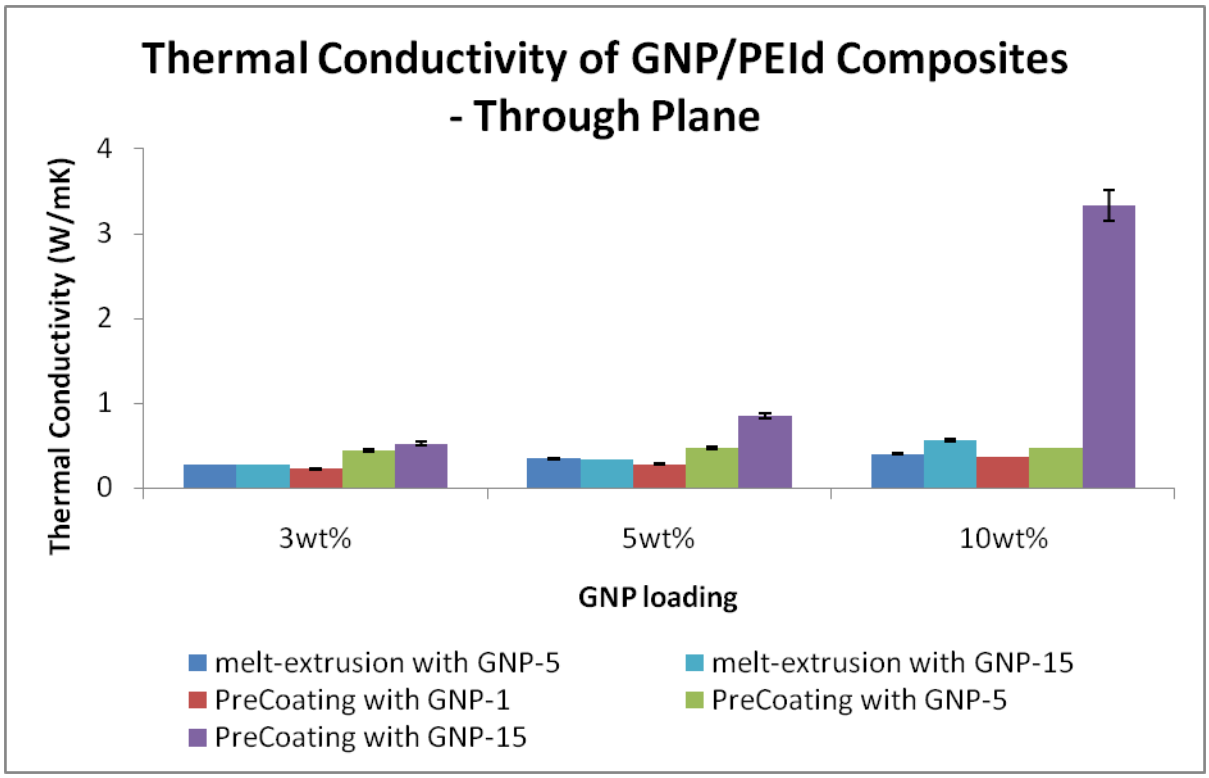

Figure 7.3, Thermal conductivity of GNP/PEI composites

The thermal conductivity of the GNP/PEI composites is shown in Figure 7.3. The melt-blended composites do not show percolation. The thermal conductivity increases with the increase of GNP-5 loading. Second, the pre-coated GNP-5/PEI composite shows a higher thermal conductivity than the melt-blended one. This indicates that there is less phonon scattering at the GNP-matrix in the composite. Although the relative improvement is around 60% as compared to melt-blended samples, the absolute value is still orders of magnitude lower than the calculated result from rule of mixture. If we take thermal conductivity of graphite Kg=2000 W/mK, then by the rule of mixtures, the thermal conductivity of the composite at 5wt% (around 2.5vol%) loading should be Kc = 0.025Kg + 0.975Kp = 500 W/mK,

where Kp is the thermal conductivity of PEI and is negligible in this equation. This simple calculation indicates a significant role of the contact resistance between particles. Although a continuous phase is formed by pre-coating and can generate electrical percolation, the thermal conductivity is still highly affected by how well the particles are touching each other. As shown in Figure 7.3, composites filled with smaller particles like GNP-1 achieve lower thermal conductivity while the ones with the larger GNP-15 particles show much higher thermal conductivity. The fact that the pre-coated GNP-1 samples exhibit an even lower value than the melt-blended GNP-5 ones indicates that the size effect is more important than particle connection. Put another way, a well-connected network with smaller particles is not as good as a partially connected network (like in 3wt% GNP-5/PEId melt-extruded sample in Figure 7.1 where percolation can be seen in some specimens) of larger particles (Figure 7.4). The same conclusion can also be drawn from comparing melt-blended 10wt% GNP-15/PEId with pre-coated 10wt% GNP-5/PEId samples. At this loading, both samples should be percolated, and the larger particle is has an advantage in the overall conductivity of the composite.

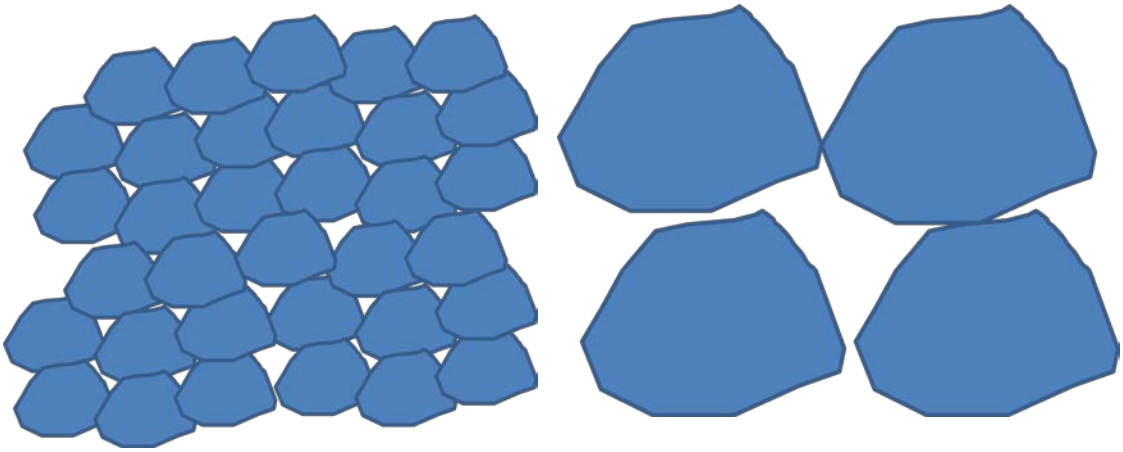

(a) Smaller particles, percolated network

(b) Larger particles, partially connected

Figure 7.4, Schematics of particle size and connectivity: (a) although the particles are well connected, the contacting resistance is huge; (b) large particles which are barely touching each other can still provide higher thermal conductivity than (a)

The explanation underneath this phenomenon is the fact that two connected GNP particles are not touching each other perfectly. A gap or a very thin layer of polymer is still spacing the particles away from each other, which will cause phonon scattering. Thus, the thermal contacting resistance is the major factor that prevents high thermal conductivity for percolated network.

Interestingly, the pre-coated 10wt% GNP-15/PEI composite shows a much higher thermal conductivity (1600% improvement compared with neat PEI) than any other samples shown in Figure 7.3. However, as shown in Figure 7.5, the thermal conductivity of pre-coated GNP-15/PEI composites has a second order polynomial dependence on the volume fraction of the GNP filler.

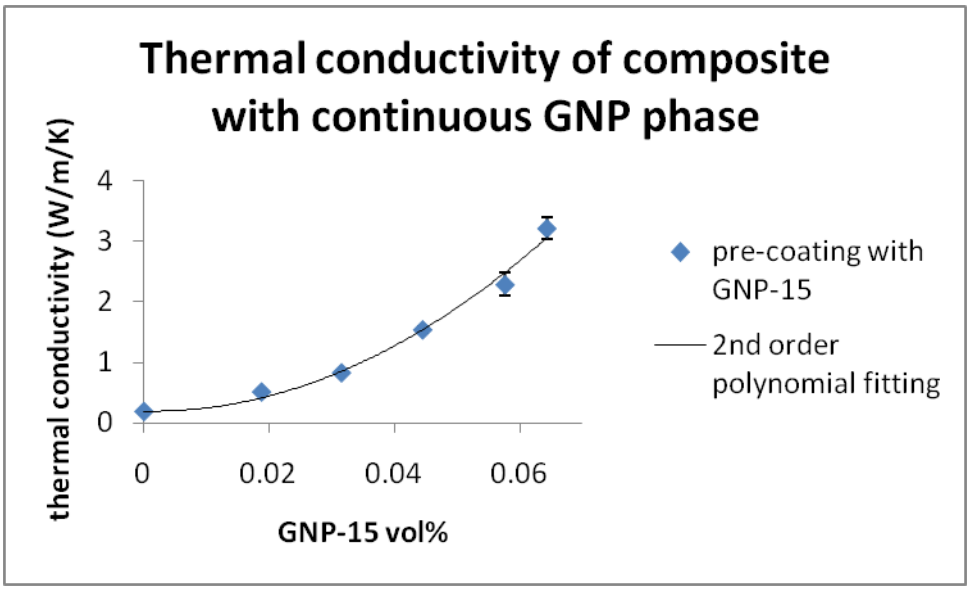

Figure 7.5, Thermal conductivity of pre-coated GNP-15/PEI composite

In Figure 7.5, the fitted line gives:

$$y = 726.32x^2 - 2.0695x + 0.192 \quad (1)$$

The second order polynomial dependence suggests that the contact between particles improves with the increase of GNP loading. This can be explained by the fact that the coated GNP layer gets thicker with higher loadings and becomes harder to be disrupted during the following compression molding.

One interesting observation of the 2nd order polynomial equation (1) is that it indicates a minimum value for thermal conductivity, at 0.14vol% GNP loading. This result is comparable with Mamunya's CNT-PVC system where the minimum thermal conductivity was obtained at around 0.5vol% of CNT loading. This loading is usually considered as the electrical percolation threshold where all the particles are connected to form a continuous phase of conductive filler. In this case, this phenomenon can be interpreted as that the PEId powder is fully covered by the GNP particles at 0.2vol% loading and the coated structure can hold together even after

compression molding.

More interestingly, if the loading is set to 100vol%, equation (1) will give out a thermal conductivity value at 724 W/mK. Although this value is somewhat lower than the thermal conductivity of graphene or CNT, it is comparable with the 380 W/mK value obtained from a monolayer assembly of GNP particles on the glass slide reported by Xiang et al [29]. The reason for the overestimation from equation (1) may be that it overestimates the best possible contacting between the GNP particles.

Conclusions

GNP/PEId composite were made from melt-blending and pre-coating. It is found that the pre-coated samples form a well connected GNP particle network which percolates the composite at very low loading (1wt%). The percolated network helps to improve the thermal conductivity to about 60% higher than that of none-percolated composites. Larger sized GNP particles can provide their composites with higher thermal conductivity due to reduced amount of contact points and lower contact resistance between filler particles even when a percolated network has been established. It is also found that the benefit of the connected network may be negated by the disadvantage of having too many contacting points. An improvement of 1600% was recorded for pre-coated 10wt% GNP-15/PEI composite. A second order polynomial dependence of thermal conductivity of percolated pre-coated GNP-15/PEId composites on GNP loading was found.

References

REFERENCES

1. Bjorneklett, A., L. Halbo, and H. Kristiansen, *THERMAL-CONDUCTIVITY OF EPOXY ADHESIVES FILLED WITH SILVER PARTICLES.* International Journal of Adhesion and Adhesives, 1992. **12**(2): p. 99-104.

2. Kowalski, L., J. Duszczyk, and L. Katgerman, *Thermal conductivity of metal powder-polymer feedstock for powder injection moulding.* Journal of Materials Science, 1999. **34**(1): p. 1-5.

3. Mamunya, Y.P., et al., *Electrical and thermal conductivity of polymers filled with metal powders.* European Polymer Journal, 2002. **38**(9): p. 1887-1897.

4. Weidenfeller, B., M. Hofer, and F.R. Schilling, *Thermal conductivity, thermal diffusivity, and specific heat capacity of particle filled polypropylene.* Composites Part a-Applied Science and Manufacturing, 2004. **35**(4): p. 423-429.

5. Mamunya, Y.P., et al., *Percolation phenomena in polymers containing dispersed iron.* Polymer Engineering and Science, 2002. **42**(1): p. 90-100.

6. Devpura, A., P.E. Phelan, and R.S. Prasher, *Size effects on the thermal conductivity of polymers laden with highly conductive filler particles.* Microscale Thermophysical Engineering, 2001. **5**(3): p. 177-189.

7. Hill, R.F. and P.H. Supancic, *Thermal conductivity of platelet-filled polymer composites.* Journal of the American Ceramic Society, 2002. **85**(4): p. 851-857.

8. Wong, C.P. and R.S. Bollampally, *Thermal conductivity, elastic modulus, and coefficient of thermal expansion of polymer composites filled with ceramic particles for electronic packaging.* Journal of Applied Polymer Science, 1999. **74**(14): p. 3396-3403.

9. Thostenson, E.T., Z.F. Ren, and T.W. Chou, *Advances in the science and technology of carbon nanotubes and their composites: a review.* Composites Science and Technology, 2001. **61**(13): p. 1899-1912.

10. Kuriger, R.J., et al., *Processing and characterization of aligned vapor grown carbon fiber reinforced polypropylene.* Composites Part a-Applied Science and Manufacturing, 2002. **33**(1): p. 53-62.

11. Choi, E.S., et al., *Enhancement of thermal and electrical properties of carbon nanotube polymer composites by magnetic field processing.* Journal of

Applied Physics, 2003. **94**(9): p. 6034-6039.

12. Moniruzzaman, M. and K.I. Winey, *Polymer nanocomposites containing carbon nanotubes.* Macromolecules, 2006. **39**(16): p. 5194-5205.

13. Tibbetts, G.G., et al., *A review of the fabrication and properties of vapor-grown carbon nanofiber/polymer composites.* Composites Science and Technology, 2007. **67**(7-8): p. 1709-1718.

14. Stankovich, S., et al., *Graphene-based composite materials.* Nature, 2006. **442**(7100): p. 282-286.

15. Fukushima, H., et al., *Thermal conductivity of exfoliated graphite nanocomposites.* Journal of Thermal Analysis and Calorimetry, 2006. **85**(1): p. 235-238.

16. Kalaitzidou, K., H. Fukushima, and L.T. Drzal, *Multifunctional polypropylene composites produced by incorporation of exfoliated graphite nanoplatelets.* Carbon, 2007. **45**(7): p. 1446-1452.

17. Yang, H., et al., *Improved mechanical and functional properties of elastomer/graphite nanocomposites prepared by latex compounding.* Acta Materialia, 2007. **55**(18): p. 6372-6382.

18. Chung, D.D.L., *Materials for thermal conduction.* Applied Thermal Engineering, 2001. **21**(16): p. 1593-1605.

19. Bailey, A.C. and B. Yates, *ANISOTROPIC THERMAL EXPANSION OF PYROLYTIC GRAPHITE AT LOW TEMPERATURES.* Journal of Applied Physics, 1970. **41**(13): p. 5088-&.

20. Kim, P., et al., *Thermal transport measurements of individual multiwalled nanotubes.* Physical Review Letters, 2001. **87**(21).

21. Hone, J., et al., *Electrical and thermal transport properties of magnetically aligned single walt carbon nanotube films.* Applied Physics Letters, 2000. **77**(5): p. 666-668.

22. Schelling, P.K. and R. Keblinski, *Thermal expansion of carbon structures.* Physical Review B, 2003. **68**(3).

23. Rudorff, W., *GRAPHITE INTERCALATION COMPOUNDS.* Advances in Inorganic Chemistry, 1959. **1**: p. 223-266.

24. Drzal, L.T. and H. Fukushima, *Expanded graphite and products produced therefrom*. 2004: US.

25. Mamunya, Y., et al., *Electrical and thermophysical behaviour of PVC-MWCNT nanocomposites.* Composites Science and Technology, 2008. **68**(9): p. 1981-1988.

26. Kim, H. and C.W. Macosko, *Morphology and properties of polyester/exfoliated graphite nanocomposites.* Macromolecules, 2008. **41**(9): p. 3317-3327.

27. Abdel-Goad, M., et al., *Preparation and rheological characterization of polymer nanocomposites based on expanded graphite.* Journal of Macromolecular Science Part a-Pure and Applied Chemistry, 2007. **44**(4-6): p. 591-598.

28. Kalaitzidou, K., H. Fukushima, and L.T. Drzal, *A new compounding method for exfoliated graphite-polypropylene nanocomposites with enhanced flexural properties and lower percolation threshold.* Composites Science and Technology, 2007. **67**(10): p. 2045-2051.

29. Xiang, J.L. and L.T. Drzal, *Thermal Conductivity of a Monolayer of Exfoliated Graphite Nanoplatelets Prepared by Liquid-Liquid Interfacial Self-Assembly.* Journal of Nanomaterials, 2010.

Chapter 8 GNP Paper: Light weight Composite having Electrical, Thermal Conductivity and Gas Barrier Properties

Abstract

Paper forms (i.e. thin free-standing films) of carbon-based materials have received increasing attention. Here we present a novel approach to fabricating a binder free, self-standing flexible paper consisting of exfoliated graphite nanoplatelets (GNPs). It is found that the electrical conductivity of the GNP paper can be as high as 2200 S/cm and the thermal conductivity reaches 313 W/mK. Both thermoset and thermoplastic matrices were used to impregnate the porous GNP paper and an extremely high tensile modulus was attained. Even with 30vol% polymer, the GNP paper composite can still exhibit ~700 S/cm electrical conductivity thanks to the highly continuous GNP network formed in the paper making process. The impregnated GNP paper was also investigated as a component in carbon fiber composite. It is found that when inserted into a layered laminate composite construction, gas permeability can be severely reduced and electrical and thermal conductivity can be greatly enhanced.

Introduction

Graphite or graphene nano platelets (GNP) have drawn a lot of interest due to their high mechanical properties (~1TB for either single layer or multi layer graphene theoretically [1, 2] and experimentally [3-5]), excellent electrical (~1.0×10^{-6} ohm/cm resistivity for pure graphene but more than two orders of magnitude higher for graphite [6]), and thermal (~5000 W/mK [7-10]) conductivity. The platelet shape of graphite also benefits the composite by providing increased tortuosity for molecular transport which enhances barrier properties to small molecules [11, 12]. One way of utilizing the excellent properties of GNP is to add it into a polymer matrix. The light weight polymer nanocomposite can serve as an alternative to metal or fiber reinforced composites with the help of GNP. However, when homogeneously dispersed in a matrix, the GNP usually cannot fully deliver its properties to its composite. For some specific systems like graphene-polystyrene, the electrical percolation threshold can be as low as 0.1 vol% and around 0.01 S/cm conductivity can be achieved at 2.5 vol% graphene loading [13-15]. However, other polymer matrices are facing much higher percolation thresholds and less improvement (~10^{-3} S/cm at 10wt% loading) [16-18]. Thermal conductivity of the GNP/polymer composites is also much lower than graphene, usually within 5 W/mK at a filler loading up to 20 vol% [19]. Moreover, increasing filler loading cannot always provide significant improvement especially after electrical percolation threshold of a given system. Meanwhile, mechanical strength would be reduced significantly due to

brittleness.

To fully use the conductivity properties of conductive nano fillers, a large continuous phase of the filler is required [18][Chapter 6]. A promising approach to realize it is to reassemble the nanometer-thick, micron-sized particles into micron-thick, multi-centimeter sized paper or film, and then incorporate this GNP paper into the polymer matrix. Carbon nanotube (CNT) Bucky paper [20-30] and graphite oxide (GO) paper [31-33] have been widely studied. Paper form materials prepared by either nanoparticle can be free-standing, self-supporting and show good flexibility [28, 31]. Electrical conductivity was reported to be 200 S/cm for Bucky paper with aligned CNT [28] and 350 S/cm for reduced GO paper [32]. Note that the paper fabricated from ref. [28] and [32] were claimed to be binder-free. Other types of paper with the presence of binder would have lower values. Compared to graphene or single-walled CNT which has a conductivity of ~2000 S/cm, these values are still one order of magnitude lower. The reason is, for CNT, the contact resistance between each tube is large due to the extremely small particle size for GO paper, the chemically reduced graphite oxide is not as conductive as pristine graphite. Li et al [34] and Biswas et al [35] both fabricated Langmuir-Blodgett thin films from exfoliated graphite. The electrical and thermal conductivity were reported to be over 1000 S/cm [35] and 380 W/mK [36], respectively. However, the Langmuir-Blodgett approach is not suitable for a paper form material with a thickness in the micron range and the porosity of the film is usually very low and hard to control, making it not an adequate solution for composites.

This research presents a novel route of fabricating binder-free, porosity-controllable, highly conductive and self-standing graphite paper consisting of graphite nanoplatelets (GNPs). The GNP particles are first dispersed in water with the addition of polyethyleneimine (PEIn). The suspension was then filtered and could be separated from the filter paper. Residual PEIn was removed by annealing the paper at a high temperature above the decomposition temperature of the PEIn. The resulting porous paper exhibits properties to other carbon based materials. Both thermoset and thermoplastic matrices were combined into this GNP paper form and the resulting material has potential to serve as a layer in laminate composites. Mechanical properties, electrical and thermal conductivity, barrier properties were measured and discussed for both GNP paper and its composites.

Experimentation

Materials

Polyetherimide (PEId) was obtained from Sabic-IP (Ultem 1010). Two thermoset systems were used including epoxy (EPON 862:Jeffamine T403=100:49 weight) and vinyl ester (Derakane 510A-40 with 1wt% MEKP). GNP 'worms' (expanded graphite with a diameter over 100 microns, 40m^2/g surface area) and GNP-15 (particles with a diameter of 15 micron, 40m^2/g surface area) were prepared in the lab [37]. The exfoliated but not pulverized GNP 'worms' were specially fabricated in order to achieve higher electrical conductivity. If not specified, GNP stands for GNP-15.

GNP Paper Fabrication

GNP particles were dispersed in water with the presence of PEIn (GNP:PEIn:Water=1:0.1~10:1000 weight). Ultrasonication was applied to the suspension to help disperse the GNP particles. After 1 min ultrasonication with a power of 10 watts, the GNP worms were broken down to individual platelets with a diameter ranging from 20 to 100 microns. The suspension was stirred overnight, and then filtered with an Anodisc filter (200 nm pore size, Whatman) or glass microfiber (1 micron opening, Whatman) filter paper under vacuum. Additional water was used to wash the filtered GNP. GNP and the filter paper were dried overnight and then separated. Due to its hydrophobic nature, the GNP layer was easily to be peeled off from the hydrophilic filter paper. The paper form GNP was then annealed under 120^{o}C for 1 hour in order to remove any residual moisture and then heated to 340^{o}C for 1 hour to decompose the remaining polyethyleneimine. Thermal gravimetric analysis (TGA) indicated that the paper was binder free after the heat treatment (Figure 8.1).

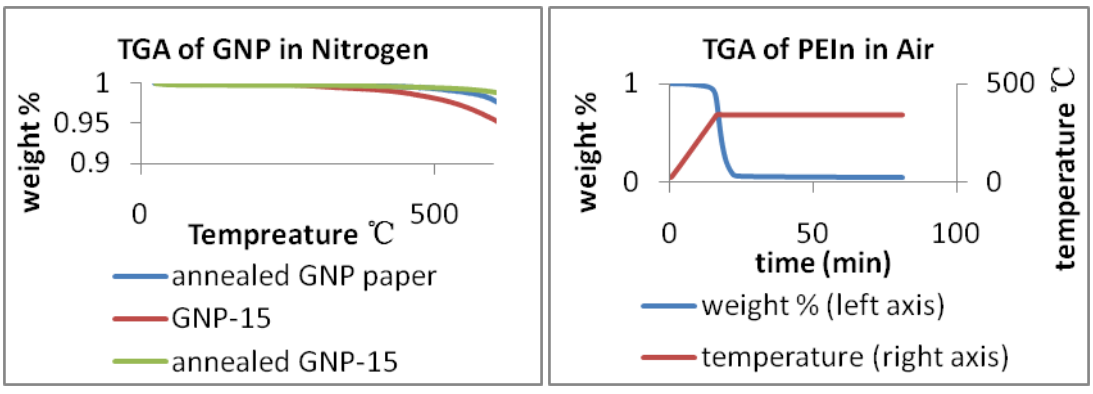

Figure 8.1, TGA result of GNP and PEIn

Figure 8.1 shows the comparison of TGA results between annealed GNP paper, un-processed GNP-15 and PEIn. After about 1 hour annealing at 340 ^{o}C in air, more than 95 wt% PEIn was decomposed. No significant weight loss was recorded before 500^{O}C for annealed GNP paper under nitrogen condition. However, for un-processed GNP-15, weight loss starts at around 300 ^{O}C. This could be due to the residual intercalant which might be washed away during dispersing GNP in water, so the weight loss won't show up in annealed GNP paper.

The filtered GNP paper possesses a porous structure. The porosity and density of the paper depend on the conditions used for filtration, e.g. the amount of suspension and the speed of filtration. Two grades of GNP paper were fabricated, one made from the Anodisc filter paper with less porosity and high density (GNP-H), and the other one made from the glass microfiber filter paper (noted as GNP-L) with lower density (Table 8.1). The porosity was calculated by assuming the density of GNP particle to be 2.1 g/cc. The GNP paper made from worms (GNP-W) generally showed higher density than GNP-15 papers, due to the more ordered layer structure formed by larger particles.

Table 8.1, Density and porosity of GNP papers, data are actual value of the particular sample, not an average

	Density (g/cc)	Porosity (vol%)
GNP-H	0.90	57
GNP-H-P	1.34	36
GNP-L	0.19	91
GNP-L-P	0.95	55
GNP-W	1.10	47
GNP-W-P	1.54	27

Note that the density of the GNP paper is very important to its properties. Porous paper can be considered as a composite consisting of GNP and air. To eliminate the effect of porosity and obtain best properties, the GNP paper was also mechanically compressed under room temperature. After applying about 100 MPa pressure, the pressed GNP paper (noted as GNP-x-P, x=H, L, W) presented a higher apparent density and lower porosity (Table 8.1 (GNP-H and GNP-H-P data are from the same paper before and after pressing), Figure 8.2). The fact that the density of pressed paper varies according to the density before pressing suggests that higher density paper has better alignment of GNP particles.

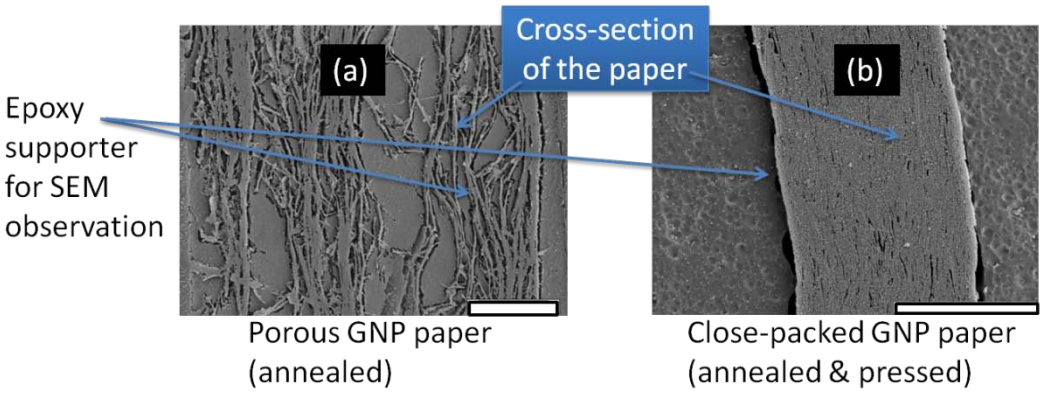

Figure 8.2, SEM images showing cross-section of the GNP paper (scale bars represent 10 micron)

Figure 8.2 shows the morphology of the cross-section of GNP paper with and without pressing. In Figure 8.2(a), the paper was not pressed. The GNP particles form a long continuous phase spaced by large pores which have a size ranging from 1 micron to 10 microns. After pressing (Figure 8.2(b)), most of the pores disappear. The GNP particles are very closely packed and have good contact with each other. However, voids are still visible in Figure 8.2(b).

The GNP paper that was fabricated in such processes exhibits very good flexibility, even without the presence of the binder after annealing. Figure 8.3(b) shows a paper plane folded from a GNP paper. The folding edge (Figure 8.3(d)) stays intact. This indicates that the Van der Waals force between GNP platelets is large enough to hold the structure that no extra binder is needed.

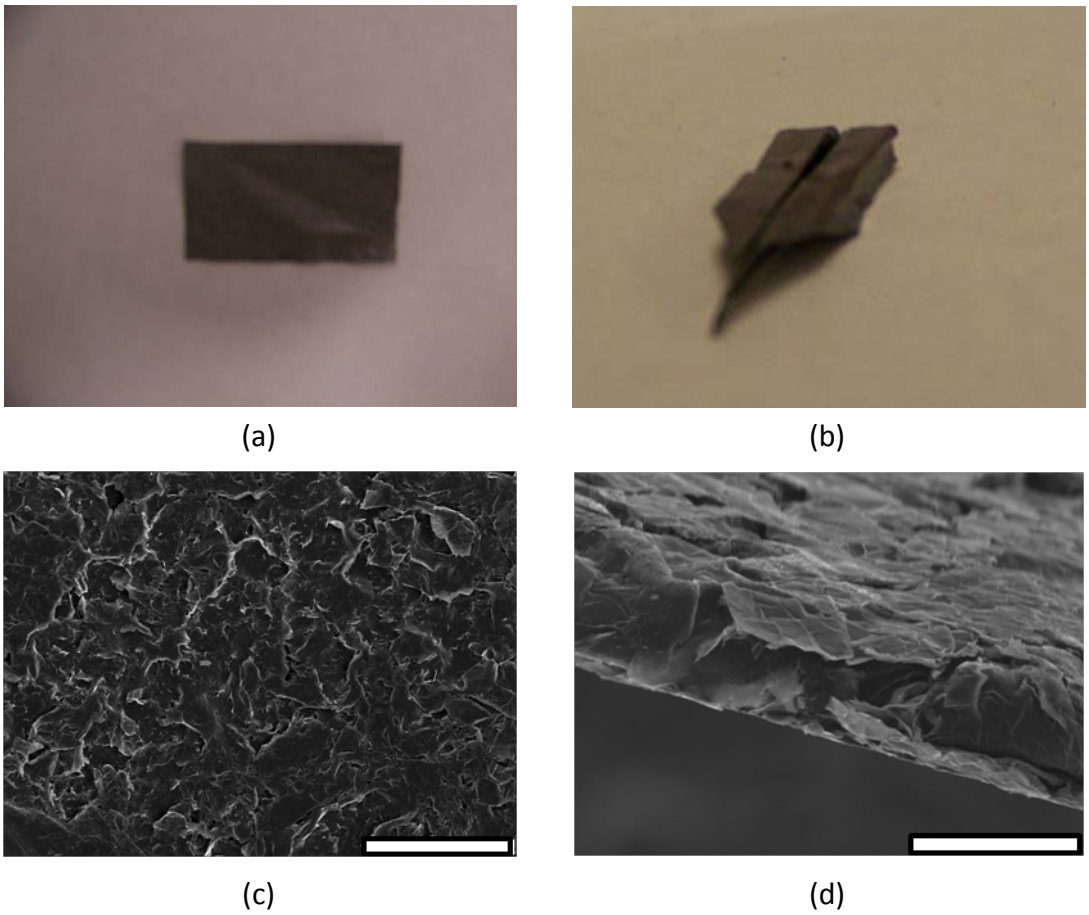

(a) (b)

(c) (d)

Figure 8.3, GNP paper and its flexibility (a) GNP paper (b) paper plane folded from GNP paper (c) morphology of the surface of the GNP paper (d) morphology of the folding edge of the paper plane (Scale bars: (c) 200 micron, (d) 50 micron)

In this research, the GNP-H was used to represent stand-alone GNP paper and for the fabrication of high GNP loading paper composites (80 wt% and 70 wt%) due to its low porosity. On the other hand, the GNP-L was mostly used for low GNP loading

paper composites (10 vol%) because of its higher porosity. The GNP papers used in CF composites were all GNP-Ls.

Impregnating GNP Paper

Due to its porosity, the GNP paper can be impregnated by either a thermoset or thermoplastic matrix. For thermoset system, the un-pressed GNP paper was soaked in the uncured liquid epoxy mixture for 1 hour and then cured in a hot press under 10 MPa and 150 ^{O}C (noted as GNP-E).

For the thermoplastic system, PEId/dichloromethane solution was prepared at 0.1 g/mL, 0.15 g/mL and 0.2 g/mL. The GNP paper was soaked in the solution for 1 hour and then dried under room temperature. Depending on the concentration of the solution, the pores can be filled with controlled amounts of PEId. The soaked paper (GNP-PEId) can also be further compressed under 10 MPa and 340^{O}C resulting in void free GNP/PEId paper composite. The loading of GNP in the paper composite is calculated by the weight change before and after impregnation.

The polymer impregnated GNP-E paper was used to fabricate laminate composite with carbon fiber/polyetherketoneketone (PEKK) prepreg (CF). Structure and notation of the composites are shown in Figure 8.4.

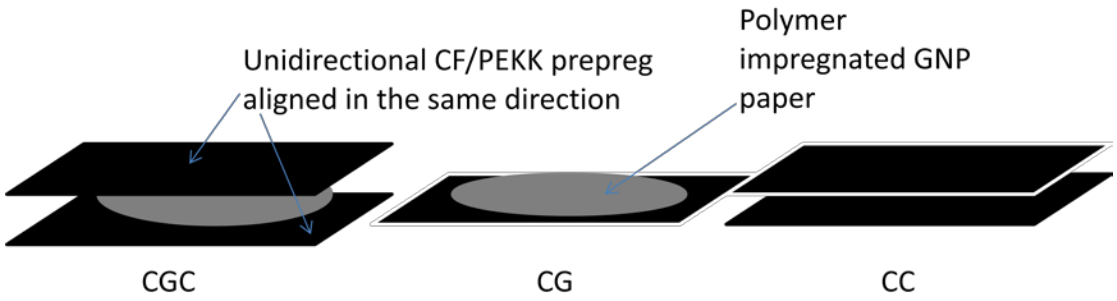

Figure 8.4, Structure and nomination of CF/GNP paper composites

Characterization

Tensile modulus was measured by Dynamic Mechanical Analyzer (DMA, TA Instruments) with film tension clamp. The strain rate was set at 0.1%/min. Representative stress-strain curves for both un-pressed and pressed GNP papers are shown in Figure 8.5. Pressed GNP paper (GNP-H-P) shows a much higher modulus and strength than un-pressed one (GNP-H). However, the elongation at break of GNP-H is greater than that of GNP-H-P. This is because in a pressed paper, GNP particles have better contact between each other which ensures a total force of attraction. Also, the layered structure has fewer voids. For GNP-H, the GNP particles have room to move and re-orient more before breaking than GNP-H-P, resulting in a greater elongation at break.

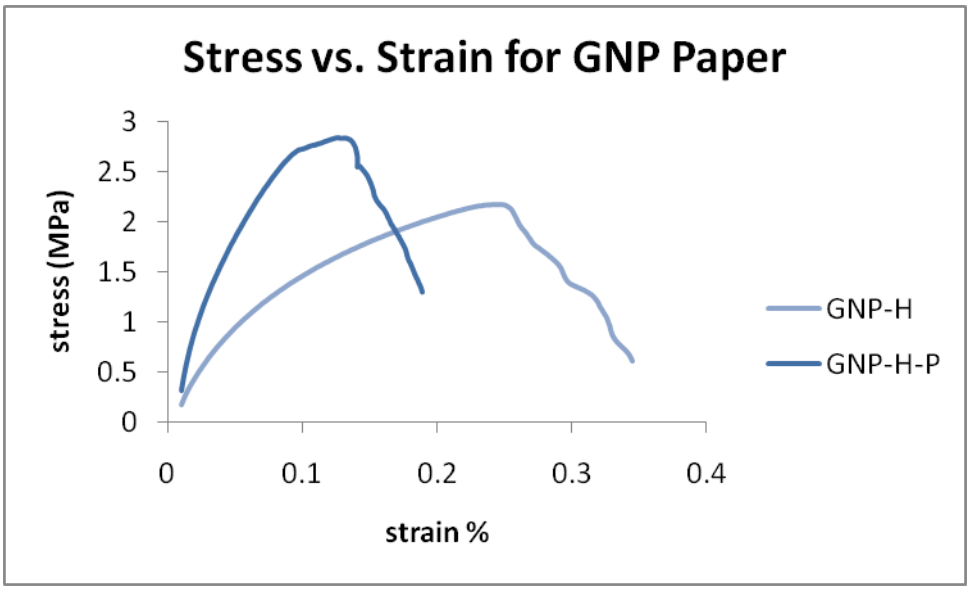

Figure 8.5, Stress-strain curve of GNP paper

Electrical conductivity was measured by 4-point method. The papers were cut into rectangular strips. Four electrode pins were pressed to the paper surface with a spacing of 1 cm. Silver paste was placed at the contacting points between the paper and the electrode pins in order to eliminate contact resistance.

Thermal diffusivity was measured by using the laser flash method. Thermal conductivity was then calculated by multiplying the diffusivity by the heat capacity and density of the paper.

O_2 permeability was measured by a MOCON OXTRAN 2/20 model (MOCON, Inc.). The composite film was sandwiched by two pieces of aluminum masks with a 1 cm^2 opening at the center. Permeation of O_2 was measured under a pressure of 30 psi and recorded with a unit of $cc/m^2/day$.

Results and discussions

Effect of Annealing and Pressing

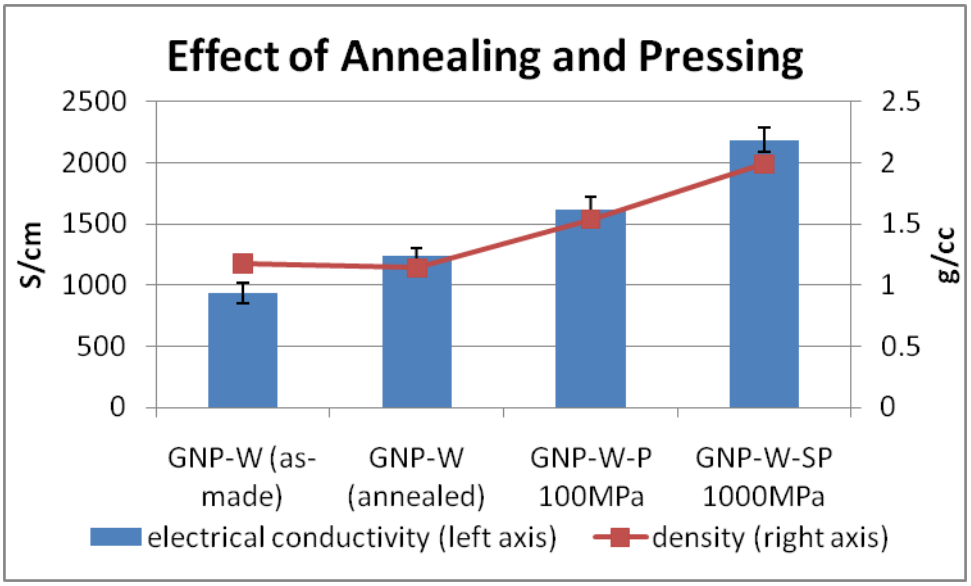

Figure 8.6, Effect of Annealing and Compression on the density and electrical conductivity of GNP-W paper. "as-made" stands for filtrated paper without annealing or pressing. Pressure is the nominal value calculated from press/sample area

GNP-W papers were used to demonstrate the effect of annealing and compression (Figure 8.6). After annealing, the density of the GNP-W paper decreased by 3wt%, indicating that about 3wt% of PEIn was left in the filtrated GNP paper. Considering the original ratio between GNP and PEIn is 1 in the suspension, it is clear that most of the PEIn was washed away by water. Considering the 5 wt% residue of PEIn after annealing under 340 ^{o}C for 1 h (Figure 8.1), a total of around 0.15 wt% PEIn residue is still in the GNP paper. However, this level is even lower than that of the un-processed GNP particle. Thus, the annealed paper can be considered as binder free. By removing the 3 wt% PEIn, the electrical conductivity of GNP-W paper increased significantly, from 900 S/cm to 1200 S/cm. This huge difference indicates the

importance of the contact resistance. Before annealing, the 3 wt% PEIn was covering the surface of all GNP particles, although the amount seems to be small. The GNP-PEIn-GNP interface is clearly inhibiting the electrical conductance.

Pressing the annealed GNP-W paper resulted in further improvement of electrical conductivity. There is a very good correlation between the density and electrical conductivity of the GNP-W paper. After compression under 100 MPa (GNP-W-P) and 1000 MPa (GNP-W-SP), the conductivity increased to 1500 S/cm and 2200 S/cm, respectively. The density of 1000 MPa pressed GNP-W-P reached 1.99 g/cc which is very close to the density of natural graphite, and it is not surprising that its conductivity is also similar to that of the natural graphite.

Properties of GNP Paper

The alignment of GNP layer and binder-free nature both benefit the properties of the GNP paper. Tensile modulus, electrical and thermal conductivity were measured for pressed and un-pressed GNP papers along with three kinds of commercially available carbon-based paper form materials including TG-411, SUPER GTO (GRAFOIL®, compressed expanded graphite from GRAFTECH) and CNT Bucky paper (NANO-LAB).

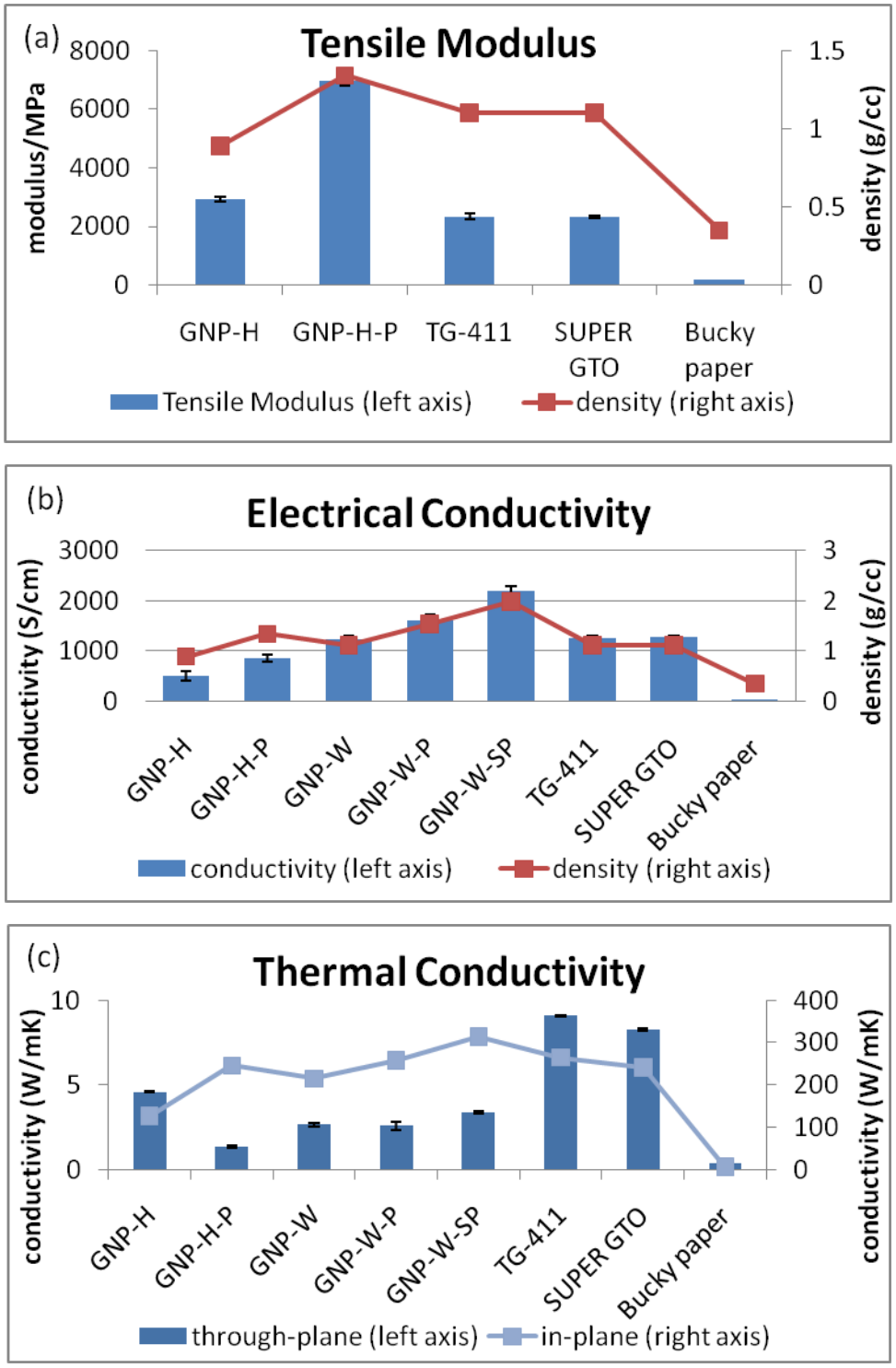

Figure 8.7, Comparison between carbon-based papers (a) tensile modulus (b) electrical conductivity (c) thermal conductivity

The comparison between GNP-H, GNP-H-P, GNP-W, GNP-W-P, GNP-W-SP (pressed under 1000 MPa nom), TG-411, SUPER GTO and CNT Bucky paper is shown in Figure

8.7. Generally, all the three kinds of properties are positively related to the density of the sample, with a couple of exceptions. First, the tensile modulus of GNP-H paper is 2900 MPa, while GRAFOIL papers have a tensile modulus of about 2500 MPa. Although the density of GRAFOIL is higher than GNP-H, unlike GNP paper where the GNP particles are highly aligned, particles do not have preferential alignment in GRAFOIL (Figure 8.8(a)). Since the properties of the GNP platelet is much higher in the in-plane direction, the alignment of GNP particles can help GNP paper to achieve maximum performance including not only modulus but also electrical and thermal conductivity. Second, the comparison between the electrical conductivity of GNP-H-P and GNP-W indicates the benefit of using larger particles. Despite its higher density, GNP-H-P falls short in electrical conductivity as compared to GNP-W. As previously stated, the size of the ultrasonicated GNP worm particles ranges from 20 to 100 microns, which is larger than GNP-15. With the same amount of material, more contacting points are present in GNP-15 paper, resulting in higher contact resistance.

The GNP-W-SP paper has the highest electrical conductivity at ~2200 S/cm. This result is much higher than other reported value for carbon-based paper in literature. Under similar density, GRAFOIL® papers have similar conductivity as compared to GNP-W. Figure 8.8(a) shows the morphology of GRAFOIL® paper. Note that the GRAFOIL® is made from expanded graphite, so the debris morphology in Figure 8.8(a) does not represent the actual size of the particles, and was more likely generated by polishing during sample preparation.

CNT Bucky paper has the lowest density, modulus, electrical and thermal

conductivity among all the materials, 0.35g/cc, 200 MPa, 39.7 S/cm and 5.28 W/mK respectively. From Figure 8.8(b), it can be observed that the CNT paper is very porous. The CNTs are loosely entangled together and can be drawn apart by relatively low force, resulting in low tensile modulus. Electrical and thermal conductivity are hindered by the high porosity and large amount of contacting points between CNT particles.

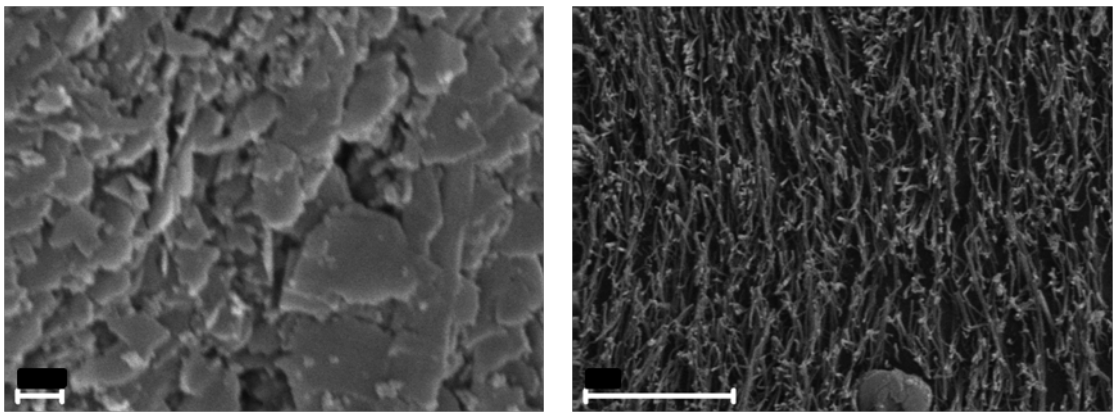

(a) (b)

Figure 8.8, SEM images showing cross-section morphology of (a) GRAFOIL® and (b) CNT Bucky paper. Samples were prepared by polishing-O_2 plasma etching process (scale bars: (a) 200 nm, (b) 2 micron)

Impregnation of GNP Paper

To investigate the morphology of impregnated GNP paper, the epoxy fixative material was mixed with fluorescent dye and used as support for the papers. An Olympus FluoView FV1000 Laser Scanning Confocal Microscope with 488 Argon laser excitation was used to detect the fluorescence signal.

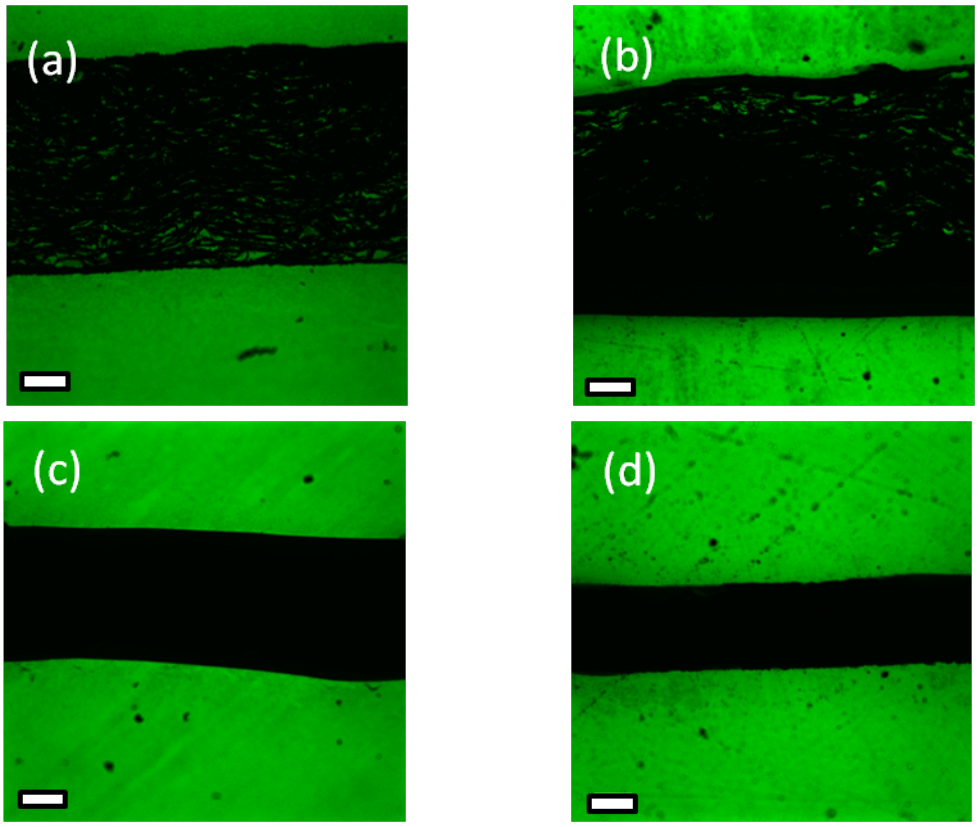

Figure 8.9, Confocal microscopic images of GNP papers impregnated by (a) 0.1 g/mL PEId/dichloromethane solution (b) 0.2 g/mL PEId/dichloromethane solution (c) pressed GNP- PEId paper (d) GNP-E paper. Green indicates fluorescence signal, black indicates GNP (scale bars represent 20 micron)

If a GNP paper is porous, the epoxy putty material can penetrate inside and give a fluorescence signal. If the GNP paper is soaked in a dilute PEId solution, the pores cannot be fully filled. Figure 8.9(a) shows uniform distributed fluorescent signal throughout the GNP paper cross-section. With the increase of PEId concentration, the area that emits fluorescent signal decreases, indicating more PEId was absorbed in the pores preventing the fluorescent tagged epoxy for penetrating into them(Figure 8.9(b)). Pressing the soaked GNP paper can close the pores and no

fluorescent signal can be seen in Figure 8.9(c). The epoxy soaked GNP paper also shows no fluorescence signal throughout the cross-section (Figure 8.9(d)).

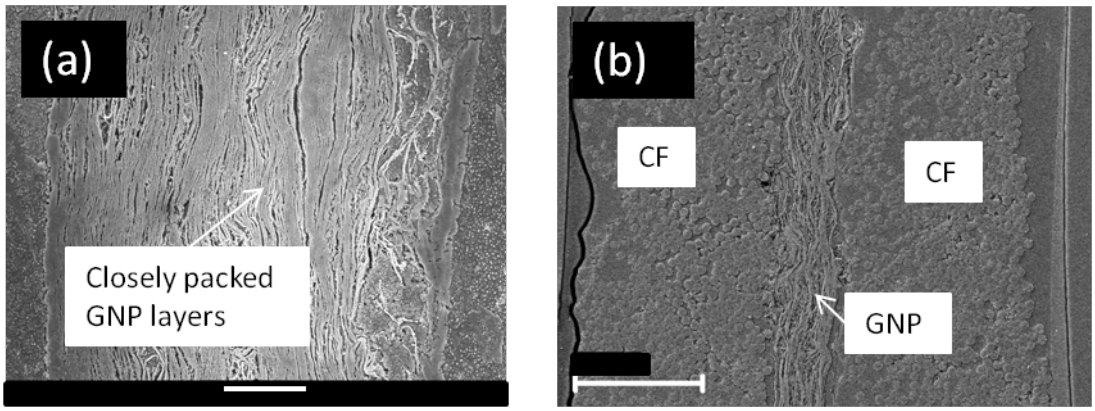

Figure 8.10, SEM images showing cross-section of (a) pressed GNP-PEId (b) CGC-PEId (Scale bars: (a) 10 micron, (b) 100 micron)

One advantage of infiltrating the GNP paper with polymer is that the tensile modulus of the composite can be greatly improved as compared with either pure GNP paper or the neat polymer. 80 wt% and 70 wt% GNP/PEId paper show a tensile modulus of 19000 MPa and 22000 MPa respectively, which are approximately 500% to 600% improvement to either pure GNP paper or neat PEId (Figure 8.11(a)). The tensile strength of the GNP paper is also improved from 2.3 MPa to 22.6 MPa and 32.3 MPa with 30 vol% and 40 vol% filled by PEId, respectively (Figure 8.11(b)).

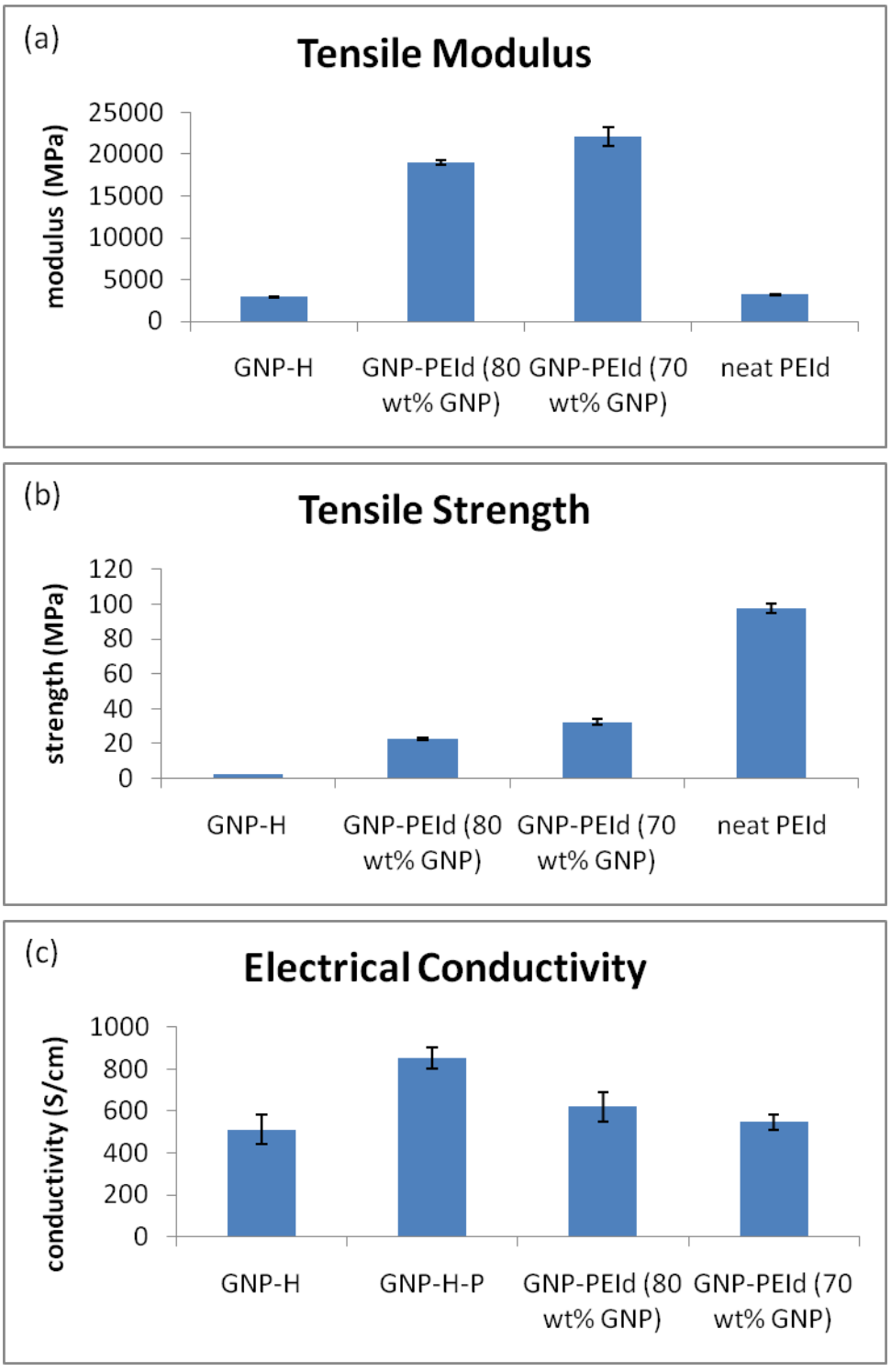

Figure 8.11, Properties of GNP paper composites from soaking

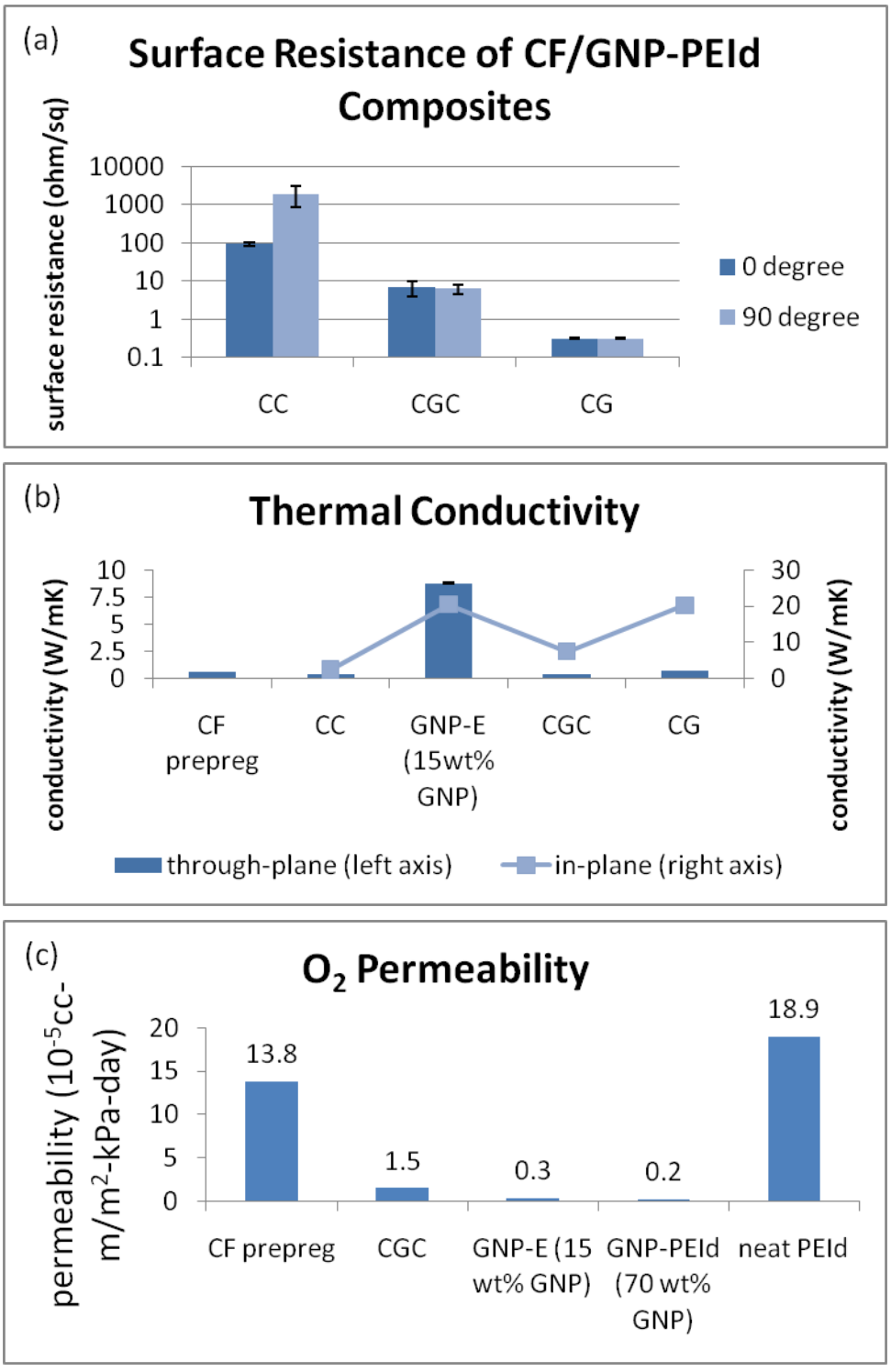

Figure 8.12, Properties of GNP paper/CF composites

Interestingly, with 10 wt% more polymer, both modulus and strength increased for GNP-PEId. This can be explained by looking at the volume fraction of GNP, PEId and voids. 70 wt% GNP-PEId has similar GNP volume fraction as the 80 wt% sample but

more polymer to fill in the voids and bind the particles, resulting in higher modulus and strength (Table 8.2).

Table 8.2, Actual composition in GNP-PEId

Sample	80 wt% GNP-PEId	70 wt% GNP-PEId	GNP-H	GNP-H-P
Actual wt%	0.79	0.71	1	1
Density	1.03	1.04	0.90	1.34
Void vol%	44	41	57	36
GNP vol%	39	36	43	64
PEId vol%	17	23	0	0

Moreover, adding 20 to 30 wt% of polymer to the GNP paper would not cause the conductivity to drop significantly (Figure 8.11(c)). In fact, compared to un-pressed GNP-H, both 80 wt% and 70 wt% GNP-PEId paper showed higher conductivity at 620 S/cm and 550 S/cm, respectively. The reason is, for pressed GNP-PEId paper, the GNP layers are also closely packed similar to pure GNP-H-P (Figure 8.10(a), Figure 8.2(b)). The PEId actually fills in those small voids between GNP particles. Certainly, the presence of PEId would add extra contacting resistance, resulting in lower conductivity for the GNP-PEId composite paper as compared to GNP-H-P. The difference in volume fraction of GNP in the paper is within 7 vol% between 70 wt% GNP-PEId and GNP-H (Table 8.2). Despite its 41 vol% voids, the O_2 permeability of 70 wt% GNP-PEId paper is only 1.1% of neat PEId (Figure 8.12(c)), indicating that the voids are not connected, which can also be observed in Figure 8.9(c) where no fluorescence signal can be observed inside the GNP-PEId paper.

The most significant effect of adding GNP paper into CF composite is the largely

reduced O_2 permeability (Figure 8.12(c)). The epoxy impregnated GNP-E paper shows a permeability that is only 2% of CF prepreg. By inserting a layer of GNP-E, the O_2 permeability of CF composite consisting of two CF layers reduced to 11% as compared to the pristine CF prepreg.

Meanwhile, with 85 wt% filled by epoxy, the GNP-E paper retains an in-plane thermal conductivity at 20.5 W/mK with a through-plane conductivity of 8.78 W/mK (Figure 8.12(b)). The presence of 85 wt% epoxy reduced the anisotropy of pure GNP paper which has a maximum anisotropic factor as high as 200 (GNP-H-P in Figure 8.7(c)). The GNP particles in this GNP-E paper were prevented from high alignment by the spacing of epoxy. If this GNP-E paper is inserted in between of two CF prepregs, both thermal and electrical conductivity can be improved for the composite. The most significant improvement was attained by structuring the GNP paper to one surface of the CF composite (Figure 8.4, Figure 8.12(a)(b)). While the CGC composite gained 200% improvement in in-plane thermal conductivity as compared to the CC construction, the increase for CG is over 700%. For surface resistance, the CG structure also benefits from the exposure of GNP phase and shows lower value (0.3 ohm/sq). For CF prepreg, the resistance in the 0 degree direction is much lower than 90 degree due to the anisotropic nature of carbon fibers. However, when a layer of GNP paper is inserted, the resistance becomes identical in both directions. This result indicates good contact between CF and GNP layers which is also shown in Figure 8.10(b). Since the conductivity of GNP is much higher than CF, the apparent surface resistance actually mainly consists of the resistance through the thickness of CF layer (Figure

8.13).

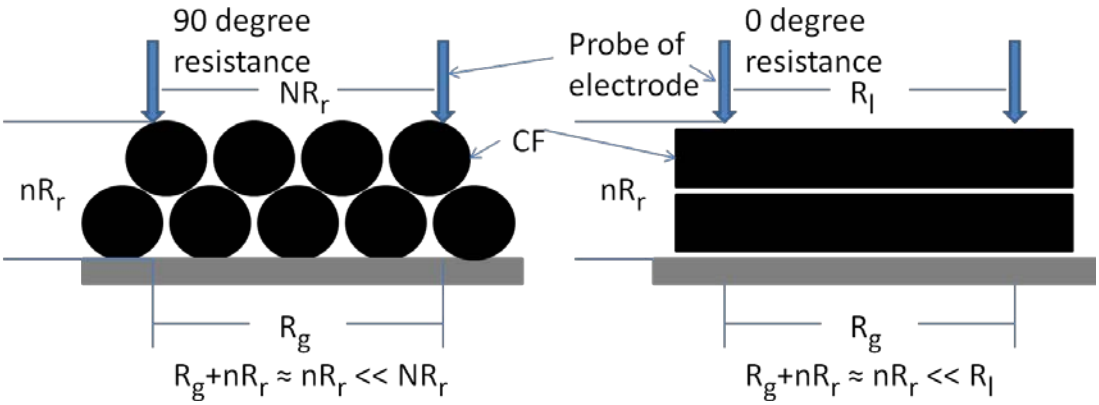

Figure 8.13, Schematics of surface resistance measurement for CF/GNP paper composite. R_r and R_l stand for resistance of CF through radius direction and through length direction, respective. R_g stands for resistance of GNP paper, which is far less than the other two. N is the number of CF between electrode probes and n is that between the probe and the GNP layer. N is usually much larger than n. When the resistance is measured along 90 degree direction, the path for electrons with the lowest resistance is through the thickness of CF layer and reaching GNP layer. The total resistance can be approximated to nR_r. When the resistance is measured along 0 degree direction, since the distance between two probes (10mm) is usually much larger than that between one probe and GNP layer (~0.2mm), R_l is still much larger than nR_r and the total resistance can also be approximated to nR_r.

Conclusions

Binder free, self-standing flexible GNP papers have been successfully fabricated through filtration of GNP/PEIn/water suspension followed by annealing. It is found that the properties are highly related to the density of the paper. The pressed GNP paper exhibited excellent electrical conductivity (~2200 S/cm) which is higher than other reported similar type of materials. The thermal conductivity (313 W/mK) is comparable to other commercially available graphite material. Processes have been

developed to impregnate the GNP paper with either thermoset or thermoplastic matrices. The resulting paper composite showed extremely high tensile modulus (22000 MPa) and reasonable strength (32 MPa) while still retaining high electrical and thermal conductivity. When inserted into a multilayer laminated composite, the additional GNP paper layer can significantly reduce the O_2 permeability and add in-plane electrical and thermal conductivity to the composite. However, through-plane properties were not improved significantly because of the anisotropic behavior and alignment of GNP particles. The GNP paper composite is believed to be a very useful addition to laminate composites, providing multifunctionality for applications such as fuel tanks, lightning strike protection, replacement for copper conductor for weight-sensitive area like aerospace, and flexible resistive heaters.

References

REFERENCES

1. Chang, T.C. and H.J. Gao, *Size-dependent elastic properties of a single-walled carbon nanotube via a molecular mechanics model.* Journal of the Mechanics and Physics of Solids, 2003. **51**(6): p. 1059-1074.

2. Meo, M. and M. Rossi, *Prediction of Young's modulus of single wall carbon nanotubes by molecular-mechanics based finite element modelling.* Composites Science and Technology, 2006. **66**(11-12): p. 1597-1605.

3. Lee, C., et al., *Measurement of the elastic properties and intrinsic strength of monolayer graphene.* Science, 2008. **321**(5887): p. 385-388.

4. Zhao, H., K. Min, and N.R. Aluru, *Size and Chirality Dependent Elastic Properties of Graphene Nanoribbons under Uniaxial Tension.* Nano Letters, 2009. **9**(8): p. 3012-3015.

5. Wong, C.L., et al., *Characterization of nanomechanical graphene drum structures.* Journal of Micromechanics and Microengineering, 2010. **20**(11).

6. Tune, L., *Physicists Show Electrons Can Travel More Than 100 Times Faster in Graphene (https://newsdesk.umd.edu/scitech/release.cfm?ArticleID=1621)*. 2008.

7. Watanabe, E., et al., *Ballistic thermal conductance of electrons in graphene ribbons.* Physical Review B, 2009. **80**(8).

8. Jiang, J.W., J.S. Wang, and B.W. Li, *Thermal conductance of graphene and dimerite.* Physical Review B, 2009. **79**(20).

9. Saito, K., J. Nakamura, and A. Natori, *Ballistic thermal conductance of a graphene sheet.* Physical Review B, 2007. **76**(11).

10. Balandin, A.A., et al., *Superior thermal conductivity of single-layer graphene.* Nano Letters, 2008. **8**(3): p. 902-907.

11. LeBaron, P.C., Z. Wang, and T.J. Pinnavaia, *Polymer-layered silicate nanocomposites: an overview.* Applied Clay Science, 1999. **15**(1-2): p. 11-29.

12. Yano, K., et al., *SYNTHESIS AND PROPERTIES OF POLYIMIDE CLAY HYBRID.* Journal of Polymer Science Part a-Polymer Chemistry, 1993. **31**(10): p. 2493-2498.

13. Stankovich, S., et al., *Graphene-based composite materials.* Nature, 2006. **442**(7100): p. 282-286.

14. Chen, G.H., et al., *Preparation of polymer/graphite conducting nanocomposite by intercalation polymerization.* Journal of Applied Polymer Science, 2001. **82**(10): p. 2506-2513.

15. Zheng, G.H., et al., *Characterizations of expanded graphite/polymer composites prepared by in situ polymerization.* Carbon, 2004. **42**(14): p. 2839-2847.

16. Zhao, Y.F., et al., *Preparation and properties of electrically conductive PPS/expanded graphite nanocomposites.* Composites Science and Technology, 2007. **67**(11-12): p. 2528-2534.

17. Vadukumpully, S., et al., *Flexible conductive graphene/poly(vinyl chloride) composite thin films with high mechanical strength and thermal stability.* Carbon, 2011. **49**(1): p. 198-205.

18. Kalaitzidou, K., H. Fukushima, and L.T. Drzal, *A new compounding method for exfoliated graphite-polypropylene nanocomposites with enhanced flexural properties and lower percolation threshold.* Composites Science and Technology, 2007. **67**(10): p. 2045-2051.

19. Fukushima, H., et al., *Thermal conductivity of exfoliated graphite nanocomposites.* Journal of Thermal Analysis and Calorimetry, 2006. **85**(1): p. 235-238.

20. Liu, J., et al., *Fullerene pipes.* Science, 1998. **280**(5367): p. 1253-1256.

21. Cooper, S.M., et al., *Gas permeability of a buckypaper membrane.* Nano Letters, 2003. **3**(2): p. 189-192.

22. Wang, Z., et al., *Processing and property investigation of single-walled carbon nanotube (SWNT) buckypaper/epoxy resin matrix nanocomposites.* Composites Part a-Applied Science and Manufacturing, 2004. **35**(10): p. 1225-1232.

23. Endo, M., et al., *'Buckypaper' from coaxial nanotubes.* Nature, 2005. **433**(7025): p. 476-476.

24. Gonnet, P., et al., *Thermal conductivity of magnetically aligned carbon nanotube buckypapers and nanocomposites.* Current Applied Physics, 2006.

6(1): p. 119-122.

25. Gou, J.H., *Single-walled nanotube bucky paper and nanocomposite.* Polymer International, 2006. **55**(11): p. 1283-1288.

26. Kim, Y.A., et al., *Fabrication of high-purity, double-walled carbon nanotube buckypaper.* Chemical Vapor Deposition, 2006. **12**(6): p. 327-+.

27. Zheng, F., et al., *Single-walled carbon nanotube paper as a sorbent for organic vapor preconcentration.* Analytical Chemistry, 2006. **78**(7): p. 2442-2446.

28. Wang, D., et al., *Highly oriented carbon nanotube papers made of aligned carbon nanotubes.* Nanotechnology, 2008. **19**(7).

29. Xu, G.H., et al., *The feasibility of producing MWCNT paper and strong MWCNT film from VACNT array.* Applied Physics a-Materials Science & Processing, 2008. **92**(3): p. 531-539.

30. Dumee, L.F., et al., *Characterization and evaluation of carbon nanotube Bucky-Paper membranes for direct contact membrane distillation.* Journal of Membrane Science, 2010. **351**(1-2): p. 36-43.

31. Dikin, D.A., et al., *Preparation and characterization of graphene oxide paper.* Nature, 2007. **448**(7152): p. 457-460.

32. Chen, H., et al., *Mechanically strong, electrically conductive, and biocompatible graphene paper.* Advanced Materials, 2008. **20**(18): p. 3557-+.

33. Park, S., et al., *Graphene oxide papers modified by divalent ions - Enhancing mechanical properties via chemical cross-linking.* Acs Nano, 2008. **2**(3): p. 572-578.

34. Li, X.L., et al., *Highly conducting graphene sheets and Langmuir-Blodgett films.* Nature Nanotechnology, 2008. **3**(9): p. 538-542.

35. Biswas, S. and L.T. Drzal, *A Novel Approach to Create a Highly Ordered Monolayer Film of Graphene Nanosheets at the Liquid-Liquid Interface.* Nano Letters, 2009. **9**(1): p. 167-172.

36. Xiang, J.L. and L.T. Drzal, *Thermal Conductivity of a Monolayer of Exfoliated Graphite Nanoplatelets Prepared by Liquid-Liquid Interfacial Self-Assembly.* Journal of Nanomaterials, 2010.

37. Drzal, L.T. and H. Fukushima, *Expanded graphite and products produced therefrom*. 2004: US.

Chapter 9 Summary and Conclusions

In summary, the possibility of using exfoliated graphite nanoplatelet (GNP) to provide multifunctionality to a composite has been investigated. Polyetherimide (PEId) was chosen as an exemplar matrix. The key idea of this research is to first reveal the relationships among processing, morphology and performance of the nanocomposites, and then use the information to guide the nanostructuring of GNP/polymer nanocomposites. The first part is based on the successful development of sample preparation method for scanning electron microscope (SEM) quantification of the nanoparticle reinforced composite morphology. The sectioning-polishing-O_2 plasma etching process is found to be very effective in revealing the morphology of the GNP/polymer nanocomposites. Sharp images can be obtained by using SEM on the sample prepared in such way. Thanks to the good contrast between nanofillers and the matrix, the image can be processed by Image-Pro software and information such as particle size and orientation can be gathered for further analysis. The complementary fluorescence image can locate the epoxy fixative material used in the preparation process and helps interpret the morphology of samples with pores or cracks inside.

By revealing the morphology, the performance of the composites such as mechanical modulus and strength, electrical and thermal conductivity, coefficient of thermal expansion, O_2 permeability can be related to the distribution, dispersion and orientation of GNP particles. It is found that high degree of alignment benefits

in-plane properties such as modulus and CTE but prevents particles from connecting with each other, resulting in poor electrical and thermal conductivity. Random orientation of the particles, on the other hand, gives the particles a better chance to touch others and helps form a continuous phase of the filler, resulting in high electrical and thermal conductivity. The quantified information about particle alignment can be used to modify models such as Tandon-Weng's equation for Young's modulus and Bharadwaj's equation for permeability. The modeling of linear thermal expansion (LTE) was also applied and explained by using the orientation information qualitatively.

Based on the morphology-performance relationship attained from morphology study, a few specially designed composites were fabricated by nanostructuring. First, the orientation of the particles in the composites is modified by annealing. With 1 hour annealing under 340^{o}C the injection molded GNP/PEId samples show significantly improved electrical conductivity, reducing its percolation threshold from 10 to 3 wt%. Secondly, uniform alignment of GNP was achieved by fabricating GNP/PEId films through extrusion casting, resulting in larger improvement in elastic modulus and strength to the neat polymer film as compared to the improvement ratio of injection molded composites. The alignment also benefits the barrier properties to O_2 permeation, resulting in over 65% reduction to O_2 permeability with 10wt% GNP-5 loading and 34 stretching ratio, while only 50% reduction if the sample is prepared by compression molding. Annealing can also be used to adjust the degree of alignment, resulting in at least one order of magnitude lower electrical resistivity and over 100%

improvement in thermal conductivity.

A new efficient, solvent-less compounding method, solid state ball milling (SSBM), has been developed. This procedure succeeds in lowering the percolation threshold by forming a continuous GNP coating on the surface of size-reduced polymer powder with good adhesion. Composites fabricated from SSBM approach showed similar percolation profile as pre-coating but with better mechanical properties without using solvent. The combination of melt-extrusion and SSBM has been found to be capable of providing a composite with both high mechanical properties and electrical conductivity. Thermal conductivity can also benefit from SSBM and pre-coating. A second order polynomial relationship is found between the thermal conductivity and the loading of GNP in pre-coated GNP/PEId composites.

Finally, in order to fully utilize the excellent properties of GNP, a novel procedure was developed to fabricate a paper form GNP assembly and make its corresponding composites. Binder free, self-standing flexible GNP paper has been successfully fabricated through filtration of GNP/polyethylene imine (PEIn)/water suspension followed by annealing. The GNP paper exhibits excellent electrical conductivity (~1800 S/cm) which is higher than other reported similar type of materials. The thermal conductivity (246 W/mK) is comparable to other commercially available graphite material. Processes have been developed to impregnate the GNP paper with either thermoset or thermoplastic matrices. The resulting paper composite (60vol% GNP) showed extremely high tensile modulus (22,000 MPa) and reasonable strength (32 MPa) while still retaining electrical and thermal conductivity. When applied to a

fiber reinforced composite laminate, the additional GNP paper layer can significantly reduce the O_2 permeability and add in-plane electrical and thermal conductivity to the composite. However, through-plane properties are not improved significantly because of the alignment of the anisotropic GNP particles.

Table 9.1, Summary of properties of GNP/PEId composites and GNP paper composites

	Loading & GNP type	Modulus (GPa)	Strength (MPa)	Electrical conductivity (S/cm)*	Thermal conductivity (W/mK)*	Relative O_2 Permeability
Injection molding	10wt% GNP-5	6.6	98	E-6.7		
	Annealed			E-3.0		
Compression molding	10wt% GNP-5	5.7	98	E-4.5	0.40	
SSBM & Pre-coating	5wt% GNP-15	3.9	65	1.25	0.85 (through-plane, 3.3 @ 10wt%)	
Extrusion cast film	10wt% GNP-5	6.8	106	E-6.1	0.29 (through-plane)	0.35
	Annealed			E-4.3	0.80	
Pressed GNP paper	100% GNP-15	7.0	2.8	850	246	
	100% worm			2200	313	
GNP paper -PEId	80wt% GNP-15	19	23	620		
GNP paper -PEId	70wt% GNP-15	22	32	550		0.01
GNP paper -epoxy	15wt% GNP-15				20.5	0.02

*: in-plane if not otherwise stated

A summary of properties of GNP/PEId composites and GNP paper composites is shown in Table 9.1, where a good variety of GNP based composites with different properties is presented. Based on the desired application, a composite with modulus as high as 22 GPa, or electrical conductivity of 2200 S/cm, or thermal conductivity of 313 W/m/K, or relative O_2 permeability as low as 1.1% as compared with neat polymer, or a combination of these properties can be produced. The possibility of synthesizing multifunctional composites with the addition of small amounts of GNP is feasible.

Future Investigations and Opportunities

Incorporating paper form GNP into composites seems to be a very promising approach for developing both structural and functional materials. Due to the high electrical conductivity, the GNP layer may be able to serve as electronic protection if inserted properly in a laminate composite. One potential new application is whether the GNP is conductive enough to serve as a primary lightning strike protector for composite aircraft. Because of the increasing interest of using composite instead of metal to construct the airplanes, the lightning strike becomes an issue. Now copper mesh is mostly used in the airplane shell for this purpose. The advantage of using GNP paper is its relatively lower density as compared with metal. Composite panels with GNP paper close to surface can be fabricated through autoclave for lightning strike testing.

The GNP/polymer composite can also be used for fuel tanks. The conductive additive

would help prevent static charge hazard while providing extra barrier properties to fuel molecules.

To further improve the performance of GNP/PEId composites, surface treatment is needed for the GNP particles. Normally, fillers with higher aspect ratio are preferred for better properties. Although high-surface-area version GNP which has a higher aspect ratio can be obtained, its direct use in PEId matrix hardly resulted in better properties. The reason is, under compounding conditions such as melt-extrusion, the thinner particles usually results in agglomerates and are hard to be dispersed well in the polymer matrix. If an adequate surfactant for GNP can be developed to enhance its compatibility with PEId, this problem can be solved and better performance may be achieved by using high-surface-area GNP. Pyrene compound, for example, is a good candidate for this kind of surfactant. The flat aromatic ring system of pyrene has a strong interaction with the graphite basal plane. Meanwhile, molecular branches that are compatible to the polymer matrix can be introduced to pyrene. If the modified pyrene compound is coated to GNP particle surface, then the added branch can help the GNP disperse well in the polymer matrix. The challenge here is to find an adequate molecular branch that has good compatibility with PEId.